MATRIX-DERIVED MICROCARRIERS FOR ADIPOSE TISSUE ENGINEERING

by

Allison Eugenia Bogart Turner

A thesis submitted to the Department of Chemical Engineering

In conformity with the requirements for

the degree of Master of Applied Science

Queen's University

Kingston, Ontario, Canada

(December, 2010)

Abstract

In vivo, adipose tissue demonstrates only a limited capacity for self-repair, and the long-term treatment of subcutaneous defects remains an unresolved clinical problem. With the goal of regenerating healthy tissues, many tissue-engineering strategies have pointed to the potential of implementing three-dimensional (3-D), cell-seeded scaffolds for soft tissue augmentation and wound healing. In particular, microcarriers have shown promise as both cell expansion substrates and injectable cell-delivery vehicles for these applications. However, limited research has investigated the engineering of tissue-specific microcarriers, designed to closely mimic the native extracellular matrix (ECM) composition. In this work, methods were developed to fabricate microcarriers from decellularized adipose tissue (DAT) via non-cytotoxic protocols. Characterization by microscopy confirmed the efficacy of the fabrication protocols in producing stable beads, as well as the production of a microporous surface topography. The mean bead diameter was 934 ± 51 μm, while the porosity was measured to be 29 ± 4 % using liquid displacement. Stability and swelling behavior over 4 weeks indicated that the DAT-based microcarriers were effectively stabilized with the non-cytotoxic photochemical crosslinking agent rose bengal, with only low levels of protein release measured within a simulated physiological environment. In cell-based studies, the DAT-based microcarriers successfully supported the proliferation and adipogenic differentiation of human adipose-derived stem cells (hASCs) in a dynamic spinner flask system, with a more favorable response observed in terms of adhesion, proliferation, and adipogenesis on the DAT-based microcarriers relative to gelatin control beads. More specifically, dynamically-cultured hASCs on DAT-based microcarriers demonstrated greater lipid loading, as well as higher glycerol-3-phosphate dehydrogenase (GPDH) activity, a key enzyme involved in triacylglycerol biosynthesis, at 7 days and 14 days in culture in an inductive medium. Overall, the results indicated that the DAT-based microcarriers provided a

uniquely supportive environment for adipogenesis. Established microcarrier sterility and injectability further support the broad potential of these tissue-specific microcarriers as a novel, adipogenic, clinically-translatable strategy for soft tissue engineering.

Acknowledgements

First and foremost, I would like to thank my supervisor Dr. Lauren Flynn, for her support, guidance, and encouragement during this project. I am honored to have been her first graduate student, and it was a pleasure to work with her. Thank you for helping me establish a strong foundation in approaching research with an open mind and a critical eye.

I would also like to thank Drs. Brian Amsden and Stephen Waldman for the use of their laboratory equipment and for their outstanding teaching during my studies at Queen's University.

Many thanks to the Flynn Lab Group, particularly Ms. Sarah Fleming, as well as Mr. Jeffery Wood, Mr. Charlie Cooney, Dr. Xiaohu Yan, Mr. Gary Contant, and Mr. James Hayami for their technical assistance during this project, and to Dr. Ronald Neufeld and Mr. Joe Steele for guidance in alginate-labeling. Thanks also to Drs. J. F. Watkins, M. Harrison, K. Meathrel, J. Davidson, C. Watters, and Mrs. K. Martin, for their clinical collaborations facilitating tissue acquisition.

To Dr. T. Kurtis Kyser, thank you for piquing my interest in pursuing graduate studies, and to Ms. Allison Laidlow, thank you for your lasting friendship along the way.

I would like to thank Drs. Donald Gerson and M. Gail Meadows for being my home away from home and for patiently discussing all things "adipose." To my husband Elliott, thank you for believing in me and supporting me at every step along the way.

Last, but certainly not least, I would like to thank my parents for their unwavering confidence in my ability to persevere, be it the best or the worst of times.

This thesis is dedicated to my father, Mr. David William Turner, who battled to hold on longer but sadly died from cancer in August of 2010. He was, and always will be, my moral compass and overwhelming motivation to contribute to the fields of engineering and medicine.

Table of Contents

List of Figures

List of Tables

List of Major Abbreviations

2-D	Two-dimensional	LN	Laminin
3-D	Three-dimensional	LPL	Lipoprotein lipase
ADD-1	Adipocyte determination- and differentiation-dependent factor-1	MSC	Mesenchymal stem cell
		PAI-1	Plasminogen activator inhibitor-1
ASC	Adipose-derived stem cell	PBS	Phosphate buffered saline
ATP	Adenosine triphosphate	PGA	Poly(glycolic acid)
BAT	Brown adipose tissue	PLA	Poly(lactic acid)
BM	Basement membrane	PLGA	Poly(lactic-co-glycolic acid)
BMI	Body mass index	PMSF	Phenylmethylsulfonyl-fluoride
BSA	Bovine serum albumin		
C/EBP	CCAAT/enhancer binding protein	PPAR	Peroxisome proliferator-activated receptor
CI	Collagen type I	PTFE	Poly(tetrafluoroethylene)
CIV	Collagen type IV	RB	Rose bengal
DAT	Decellularized adipose tissue	RGD	Argenine, glycine, aspartic acid
DMEM	Dulbecco's Modified Eagle's Medium	Rib	Riboflavin
		RXR	Retinoid X receptor
DNA	Deoxyribonucleic acid	SEM	Scanning electron microscopy
ECM	Extracellular matrix		
FBS	Fetal bovine serum	SREBP-1c	Sterol regulatory element-binding protein-1c
FITC	Fluorescein 5(6)-isothiocyanate	STAT	Signal transducers and activators of transcription
GPDH	Glycerol-3-phosphate dehydrogenase	SVF	Stromal vascular fraction
GTA	Glutaraldehyde	TCPS	Tissue culture poly(styrene)
IBMX	Isobutylmethylxanthine	TNF-α	Tumor necrosis factor-α
IL	Interleukin	WAT	White adipose tissue

Chapter 1
Introduction

1.1 Clinical Motivation

Tumor resections, trauma and burns, changes with age, and congenital abnormalities can result in soft tissue defects or voids within the dermis and underlying subcutaneous layer of fat, impairing function and appearance [1]. Such defects are primarily due to the loss of adipose tissue, or fat, which has an extremely limited capacity for self-repair [1, 2]. According to the American Society of Plastic Surgery, approximately 5.2 million reconstructive surgeries were performed in 2009, 3.9 million of which were attributed to tumor removal [3]. Additionally, almost 12.5 million cosmetic procedures employing a range of synthetic and/or naturally-derived filler materials were reported in 2009, representing a 69% increase compared to the year 2000 [3].

The need for treatment of soft tissue defects remains an unresolved problem in reconstructive and plastic surgery [4]. To date, clinical approaches have demonstrated little success in achieving long-term volume restoration [5]. The available methods rely largely on synthetic implants or injectables, or the transfer of free fat and pedicled flaps, in which autologous tissue is transplanted from a donor site and relocated to fill a defect [6-8]. However, synthetic materials consistently induce a foreign body response and are subject to implant migration and poor integration within the surrounding host tissues [1, 9]. Many available naturally-derived materials shrink extensively and unpredictably *in vivo,* and depending on sourcing, may pose disease transmission concerns [4, 10]. Despite the superior biocompatibility of autologous tissues, long-term success of adipose tissue grafting has been limited to date, resulting in donor site defects and demonstrating significant graft resorption, with replacement by fibrous tissue and oil cysts due to insufficient vascularization [10, 11]. The development of a minimally-invasive product capable of restoring function and appearance to damaged

subcutaneous tissues, while inducing a minimal immune response, would greatly enhance clinical outcomes in reconstructive and cosmetic procedures [6].

1.2 Thesis Overview

Tissue engineering holds exciting promise for the regeneration of functional living tissues [12]. To date, many strategies point to the potential of cell-seeded scaffolds, or support structures intended to mimic the native extracellular matrix (ECM), to contribute to the regenerative response [6, 7, 9, 13]. In particular, scaffolds derived from decellularized adipose tissue (DAT) have been shown to provide a microenvironment inductive of adipogenesis, without the need for exogenous differentiation factors [14]. This work highlights the critical role of the ECM in mediating the cellular response, and suggests that tissue-specific bioscaffolds, engineered to mimic the extracellular environment of the cells of interest, may be an effective strategy for promoting more normal cellular behavior. However, to date, no methodology has been developed which incorporates the composition of a fully decellularized tissue in combination with a tailored scaffold microgeometry, more specifically, in the form of spherical engineered microcarriers. As DAT provides a highly purified form of the adipose matrix [14], the fabrication of DAT-based microcarriers could provide an adipogenic scaffold approximating the native matrix in composition, while ensuring the removal of most antigenic components.

This thesis encompasses the development and characterization of novel porous microcarriers fabricated from DAT, intended for use in adipose-derived stem cell (ASC) culture and incorporation within adipose tissue-engineering strategies. Initial work focused on designing and assembling a sterile microdroplet fabrication system, and developing DAT solubilization protocols to permit the production of DAT/alginate composite microspheres. Prior to extracting the alginate phase, non-cytotoxic crosslinking methods were explored to stabilize the DAT phase within the microcarriers. The microcarrier formulations produced were characterized in terms of

architecture, stability and swelling behavior, particle size and porosity, sterility, and injectability. Finally, studies on the *in vitro* ASC proliferative and adipogenic responses were assessed in a three-dimensional (3-D) dynamic spinner culture system.

1.3 Research Hypothesis and Objectives

This research tested the hypothesis that porous DAT-based microcarriers fabricated via non-cytotoxic protocols could facilitate the attachment, proliferation and adipogenic differentiation of seeded human ASCs.

The specific objectives of this project were to:

i. Develop and optimize a protocol for the solubilization of decellularized adipose tissue

- Establish a reproducible method to yield DAT solutions with a controlled total protein content.

ii. Develop and optimize methods for the production of porous DAT-based microcarriers

- Design and assemble an air-jet droplet apparatus for the fabrication of sterile spherical droplets of controlled diameter.
- Develop methods for the production of sterile, composite DAT/alginate microcarriers.
- Establish protocols for the effective stabilization of DAT within the microcarriers, via non-cytotoxic photochemical crosslinking methods, prior to extracting the alginate to yield a porous microstructure.
- Using similar methods, produce a gelatin-based microcarrier model for use as a control during *in vitro* culturing experiments.

iii. Characterize the DAT-based microcarriers

- Evaluate the microcarriers and confirm alginate extraction by scanning electron microscopy (SEM), optical microscopy, and fluorescence microscopy.
- Characterize the microcarrier percent porosity via liquid displacement.

- Characterize the microcarrier stability and swelling behavior in a simulated physiological environment.
- Assess microcarrier sterility and injectability.

iv. Evaluate the potential for DAT-based microcarriers to support adipose-derived stem cell proliferation and adipogenic differentiation during *in vitro* culturing experiments

- Develop preliminary seeding protocols and culturing techniques for ASCs on DAT-based microcarriers in a dynamic spinner culture system.
- Confirm cell attachment and proliferation by total deoxyribonucleic acid (DNA) quantification and microscopic imaging of fluorescently-labeled ASCs.
- Characterize the *in vitro* adipogenic response by assessing intracellular lipid accumulation and glycerol-3-phosphate dehydrogenase (GPDH) activity.

Chapter 2
Literature Review

2.1 Physiology of Adipose Tissue

To develop a successful adipose tissue-engineering strategy, it is critical that the complex physiology of native adipose tissue be understood. Adipose tissue, commonly denoted as fat, is a highly-specialized, dynamic, and multifunctional connective tissue, distributed ubiquitously throughout the human body [1, 15]. Principally functioning to achieve the body's energy balance, adipose tissue also maintains body contours, provides thermal and mechanical insulation to surrounding tissues, and produces a myriad of autocrine, paracrine, and endocrine factors [16]. As a result, adipose tissue is classified as an endocrine organ, with functions extending far beyond simply supporting the energy requirements of other tissues [16, 17]. In lean mature humans, the adipose organ accounts for 9-18% of body mass in males and 14-28% in females [18]. Males tend to accumulate adipose tissue in the central or abdominal regions of the body, whereas females distribute fat throughout the gluteofemoral or peripheral adipose depots [19].

In vivo, specialized terminally-differentiated cells termed adipocytes are organized in combination with other cells, cytokines, growth factors, and the extracellular matrix (ECM), to form the different types of adipose tissue [9]. More specifically, depending on the cellular morphology and tissue function, adipose tissue may be classified as white or brown [15]. Each type and depot is extensively innervated and vascularized, and the blood supply is essential for the delivery and removal of metabolic substrates and products, respectively [20, 21].

2.1.1 White Adipose Tissue

White adipose tissue (WAT) forms the subcutaneous layer between the muscle and the dermis, as well as the intra-abdominal and visceral depots surrounding the heart, kidneys, and other internal organs [18]. WAT is also localized throughout skeletal muscle, at periarticular

regions, and within the marrow [7]. Although less densely vascularized than brown adipose tissue, each cell in WAT contacts at least one capillary [6].

From a cellular perspective, WAT is comprised mainly of unilocular white adipocytes, which accumulate and store intracellular lipids in the form of triacylglycerols during periods of positive energy balance, and distribute fatty acids when metabolic energy requirements exceed intake, as mediated by paracrine and endocrine factors [17]. White adipocytes are spherical in morphology, and possess an acentric rod-like flattened nucleus and thin elongated mitochondria, adjacent to a single large lipid-filled vacuole [22]. Approximately 90% of the cell volume of a mature white adipocyte is comprised of intracellular lipid, giving rise to the macroscopic white/yellow color of WAT [15, 22]. Given the unique ability for mature white adipocytes to significantly lipid-load, WAT is the only tissue in humans capable of extensively increasing in mass, once fully differentiated [18].

2.1.2 Brown Adipose Tissue

In humans, brown adipose tissue (BAT) is present in significant collections only during the neonatal period, where it functions to generate heat to help adapt to changes in the body temperature [7]. The brownish appearance of BAT is attributed to its greater vascular density, as well as the structurally- and functionally-distinct brown adipocytes, which are rich in mitochondrial cytochromes [20, 23]. Morphologically, brown adipocytes are considerably smaller than white adipocytes, with a central rounded nucleus and a multilocular distribution of many small intracellular lipid droplets [22]. Brown adipocytes also contain larger, more numerous specialized mitochondria that express uncoupling protein-1 (UCP-1), which allows for the uncoupling of oxidative phosphorylation to generate heat rather than adenosine triphosphate (ATP), without the need to perform mechanical work [24]. Overall, through the breakdown of intracellular lipids, BAT functions to generate heat via non-shivering thermogenesis [23].

At birth, BAT is distributed throughout the body [7]. However, as the body ages, BAT is replaced by WAT, with BAT largely undetectable in mature adults [25]. Adipose tissue biopsies from normal human adults contain only one brown adipocyte for every 100-200 white adipocytes [22]. As WAT is the predominant form of adipose tissue in mature humans, most adipose tissue-engineering strategies focus on WAT and its repair and/or regeneration [7].

2.1.3 Cellular Components

Terminally-differentiated lipid-filled adipocytes form the bulk mass of WAT, based on their significantly larger size as compared to the other resident cells of adipose tissue, including fibroblasts, endothelial cells, macrophages, mast cells, and the heterogeneous population of adipose-derived stem cells (ASCs), sometimes also referred to in the literature as preadipocytes, adipose stromal cells, adipose precursor cells (APCs), or processed lipoaspirate (PLA) cells [26-28]. Additionally, blood and nerve cells are present in the extensive vascularization and innervation of adipose tissue [29, 30]. Depending on the type, depot, and anatomical location of the adipose tissue, the cellular composition and stem cell fraction may vary significantly [22, 31].

2.2 Adipose-Derived Stem Cells

Adipose-derived stem cells (ASCs) are readily isolated from the stromal vascular fraction (SVF) of adipose tissue, and form a collective population of highly proliferative cells including mesenchymal stem cells (MSCs), and the more-committed adipose progenitor cells, adipoblasts (determined) and preadipocytes (committed) [30]. Therefore, adipose tissue is widely recognized as an abundant source of multipotent stem cells [13, 32, 33]. Freshly excised adipose tissue from surgical reductions or biopsy procedures, as well as lipoaspirate material, may be processed via enzymatic digestion, filtration, and centrifugation isolation steps to yield high numbers of ASCs [32]. While human bone marrow-derived MSCs (hBMSCs) have shown promise, ASCs are significantly more abundant, with the SVF of adipose tissue containing between 1.2-5.1% ASCs,

as compared to the frequency of MSCs in the bone marrow, which is commonly in the range of 0.001%–0.01% [31]. Furthermore, ASCs may be procured through less surgically-invasive techniques than hBMSCs, from readily available and otherwise discarded tissues [34].

Depending on the culturing environment, ASCs can be induced to differentiate along the adipogenic, angiogenic, chondrogenic, osteogenic, myogenic, and putative neuronal lineages, under the influence of various hormones, growth factors, and cell-cell and/or cell-matrix interactions [32, 35-37]. ASCs also demonstrate significant plasticity, meaning that more-committed ASCs and mature adipocytes can dedifferentiate, and in turn either redifferentiate along the adipogenic lineage, or toward an alternative mesenchymal lineage [27].

2.2.1 Adipose-Derived Stem Cell Markers

Human ASCs (hASCs) display similar immunophenotypic surface marker profiles to hBMSCs and skeletal muscle-derived cells, although variations in cell sources and culture methods have resulted in some differences in expression patterns between studies reported in the literature [33]. Both hASCs and hBMSCs express the adhesion molecules CD9 (tetraspanin), CD29 (β-1 integrin), CD54, CD105 (endoglin), and CD166 (activated lymphocyte cell adhesion molecule) [15]. hASCs and hBMSCs also share the expression of the receptor molecules CD44 (hyaluronate) and CD71 (transferrin), the surface aminopeptidases CD10 and CD13, specific extracellular matrix proteins including collagens, CD90 (Thy-1), the intracellular proteins α-smooth muscle actin and vimentin, and the complement regulatory proteins CD55 (decay accelerating factor) and CD59 (complement protectin) [15, 33]. While hASCs and hBMSCs have demonstrated positive expression of the Class I major histocompatibility complex (MHC) protein HLA-ABC, neither have been shown to express the Class I protein HLA-DR or MHC Class II markers [15]. Additionally, neither cell population expresses the hematopoietic cell markers

CD14 and CD45, nor do they express CD18 (β-2 integrin), CD50, or CD62 (endothelial-selectin) [15].

However, as discussed, while this profile is generally consistent, it is by no means comprehensive. To date, discrepancies remain in the characterization of the hASC phenotype, specifically in the detection of CD34, Stro-1, and CD106 [32]. As ASC behavior is significantly impacted by culturing conditions, such discrepancies could be attributed to inconsistencies between cell isolation and/or culturing methods, in addition to differences in sensitivity between detection methods employed [32]. Overall, hASCs demonstrate a phenotype similar to hBMSCs and skeletal muscle cells, with direct immunophenotypic comparisons between hASCs and hBMSCs as high as 90% identical [33].

The phenotypic characterization of hASCs as a function of cell passage has also been conducted [33]. Early passage hASCs have been shown to express CD90, CD34, ATP-binding cassette subfamily G member 2 (ABCG2), and aldehyde dehydrogenase (ALDH) [38]. Preadipocyte factor-1 (Pref-1) and the multilineage marker Stro-1 are also expressed by undifferentiated hASCs [38]. Additionally, there are cells in early passages that are positive for endothelial markers, including vascular endothelial growth factor receptor (Flk-1), CD31 (platelet endothelial cell adhesion molecule-1; PECAM-1), CD144 (vascular endothelial-cadherin), and von Willebrand factor (vWF) [38]. As a result, the expression of these early passage markers by techniques such as flow cytometry during cell characterization is one method to assess the differentiation state of cultured hASCs [33].

2.3 Adipogenesis

Adipose tissue expansion involves both cellular hypertrophy and hyperplasia [17, 18]. Hypertrophy refers to the increase in size of existing adipocytes as they accumulate

triacylglycerol intracellularly [18]. Hyperplasia refers to the increase in adipocyte number through the proliferation and adipogenic differentiation of ASCs into new mature adipocytes [18]. Adipocytes cannot expand in volume indefinitely, and when their maximum physical cell size is reached due to lipid uptake, ASCs are signaled to differentiate into mature adipocytes and commence intracellular lipid accumulation [36]. During positive energy balance, both adipocyte hypertrophy and hyperplasia occur in a cyclical fashion, with adipocyte hypertrophy preceding hyperplasia [17].

Proliferation refers to the replication or expansion of the ASC population, while adipogenic differentiation denotes the transformation of ASCs into lipid-filled adipocytes [39]. Before differentiating, ASCs must reach an initial state of growth arrest to trigger the development of adipoblasts into more-committed preadipocytes, which may also undergo additional rounds of cell division or mitotic clonal expansion, once committed to the adipogenic lineage [36, 39]. A second state of growth arrest is reached as terminal adipogenic differentiation ensues [39]. During this phase, synthesis of adipocyte-secreted products begins, and intracellular lipid droplets form and coalesce over time to yield unilocular mature adipocytes [39]. Adipogenic differentiation is characterized by a transcriptional cascade of regulatory factors responsible for inducing the expression of adipogenic genes [40]. Overall, adipogenesis is a complex regulatory process controlled by the temporal up- or down-regulation of hundreds of genes during adipogenic differentiation [18].

2.3.1 Transcriptional Regulation of Adipogenesis

The principal transcriptional regulators of adipogenesis are peroxisome proliferator-activated receptor γ (PPARγ), members of the CCAAT/enhancer binding protein (C/EBP) family, and the adipocyte determination- and differentiation-dependent factor-1/sterol regulatory element-binding protein-1c (ADD-1/SREBP-1c) [41, 42]. Overall, expression of C/EBPβ and

C/EBPδ leads to the activation and the expression of PPARγ and C/EBPα, which regulate the expression of many genes characteristic of the adipocyte phenotype, including lipoprotein lipase (LPL), glucose transporter type-4 (Glut-4), adipocyte-specific fatty acid binding protein 2 (aP2), fatty acid synthase (FAS), acetyl CoA carboxylase, malic enzyme, insulin receptor, and glycerol-3-phosphate dehydrogenase (GPDH) [42]. Specifically, the activation of PPARγ is thought to mark the end of post-mitotic arrest, after which C/EBPα and PPARγ in turn feed back to induce their own expression [17]. Upon reaching the second growth arrest period, the expression of the fully-differentiated adipogenic phenotype occurs (Figure 2.1).

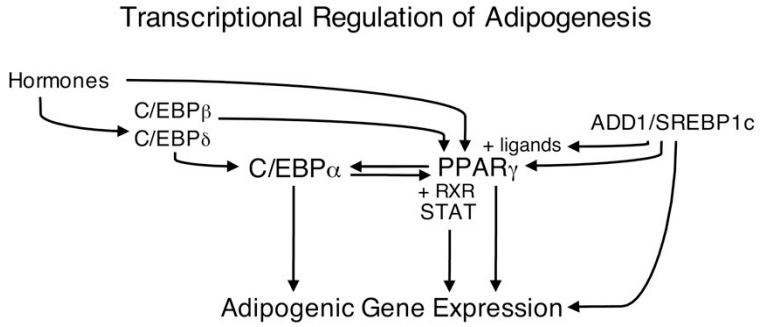

Figure 2.1: Generalized transcriptional cascade for the adipogenic differentiation of ASCs.

2.3.1.1 PPARγ

The transcription factor PPARγ belongs to the ligand-regulated PPAR subgroup of the nuclear receptor superfamily [41, 42]. In humans, the identification of PPARγ was preceded by the discovery of PPARα and PPARδ (also referred to as PPARβ) [41]. While the three PPAR isoforms share similar amino acid sequencing of their DNA- and ligand-binding domains, all serve different roles *in vivo* [41] and have affinities for different ligands and peroxisome proliferator response elements (PPREs), which are specific DNA regions on target genes that bind PPAR factors [41]. Of the three PPAR isoforms, PPARγ is most highly expressed in adipose tissue, while demonstrating little to no expression in other tissues [41]. Furthermore, the gene

encoding PPARγ has two specific promoter regions that produce different isoforms, denoted PPARγ1 and PPARγ2 [37, 43], with PPARγ2 expressed exclusively in adipose tissue [41]. During cell culture, PPARγ appears to be required for ASC adipogenic differentiation [44]. Therefore, PPARγ has been denoted as one of the master regulators of adipogenesis, while PPARα and PPARδ play more secondary roles [43].

To be transcriptionally activated, PPARγ must heterodimerize with the retinoid X receptor α (RXRα) before binding to PPREs and initiating RNA synthesis [41]. More specifically, PPARγ must be activated through binding ligands to its carboxyl-terminated ligand-binding domain [36]. Endogenous PPARγ ligands discovered to date include prostaglandins and polyunsaturated fatty acids [36, 41]. *In vitro*, the activation of PPARγ can be achieved through cell exposure to synthetic ligand compounds called thiazolidinediones (TZDs) such as troglitazone and rosiglitazone, which enhance insulin sensitivity [42].

2.3.1.2 C/EBP Family

The C/EBP family belongs to the basic-leucine zipper (bZIP) class of transcription factors [36]. The basic region permits the binding of DNA, while the leucine zipper enables C/EBPs to form homodimers or heterodimers with other proteins in this family [36, 41]. Adipogenic differentiation implicates three isoforms of the C/EBP family of transcription factors, specifically C/EBPα, C/EBPβ, and C/EBPδ [41]. *In vivo*, the distribution of C/EBPs is not limited to adipose tissue [36]. During adipogenesis, C/EBPα plays a critical role in the activation of adipogenic differentiation [44]. C/EBPα is also thought to aid in maintaining adipocytes in their differentiated form [41].

2.3.1.3 ADD-1/SREBP-1c

ADD-1/SREBP-1c is another key transcription factor involved in adipogenic differentiation and lipid metabolism [39], and is a member of the basic helix-loop-helix (bHLH) family of transcription factors [42]. During adipogenesis, expression of the gene encoding ADD-1/SREBP-1c is up-regulated [45]. In fact, ADD-1/SREBP-1 has been proposed as a modulator of the activation of PPARγ through interactions with the PPARγ2 promoter, thereby inducing gene expression of PPARγ [36]. ADD-1/SREBP-1c is also known to stimulate the expression of many genes required for lipogenesis, such as LPL and FAS [42].

2.3.1.4 Other Transcriptional Mediators of Adipogenesis

In addition to PPARγ, the C/EBP family members, and ADD-1/SREBP-1c, several other factors can act to modulate adipogenesis [39, 43]. Specifically, the expression of the GATA-binding transcription factors GATA-2 and GATA-3 has been shown to inhibit adipogenic differentiation of adipose precursor cells through suppressing the activity of the PPARγ2 promoter and/or by reducing the activity of C/EBPβ and C/EBPδ [39]. Conversely, the expression of the cyclic adenosine monophosphate (cAMP) response element binding protein (CREB) is thought to be a critical initiator of adipogenesis [39]. The expression of members of the signal transducers and activators of transcription (STAT) family, STAT1, STAT5A, and STAT5B, also occurs downstream of PPARγ in a ligand-dependent manner [46].

2.3.2 Inhibitors of Adipogenesis

Other signaling molecules have been identified as potent inhibitors of adipogenic differentiation. Cytokines including tumor necrosis factor-α (TNF-α) and interleukin-1 (IL-1) suppress ASC adipogenic differentiation *in vitro*, as do the growth factors platelet-derived growth factor (PDGF), fibroblast growth factor (FGF), epidermal growth factor (EGF), and transforming

growth factors- α and β (TGF-α and TGF-β) [36], which generally promote proliferation. Pref-1 is a transmembrane molecule that inhibits adipogenic differentiation and must be down-regulated for adipogenesis to proceed [39].

Wnt and Hedgehog (Hh) signaling have also been shown to inhibit adipogenesis. More specifically, the canonical, or Wnt/β-catenin signaling pathway has been shown to maintain the undifferentiated state of ASCs through blocking the activation of C/EBPα and PPARγ [47]. Interestingly, while inhibiting adipogenesis, the up-regulation of the Wnt/β-catenin signaling pathway promotes osteogenic and chondrogenic differentiation in mesenchymal progenitors, pointing to Wnt signaling as a selective switch modulating the differentiative response [48]. Hh signaling has been shown to reduce intracellular lipid accumulation and decrease expression of adipocyte-specific genes, presumably through interfering with the function of C/EBPα and PPARγ [7]. Overall, inhibition of specific elements from the Wnt and Hh signaling pathways are required for adipogenesis [7].

2.3.3 *In Vitro* Adipogenic Factors

Culturing studies have led to the establishment of protocols for the induction of ASC differentiation *in vitro*. During proliferation, ASCs are typically provided with fetal bovine serum (FBS), which contains several of the adipogenic inhibitors previously outlined [9]. By supplying ASCs with a serum-free differentiation cocktail incorporating a variety of growth factors, hormones, and cytokines known to target adipogenic pathways, at physiological concentrations or higher [9], ASCs may be successfully induced to differentiate into lipid-loading adipocytes. Specifically, adipogenic cocktails are commonly supplemented with insulin, triiodothyronine (T3), and glucocorticoids (hydrocortisone or dexamethasone) [9]. Additionally, biotin, pantothenate, isobutylmethylxanthine (IBMX) (a phosphodiesterase inhibitor that prevents cAMP

degradation), and TZDs (troglitazone and rosiglitazone) have shown positive results when included in adipogenic medium formulations [9].

2.3.4 Vascularization of Adipose Tissue During Adipogenesis

Extensive vasculature is necessary to support the expansion of adipose tissue through hypertrophy or hyperplasia [27]. Therefore, adipogenesis is tightly associated with angiogenesis, during which the parallel ingrowth of capillaries occurs [26]. Newly-formed primitive capillary networks are thin and tenuous, with oxygen and nutrient transport to the resident cells limited to a distance of 150 μm from each capillary [8]. Therefore, each cell must be in close proximity to at least one or more capillaries [27]. This renders continuous remodeling and/or expansion of the existing vasculature necessary to permit tissue growth and survival [6]. More specifically, vascular homeostasis is achieved through the dilation and remodeling of existing capillaries during hypertrophy, or neovascularization during hyperplasia [26], as modulated by a wide range of angiogenic factors secreted by WAT (Table 2.1) [27].

Table 2.1: Angiogenic factors produced in adipose tissue [27].

Pro-Angiogenic Factors	- Vascular Endothelial Growth Factors (VEGF-A, VEGF-B, VEGF-C) - Hepatocyte Growth Factor (HGF) - Fibroblast Growth Factor-2 (FGF-2) - Secreted Protein Acidic and Rich in Cysteine (SPARC)/osteonectin - Angiopoietins (Ang-1, Ang-2) - Leptin - Platelet-Derived Growth Factor-β (PDGF-β) - Transforming Growth Factor-β (TGF-β) - Tumor Necrosis Factor-α (TNF-α) - Tissue Factor (TF) - Matrix Metalloproteinases (MMP-2, MMP-9)
Anti-Angiogenic Factors	- Adiponectin - Thrombospondins (TSP-1, TSP-2) - The "A Disintegrin And Metalloproteinase" Family (ADAMTS-1, ADAMTS-8)

The primary pro-angiogenic growth factors produced by adipose tissue are vascular endothelial growth factor-A (VEGF-A) and hepatocyte growth factor (HGF) [26, 27]. Both

adipocytes and ASCs contribute to VEGF production [26]. Key anti-angiogenic factors produced by adipose tissue to maintain homeostasis include adiponectin, thrombospondins (TSPs), and members of the "A Disintegrin And Metalloproteinase (ADAM)" family containing a thrombospondin motif (ADAMSP) [26]. Overall, the modulation of angiogenesis and neovascularization in adipose tissue is achieved through the tightly regulated balance of pro- and anti-angiogenic factors [49]. Significant research is required to elucidate the complex interactions that mediate angiogenesis during adipogenesis, and the ability to achieve adequate vascularization is critical for the long-term success of adipose tissue-engineered constructs [27, 50].

2.4 Adipose Tissue Metabolism

In vivo, WAT provides a buffer for metabolic energy imbalance [51]. The synthesis (lipogenesis) and hydrolysis (lipolysis) of triacylglycerols occurs simultaneously *in vivo*, and whether there is an accumulation or loss of lipid depends on the relative rates of lipogenesis and lipolysis [52]. The pathways controlling lipogenesis and lipolysis are tightly regulated, with insulin and glucocorticoids acting as promoters of lipogenesis, and glucagon and the catecholamines largely supporting lipolysis [53].

2.4.1 Lipogenesis

Most plasma triacylglycerols are acquired through dietary intake, and are either secreted from the small intestine in chylomicrons (large lipoprotein particles), or from the liver bound to lipoproteins [16]. Triacylglycerol is composed of fatty acids esterified with glycerol-3-phosphate [52]. Fatty acids may be synthesized within adipocytes and the liver via *de novo* lipogenesis, facilitated by FAS and acetyl CoA carboxylase, or they may be acquired from plasma carriers as albumin-bound fatty acids or from lipoprotein-bound triacylglycerols [54]. Prior to uptake by white adipocytes, triacylglycerols must be hydrolyzed to release the fatty acids within adjacent capillaries by the enzyme LPL [54]. Transport proteins including CD36, Fatty Acid Transport

Protein (FATP), and aP2 then mediate the transfer of fatty acids across the adipocyte membrane [54].

Glycerol-3-phosphate is derived from the glycolysis and glycerogenesis of glucose [52]. Glucose uptake by adipocytes is modulated by insulin, and is facilitated by membrane glucose transporters (Glut), particularly the insulin-sensitive Glut-4 transporter [54]. Ultimately, glycerol-3-phosphate is esterified with fatty acids by acyltransferase enzymes within the adipocyte cytoplasm to yield intracellularly-stored triacylglycerol [54].

2.4.2 Lipolysis

Mature adipocytes are uniquely equipped to mobilize their lipid reserves to meet metabolic energy needs, possessing the enzymes and regulatory proteins required for not only lipogenesis, but also lipolysis [39]. During lipolysis, triacylglycerol is sequentially hydrolyzed intracellularly into diacylglycerol, monoacylglycerol, and glycerol, thereby releasing one fatty acid chain upon each hydrolysis step [51]. To date, three enzymes have been indicated in the breakdown of triacylglycerol stored within white adipocytes, which are adipose triglyceride lipase (ATGL), hormone-sensitive lipase (HSL), and monoglyceride lipase (MGL) [51]. ATGL is now accepted as the major triacylglycerol lipase, whereas HSL has been designated a diacylglycerol lipase [51]. Lipase-liberated fatty acids are transported out of the cell and subsequently distributed to tissues that require energy, or reincorporated into adipocytes [54]. Activation of lipases is tightly regulated during lipolytic activities at the post-transcriptional level, through reversible lipase phosphorylation and/or co-activator binding [51]. Perilipin A, an abundant structural protein that is found within the intracellular lipid of white adipocytes, appears to play a critical role in mediating the activation and activity of lipases during lipolysis [51].

2.5 Adipose Tissue as an Endocrine Organ

The ability of adipose tissue to synthesize and release important regulatory molecules defines its function as an endocrine organ [55]. Quantitatively, fatty acids are the major secretory product of adipose tissue, with WAT also involved in storing cholesterol and the metabolism of steroid hormones [16]. To date it is estimated that hundreds of synthesized peptide hormones and endocrine factors are also secreted from the resident cells of adipose tissue [56]. Some of these factors play a role in glucose or lipid metabolism and appetite regulation, while others are inflammatory cytokines or are involved in the immune response, vascular homeostasis, or the complement system [16]. ASCs secrete factors involved in their own differentiation, while mature adipocytes secrete factors to communicate with the brain, liver, and skeletal muscle, as well as with nearby ASCs, endothelial cells, and macrophages [56]. Therefore, adipose tissue represents the largest endocrine gland in the body [49]. The major adipose tissue secretory products are listed in Figure 2.2.

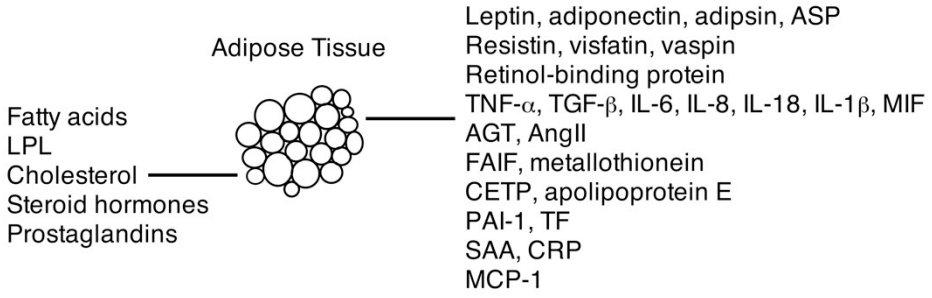

Figure 2.2: Major secreted factors from human WAT [16, 56, 57]
AGT, angiotensinogen; AngII, angiotensin II; ASP, acylation-stimulating protein; CETP, cholesterol ester transfer protein; CRP, C-reactive protein; FAIF, fasting-induced adipose factor; IL, interleukin; LPL, lipoprotein lipase; MCP-1, monocyte chemoattractant protein-1; MIF, macrophage inhibitory factor; PAI-1, plasminogen activator inhibitor-1; TF, tissue factor; SAA, serum amyloid A; TGFβ, transforming growth factor-β; TNFα, tumor necrosis factor-α.

Factors released from WAT include the cytokines (often termed adipokines) leptin and adiponectin, and other factors such as interleukins, angiotensinogen, and prostaglandins [39], and the effects may be autocrine or paracrine, or may occur in distant locations [16].

2.5.1.1 Leptin

Leptin, the first adipokine discovered, is a cytokine-like polypeptide encoded by the obese (*ob*) gene [16, 55-57]. *In vivo*, leptin is expressed and secreted predominantly by mature adipocytes in direct proportion to adipose tissue mass [55], effectively signaling the size of the available energy store to the hypothalamus in the brain [57]. As a result, this satiety hormone plays a critical role in energy homeostasis and body weight regulation [57]. Leptin receptor activation acts to suppress the urge for dietary intake, and promotes energy expenditure pathways [19].

Leptin expression and secretion is up-regulated by insulin, glucocorticoids, TNF-α, IL-1, estrogens, and C/EBPα, and down-regulated by factors including catecholamines, androgens, free fatty acids, and PPARγ agonists [52, 55]. During caloric restriction and weight loss, leptin levels significantly decrease [55]. Leptin deficiencies result in severe obesity with overeating that persists, despite elevated insulin levels [19]. However, common obesity is characterized by elevated leptin concentration, often coupled with leptin resistance [55, 56]. Additionally, leptin has several peripheral endocrine effects including the regulation of immune function, hematopoiesis, angiogenesis, reproduction, and bone development, supporting the importance of adipocyte-generated leptin throughout the body [52, 55]. Although primarily secreted from adipocytes, leptin is also expressed and secreted by the stomach, skeletal muscle, and the placenta [58].

2.5.1.2 Tumor Necrosis Factor-α

TNF-α is a transmembrane protein expressed and secreted from WAT that functions as a cytokine implicated in insulin resistance and obesity [55]. In particular, the expression of TNF-α is positively correlated with obesity and insulin resistance, and is associated with impaired insulin signaling, reduced LPL activity, as well as lower Glut-4 protein expression in adipocytes [19, 52]. TNF-α also represses the transcription of genes involved in adipogenesis and lipogenesis, and may increase leptin secretion to help attenuate appetite during positive energy balance [52, 55].

2.5.1.3 Plasminogen Activator Inhibitor-1

Plasminogen activator inhibitor-1 (PAI-1) is a pro-inflammatory thrombosis-associated cytokine secreted by many cell types within WAT, with expression levels greater in visceral depots, relative to subcutaneous adipose tissue [55]. Plasma PAI-1 levels are positively correlated with obesity, insulin resistance, and features of cardiovascular disease, with PAI-1 concentration being highly associated with visceral adiposity [55]. The most potent stimulator of PAI-1 expression in adipose tissue is paracrine- and autocrine-secreted TGF-β [57]. TNF-α also contributes to the elevated PAI-1 levels observed during obesity and insulin resistance [55]. Overall weight loss results in a significant reduction in PAI-1 expression and secretion [55].

2.5.1.4 Adiponectin

Adiponectin (apM1, Acrp30, adipoQ, or GBP28) is a polypeptide expressed specifically by adipocytes, with expression levels characteristically higher in subcutaneous as compared to visceral adipose tissue depots [55, 56]. Contrary to many other adipokines, adiponectin expression levels decrease with obesity, and are negatively correlated with insulin resistance [57]. Adiponectin works to lower hepatic glucose production and increases glucose uptake and fatty acid oxidation in skeletal muscle [56]. Adiponectin has also been identified as an anti-inflammatory and vasculo-protective factor [19]. Loss of adipose tissue results in increased

adiponectin secretion from WAT, with low adiponectin levels being linked not only to obesity and insulin resistance, but also to atherosclerosis [16, 19]. TNF-α and interleukin-6 (IL-6) expression during obesity leads to a decrease in adiponectin production [27].

2.5.1.5 Interleukin-6

IL-6 is another cytokine released from adipose tissue involved in the regulation of many metabolic and endocrine systems [55]. Expression levels are positively correlated with obesity, impaired glucose tolerance, and insulin resistance [57], with greater secretion of IL-6 in visceral as compared to subcutaneous adipose tissue [19]. Both expression and circulating IL-6 levels decrease with fat loss [55]. IL-6 inhibits adipogenesis and decreases adiponectin levels [55].

2.6 Adipose Tissue Extracellular Matrix

The development of a successful tissue-engineering strategy requires an understanding of how resident cells form, maintain, and repair their respective tissues. In general, the ECM is a complex mixture of structural and functional proteins, glycoproteins, and proteoglycans [59]. More specifically, the ECM is secreted by endogenous matrix-producing cells, and arranged with a tissue-specific organization and compositional architecture, to give rise to the overall three-dimensional (3-D) tissue ultrastructure enriched with cellular components and a variety of growth factors, cytokines, ions, and water [60]. Therefore, the ECM is a multifunctional natural scaffold that not only imparts structural integrity to the tissues, but also modulates a wide range of cellular behaviors, including cell morphology, adhesion, migration, proliferation, and differentiation [61]. Moreover, the ECM is dynamic and subject to constant remodeling, for instance during hypertrophic expansion and adipogenesis [59]. Cell responses to the ECM are mediated by specific cell-surface receptors, which interact with different active sites on the components of the

ECM [62]. The ECM also modulates inflammatory and immune responses, particularly during wound healing [60].

Adipose tissue has an ECM enriched in the fibrillar protein collagen type I, secreted by both mature adipocytes as well as the SVF, including ASCs and more-committed adipose progenitor cells [59]. Additionally, each adipocyte is surrounded by a thin basement membrane (BM), rich in collagen type IV and laminin [59]. The unique capacity of adipocytes to significantly increase in volume during intracellular uptake renders them fragile and easily ruptured due to mechanical stresses [59]. The specialized basal lamina of adipose tissue is thought to promote cell survival through dissipating the mechanical stress experienced by lipid-filled adipocytes over a larger tissue area, such that the fibrillar collagen is the primary load bearing material [59]. The adipose ECM is also comprised of collagen types III, V, and VI, fibronectin, and nidogen (entactin), and other components (Table 2.2) [59, 63].

Table 2.2: Core proteins found in the extracellular matrix of mature adipose tissue [59].

- Perlecan (heparan sulfate proteoglycan)	- Mimecan (osteoglycin)
- Calreticulin	- Nidogen 1 (entactin)
- Collagen types I, III, IV, VI	- Nidogen 2 (osteonidogen)
- Collagen types XII, XIV, XV, XVIII	- Periostin
- Dermatopontin	- Proteoglycan 4
- Elastin	- SPARC (osteonectin)
- Fibronectin	- Spondin-1 (vascular smooth muscle cell growth-promoting factor)
- Fibulin	
- Galectin	- Spondin-2 (mindin)
- Laminin	- Tenascin-C, Tenascin-X
- Lumican (keratan sulfate proteoglycan)	- Thrombospondin-1, Thrombospondin-2
- Matrilin	- Versican core protein (fibroblast proteoglycan)
- Microfibril-associated glycoprotein 4	

2.6.1 Collagen Type I

Collagen type I (CI) is the most prevalent ECM component within adipose tissue [59]. As is the case for all collagens (of which more than 20 have been identified), CI forms a right-handed triple helix comprised of three α-chains (Figure 2.3) [64].

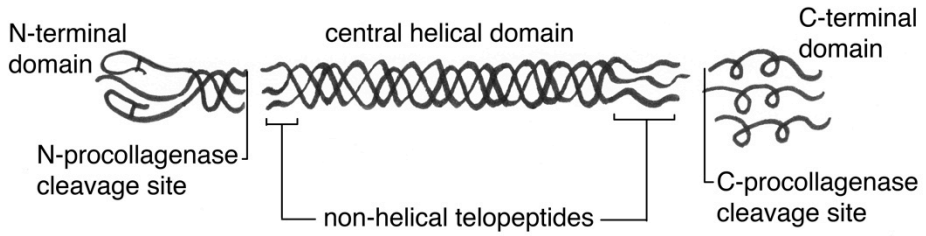

Figure 2.3: The general structure of collagen type I, adapted from Gelse *et al.* (2003) [64].

Each α-chain forms an extended left-handed helix with a pitch of 18 amino acids per turn [64]. The α-chains, staggered by one residue relative to one another, are supercoiled around a central axis to form the right-handed triple helical structure [64]. A glycine (Gly) residue occurs in every third position on the polypeptide chains, resulting in the characteristic $(Gly\text{-}X\text{-}Y)_n$ collagenous domain [64]. During assembly of the α-chains to form the helix, Gly residues are positioned toward the central axis, while the more bulky X and Y amino acid side chains, often proline and hydroxyproline respectively, occupy the outer positions to yield a tightly-packed molecule [65]. In fibrillar collagens including CI, the $(Gly\text{-}X\text{-}Y)_n$ repeat dominates, resulting in triple helical domains of 300 nm in length [64]. Interestingly, the N (amino)- and C (carboxy)-terminal non-helical domains (flanking the central helical domain) are thought to be involved in initiating triple helix formation and regulating fibril diameter, respectively [64].

Structurally, CI is a heterotrimer comprised of two identical α1(I)-chains and one α2(I)-chain [64]. These heterotrimer molecules, known as procollagen [65], are in turn arranged to form highly-organized quarter-staggered fibril bundles [64], which give rise to the biomechanical properties of CI [66]. Kinks form due to regions containing lower levels of proline and hydroxyproline, as compared to the regions of fibril overlap [66]. The resulting overall structure is less densely packed, imparting CI with tensile strength and load-bearing capacity [66].

2.6.2 Collagen Type IV

Collagen type IV (CIV) is a heterotrimer comprised of α-chains coiled into a helical structure [67]. CIV is a network-type collagen that is the most abundant structural component of the BM [65], including the BM in adipose tissue. The triple helical domain of CIV contains interruptions at several positions that impart greater flexibility to CIV, as compared to CI [68]. These interruptions also result in a longer triple-helical domain of 400 nm [64]. The globular C-terminal domain has internal regions that covalently link via disulfide bonds to form dimers [66], whereas the helical N-terminal domain is separated from the main triple-helical domain by a molecular kink [65]. N-terminal domains of adjacent CIV molecules form covalent disulfide crosslinks, yielding a tetrameric structure, and ultimately leading to the stable 3-D meshwork characteristic of CIV [66]. CIV can also associate with other ECM proteins, such as laminin, to form the supramolecular network structure of the BM [69].

2.6.3 Laminin

Laminin (LN), the most abundant glycoprotein in the BM [69], has a complex, heterotrimeric cross-shaped molecular structure, with three distinct regions, denoted as the α, β, and γ chains (Figure 2.4) [70]. The N-terminus of each chain forms the short arms of the cross, while the C-terminal regions combine to form the long arm [69, 71]. Several distinct α, β, and γ chains have been discovered, which combine to yield the 16 isoforms isolated to date [72].

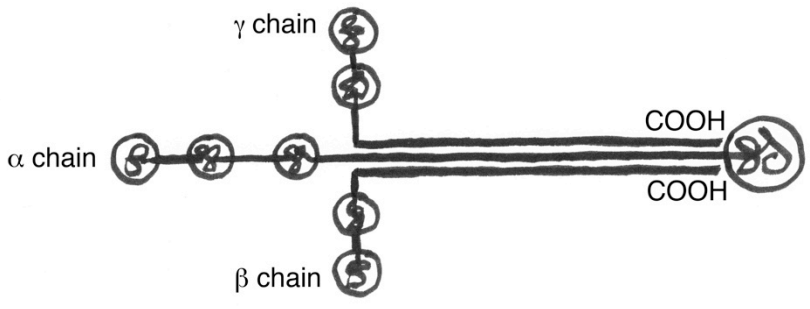

Figure 2.4: The overall cross-like molecular structure of laminin.

LN plays a significant role in the assembly and architecture of the BM, particularly during the early stages of its development [71]. LN may polymerize with other LN molecules via N-terminal interactions [72], in addition to interacting with other proteins, such as CIV and nidogen, to form the organized structure of the BM [69]. Cells bind with LN through receptor-ligand interactions that influence cell responses such as adhesion, migration, and differentiation [72]. Overall, LN is an important regulatory and structural molecule [69], and culturing experiments to date indicate that interactions with LN may enhance the adipogenic response of adult mouse BMSCs *in vitro* [73].

2.6.4 Other Extracellular Matrix Components

Glycosaminoglycans (GAGs) play an important role in the ECM, influencing cellular adhesion by binding growth factors and cytokines, as well as promoting water retention to contribute to the overall mechanical properties of the hydrated matrix environment [70]. The ECM has also been identified as a rich reservoir of growth factors, including VEGF, FGF, EGF, TGF-β, HGF, and PDGF [60].

2.6.5 Adipose Extracellular Matrix Organization

During adipogenesis and the commitment of adipose progenitor cells, synthesis of BM-associated collagen type IV, laminin, and nidogen is increased, while the network of fibrillar collagen (predominantly type I) is maintained, despite the decrease in expression of fibronectin and collagen types I and III [39, 59]. Through a complex series of enzymatic processes, the committed cells become embedded within the BM, which will ultimately form a mesh that surrounds the mature adipocytes [59]. The overall resulting ECM structure is a fibrillar network incorporating network-rich regions enriched in laminin [59]. ECM formation is induced by insulin through the transcriptional up-regulation of processing enzyme genes, and by glucose-induced stimulation of enzyme activity [59].

2.7 Current Clinical Strategies for Adipose Tissue Repair

Current clinical strategies for restoring volume to subcutaneous soft tissue defects employ autologous, allogenic, xenogenic and/or synthetic biomaterials [9]. For the repair of larger-volume soft tissue defects, treatments rely largely on autologous transfer of tissue flaps, in which a vascularized pedicle of adipose tissue is transferred with an intact blood supply to the defect site [7]. However, these flap transfers are major surgical procedures, and often result in significant donor site morbidity, in addition to graft resorption over time [6]. Synthetic alternatives, such as silicone and paraffin, have demonstrated poor outcomes involving device rupture and migration, coupled with undesirable fibrous encapsulation and contraction [74]. For the repair of small-volume or irregularly-shaped defects, injectable products are highly attractive.

2.7.1 Autologous Injectable Products

Autologous injectables do not pose immunogenic concerns, nor do they evoke a significant foreign-body response upon transplantation *in vivo* [11, 75]. Extensive clinical efforts have been made to use readily available and expendable lipoaspirate material, obtained from routine liposuction procedures, for soft tissue augmentation and reconstruction [11, 76]. However, free fat transfer has yielded unsatisfactory results [77]. Lipoaspirates and free fat grafts lack the supporting vasculature needed to enable vascularization and tissue survival, ultimately leading to graft resorption and replacement with fibrous tissue, and repeated treatments are required to maintain the corrected volume [6, 11]. Other efforts to develop an autologously-sourced injectable filler have focused on collagen-based injectables prepared from autologous biopsies [63]. However, the volume of transplantable tissue obtainable by this approach is significantly limited by the tradeoff of donor site defects, often unjustified by the resorption of the transplanted tissue over time [63].

2.7.2 Allogenic and Xenogenic Injectable Products

Allogenic materials have also been investigated as filler materials for the repair of small-volume defects [11]. Collagen from engineered human dermal fibroblasts has been developed and approved for clinical use (CosmoDerm® and CosmoPlast®) [78]. Cymetra®, the micronized form of the product Alloderm® (decellularized human cadaveric dermis), presents another allogenic injectable [11, 34]. However, for all three products, complete *in vivo* resorption is exhibited within approximately 6 months, rendering repeated treatments required [78]. Xenogenic injectable materials including bovine collagen (Zyderm®) and rooster comb-sourced hyaluronan (Hylaform®) face similar disadvantages of implant resorption over time, and the possible risk of disease transmission particularly in the case of xenogenic collagen-based products [78].

2.7.3 Synthetic Injectable Products

Synthetic injectables may avoid disease-transmission risks. Moreover, synthetics offer the advantage of tunable material properties [79]. Poly(lactic acid) (PLA) is an injectable biodegradable polyester that is used in the treatment of lipoatrophy in patients with HIV [80]. For more permanent volume augmentation, injectable poly(tetrafluoroethylene) (PTFE) has been tested [80]. However, PLA injections induce subcutaneous nodule formation, and PTFE is associated with a foreign body response [11, 78]. Furthermore, the mechanical properties of many synthetics differ from those of native adipose tissue, potentially creating patient discomfort and extensive scarring if rigid materials are employed [74]. Substrate elasticity has also been shown to direct the differentiation response of seeded MSCs, supporting the need to engineer tissue-specific matrices in terms of both composition and architecture [81].

2.8 Adipose Tissue Engineering

To date, clinical approaches focus largely on temporary volume restoration, rather than adipose tissue regeneration [34]. However, through tissue engineering, researchers aim to

regenerate new and functional adipose tissue for the repair and augmentation of soft-tissue defects [81]. The ability to predictably induce the formation of stable adipose tissue would be invaluable to the fields of reconstructive and plastic surgery [33, 34]. Many approaches to date point to the ability of cell-seeded 3-D scaffolds, which act as cellular support structures intended to mimic the native ECM environment, to significantly contribute to the regenerative response, as characterized through *in vitro* and/or *in vivo* studies [6, 9, 82]. However, limited success in achieving stable adipose tissue formation *in vivo* has been achieved.

2.8.1 Design Criteria for Adipose Tissue Engineering

In developing an adipose tissue-engineering strategy, coordination must exist between the cell source selected, the scaffold material, and the resulting microenvironment [34]. Strategies must be biocompatible *in vivo*, and a construct should not elicit a strong immune or inflammatory response upon transplantation, nor should it yield toxic or immunogenic products upon degradation [7]. Materials employed should be biodegradable, such that cells may remodel the construct over time [7]. Additionally, the mechanical properties and the bioactivity of the scaffold should mimic native fat, such that physical discomfort is minimized, and the incorporation of blood vessels, lymph supply, and nerves is achieved [7, 34]. Overall, the approach should promote the predictable formation of functional and stable adipose tissue.

2.8.2 Cell Sources for Adipose Tissue Engineering

The selection of an appropriate cell source for use in adipose tissue-engineering strategies is critical. Cells employed in regenerative approaches should not only contribute to the adipogenic and angiogenic responses, but should also be clinically translatable and available in abundant quantities, preferably obtained through minimally-invasive techniques [83]. To date, multiple cell sources have been investigated including mature adipocytes, ASCs (including committed preadipocyte populations from rat, mouse, and human sources), embryonic stem cells

(ESCs), and bone marrow-derived MSCs [7, 53]. Mature adipocytes form the major cellular component of adipose tissue. However, adipocytes are terminally-differentiated cells that do not proliferate extensively in their mature form, and their lipid-filled cytoplasm renders them highly susceptible to damage during isolation procedures [34]. As a result, adipocytes are not an attractive cell source for applications in adipose tissue engineering.

Genetically-modified preadipocyte cell lines from rat and mouse sources have a high proliferative capacity, and under the appropriate conditions, have been shown to accumulate intracellular lipids and adopt a rounded morphology characteristic of mature adipocytes [53]. The most commonly-investigated preadipocyte cell lines are the 3T3-L1 and 3T3-F442A sister cell lines derived from disaggregated mouse embryos [53]. These cells are committed progenitors to the adipogenic lineage, as are the less-extensively investigated Ob17-derived cell lines, sourced from epididymal fat pads of *ob/ob* (obese) mice, and the TA1 and 30A5 cell lines derived from multipotent 10T1/2 cells, which are cloned from mouse embryos [53]. Other potential cells of interest include the CHEF/18, Balb/c 3T3, RCJ 3.1, and 1246 lines, which also demonstrate multipotent differentiation capacity, including the adipogenic lineage [53].

Insights gathered from studies involving cell lines have significantly contributed to the current model of adipogenic differentiation, as well as to the understanding of the impact of scaffold and culturing conditions on cell response [7]. Overall, clonal cell lines are well defined, can readily proliferate and differentiate *in vitro*, and are commercially available, as compared to primary cells isolated from tissues [6]. However, immortalized lines have chromosomal abnormalities, and are therefore not necessarily representative of primary diploid cells [53]. Similarly, primary cells isolated from other species are not always representative of human cell behavior, and are generally prohibited for clinical use [8].

Human pluripotent stem cells sourced from embryos are primary cells that can be induced to adipogenically differentiate *in vitro* [7]. However, significant concerns regarding tumorigenicity coupled with ongoing ethical challenges have resulted in only limited human embryonic stem cell use in the field of adipose tissue engineering to date [7].

As discussed, primary MSCs are multipotent and may be derived from adult tissues including human fat (hASCs) or human bone marrow (hBMSCs) [53]. Overall, MSCs are heterogeneous populations of stem and progenitor cells displaying varying degrees of commitment [39], that give rise to connective tissues including bone, cartilage, muscle, tendon, and fat [84]. hBMSCs have been widely investigated for use in adipose tissue-engineering strategies to date [7]. hBMSC-seeded constructs fabricated from a variety of different synthetic and naturally-derived biomaterials have demonstrated promise in their ability to support adipogenesis [7, 85]. However, the clinical applicability of hBMSCs is limited due to the painful drilling and aspiration cell acquisition procedures required, which yield only low numbers of multipotent hBMSCs, with the population density decreasing with the age of the patient [86].

As previously described, hASCs represent an alternative and more abundant multipotent stem cell source isolated from the stromal vascular fraction of routinely-discarded adipose tissue [86]. This heterogeneous stem cell and progenitor population can be procured via significantly less invasive methods than hBMSCs, while maintaining a comparable surface phenotype expression, secretory profile, and multilineage capacity [33]. *In vitro*, hASCs demonstrate a high proliferative capacity [30]. Furthermore, hASCs have been shown to repress histocompatibility antigen expression following serial passaging *in vitro*, potentially minimizing the immune response *in vivo* [33]. Both autologous and allogenic hASCs may be promising for clinical use, and attractive for adipose tissue-engineering research. Therefore, research has largely shifted from using hBMSCs to hASCs [7].

Adipogenic differentiation of ASCs into mature adipocytes is accompanied by the intracellular accumulation of lipid droplets [39]. Therefore, the presence of intracellular lipids can be used to indicate early adipogenic activity. Oil Red O histological staining and measuring the enzymatic activity of GPDH, a key enzyme involved in triacylglycerol biosynthesis, can be performed to assess lipid accumulation [7]. Reverse transcriptase-polymerase chain reaction (RT-PCR) can also be performed to detect the expression of key transcriptional regulators of adipogenesis, including PPARγ and C/EBPα, or the expression of lipogenic genes such as LPL and Glut-4 [7]. Additionally, the synthesis and secretion of adipokines or ECM proteins may be assessed, or metabolic glucose uptake may be quantified [7].

2.8.3 Adipose Tissue-Engineering Scaffolds

The material and geometry used in developing adipose tissue-engineering scaffolds significantly influence the outcome of the repair strategy [87]. *In vivo*, dynamic interactions between cells and the ECM allow for the continuous and necessary exchange of information between the cells and their environment [64]. During adipogenesis, cellular adhesion of ASCs to the ECM is required for proper cell development and tissue organization to occur [73]. To restore fully functional soft tissues in defect sites, this ECM structure must be recapitulated by scaffolds applied in adipose tissue engineering. A wide variety of synthetic and naturally-derived biomaterials, prepared in a range of different geometries including porous sponges, discs, and microcarriers, have been explored in adipose tissue-engineering strategies to date [88].

2.9 Synthetic Biomaterials in Adipose Tissue Engineering

Synthetic materials have been widely investigated based on their tunable material parameters and the elimination of disease transmission concerns, as previously described. Significant work has assessed biodegradable polyester scaffolds made from poly(lactic acid)

(PLA), poly(glycolic acid) (PGA), and poly(lactic-co-glycolic acid) (PLGA). *In vivo* studies examining PGA and PLA constructs seeded with 3T3-L1 preadipocytes, have shown promise for the support of short-term adipogenesis, but are rapidly degraded *in vivo* over 4-12 weeks [7]. Adipose tissue-engineering strategies incorporating PLGA loaded with basic fibroblast growth factor (bFGF) have shown promise in supporting adipogenesis, as well as vascularization. However, longer-term studies have not been performed [7]. Other strategies have investigated peptide-modified poly(caprolactone) (PCL), poly(ethylene) terepthalate (PET), modified poly(tetrafluoroethylene) (PTFE), silicones, poly(ethylene glycol) (PEG), and poly(ethylene glycol) diacrylate (PEGDA), each of which carries specific advantages and limitations [7]. Overall, synthetic materials have demonstrated varying degrees of success in short-term adipose tissue-engineering studies to date [9]. However, longer-term studies remain ambiguous, and despite the flexibility in material design, as well as the convenient availability of synthetic polymers, these materials inherently lack the naturally-derived molecules that are required to facilitate normal cell-matrix interactions that significantly impact the overall cell response [89].

2.10 Naturally-Derived Biomaterials in Adipose Tissue Engineering

Naturally-derived biomaterials are obtained from tissues or other biological systems [89]. Based on their inherent similarities to the native ECM and potential for enhanced biocompatibility, a multitude of naturally-derived materials have been investigated for use in adipose tissue engineering to date, including modified alginate, chitosan, collagen type I, gelatin, modified hyaluronan, fibrin, silk, ECM-derived gels, and decellularized tissues [89].

2.10.1 Collagen

CI has been extensively investigated in adipose tissue-engineering research. Upon transplantation, depending on the source and processing methods, collagen scaffolds can demonstrate low antigenicity and are biodegradable, rendering them relatively biocompatible as

compared to many other materials [90]. Moreover, collagen-based scaffolds have shown promise in supporting adipogenesis in seeded cells from various sources [7, 9]. However, collagen and its denatured forms such as gelatin, demonstrate significant shrinking and resorption *in vivo* unless modified or stabilized [91]. Collagen is highly hydrophilic, and swells upon hydration, thereby reducing scaffold mechanical stability and the ability to retain a specific shape [92].

2.10.1.1 Collagen Stabilization by Crosslinking

Toward the goal of strengthening collagenous materials, a variety of crosslinking agents have been investigated. Physical crosslinking methods such as heat and dehydrothermal treatment can risk protein denaturation, thereby compromising stability [93]. As a result, chemical crosslinking using bifunctional agents such as glutaraldehyde (GTA) is more commonly employed [94]. GTA is highly effective at stabilizing collagenous materials, is widely available, and relatively inexpensive [95]. Aldehyde groups on GTA react with free lysine or hydroxylysine amino acid residues on the polypeptide chains to form crosslinks [94, 96]. However, GTA is cytotoxic, rendering alternative crosslinking approaches desirable [94].

Photochemical crosslinking methods that use photosensitizing dyes in the presence of light, present an effective alternative [91, 93, 97]. Specifically, photosensitizing dyes including rose bengal and riboflavin have shown great promise as less cytotoxic crosslinking agents for stabilizing collagenous materials [91, 98]. Overall, photochemical crosslinking is achieved by the activation of photosensitizers by light, and the subsequent photochemical reactions producing highly-reactive oxygen species (i.e. oxygen free radicals or hydrogen peroxide) that react with surrounding protein molecules to form crosslinks [91]. The light-activated photosensitizer may also activate ground-state oxygen substrate to crosslink the protein molecules by oxidation [97]. The amino acid groups including tryptophan, tyrosine, histidine, cysteine, and methionine have been suggested as particularly vulnerable to photochemical crosslinking [97, 99].

Enzymatic crosslinking of collagenous materials is another less cytotoxic approach as compared to conventional glutaraldehyde stabilization [100]. In particular, commercially available microbial transglutaminase derived from *Streptoverticillium mobaraense* has shown promise as an effective and natural crosslinking agent for collagen, through the formation of intramolecular or intermolecular glutamyl-lysine bonds [100].

2.10.2 Alginate

Alginate is a natural hydrogel derived from the brown seaweed *Macrocystis pyrifera*, and produced commercially by bacteria [101]. Structurally, alginates combine unbranched binary copolymers of 1-4 linked β-D-mannuronic acid (M) and α-L-guluronic acid (G) in varying sequences and ratios, depending on their source [101]. High-G content results in increased structural rigidity of the chains, whereas low-G alginates form softer, more flexible gels [101]. In the presence of divalent cations, such as Ca^{2+}, alginates crosslink to form reversible gels that can be solubilized by chelating agents [101, 102]. As alginates do not facilitate strong cellular attachment, they are often subjected to surface modification techniques that incorporate cell adhesion peptides such as the 'argenine, glycine, and aspartic acid' (RGD) domains that bind integrins [103].

2.10.3 Decellularized Tissues

Tissue decellularization aims to remove cellular and antigenic components from biological tissues, while preserving the native matrix as well as possible [104]. In doing so, naturally-derived scaffolds are obtained that incorporate the complex structural proteinaceous composition of the native ECM *in vivo* [70]. Overall, decellularized tissues are favorable culturing substrates for achieving cellular attachment, proliferation, and differentiation, as they represent the natural cell-secreted scaffold [70].

Decellularization is commonly achieved through a combinatory approach incorporating various physical, chemical, and enzymatic treatments delivered in a systematic order. Physical disruption of cell membranes may involve snap freezing, homogenization, or mechanical agitation [105]. Chemical treatments often employ a selection of hypotonic and hypertonic solutions to achieve cell lysis by osmotic shock, in addition to a range of non-ionic, ionic, and zwitterionic detergents that disrupt lipid-lipid and lipid-protein interactions, and chelating agents, such as EDTA, that disrupt cell adhesion to the ECM [105]. Enzymatic treatments include trypsin, endonucleases, and exonucleases that digest residual nucleic acids [105]. Most decellularization regimes also include protease inhibitors such as phenylmethylsulfonylfluoride (PMSF) to prevent the degradation of the ECM by proteases released during cell lysis, and antibiotics and antimycotics to prevent bacterial and fungal contamination and degradation of the matrix during processing [105].

Decellularization protocols have been successfully established for many human tissues to date, including the dermis, intestine, bladder, liver, pericardium, arteries, heart valves, nerves, skeletal muscle, placenta, and most recently, adipose tissue (DAT) [14, 106-119]. Established detergent-free protocols for the decellularization of human fat have confirmed the preservation of not only the fibrillar collagen type I structure of the adipose matrix, but also the presence of the BM proteins, collagen type IV and laminin [14]. During *in vitro* culture with hASCs, DAT has demonstrated the ability to significantly modulate the adipogenic response [14]. Specifically, intact DAT scaffolds have induced the expression of the master adipogenic regulators, PPARγ and C/EBPα, in seeded hASCs without the addition of exogenous factors [14]. This work highlights the capacity for the ECM to direct cell fate, and renders DAT an exciting naturally-derived biomaterial for use in adipose tissue engineering. This research also points to the broad potential for tissue-specific approaches in scaffold design.

2.11 Culturing Environments for Adipose Tissue Engineering

To realize cell-based therapies on a clinically-relevant scale, methods to rapidly expand appropriate cell populations *in vitro* must be established [8, 120-122]. Overall, ASC expansion to date has remained largely dependent on the use of two-dimensional (2-D) tissue culture poly(styrene) (TCPS) plates in a static environment [123]. While convenient, the use of TCPS carries significant disadvantages. Specifically, ASCs cultured on TCPS adopt a fibroblast-like morphology, as opposed to the rounded morphology characteristic of ASCs *in vivo* [39, 123]. Furthermore, the native immunophenotype is not retained, and the ECM secretion profile differs from the native ECM, based on the inability to recapitulate the complex 3-D architecture of the *in vivo* microenvironment in 2-D culture [123]. Enzymatic treatments such as trypsinization that are required to release ASCs from TCPS during passaging can also negatively impact cell behavior [124]. Overall, appreciable cell expansion requires significant incubator space and many single-use TCPS flasks, which is associated with a high operating cost [125]. Moving to a 3-D environment, ASCs cultured statically on 3-D constructs demonstrate cell necrosis at the construct cores due to inadequate supply of nutrients and oxygen [7].

Therefore, significant efforts are underway to move from a 2-D static environment to a 3-D dynamic environment, via the use of dynamic culture systems, such as rotating-wall bioreactors and spinner flasks [122]. Cells cultured under dynamic conditions in these low-shear systems may be expanded on a variety of spherical 3-D microscaffolds, commonly termed microcarriers [126]. Promisingly, a more native phenotype and rounded cell morphology are retained through the 3-D dynamic culture of ASCs in such systems [127]. Moreover, the ECM secreted by ASCs cultured under dynamic conditions tends to more closely resemble the native ECM *in vivo* [123].

Spinner flasks are glass or plastic culturing vessels equipped with magnetic impellors that are driven by a magnetic stir plate on which the spinner flasks are positioned during cell culture

[122]. Two side ports are present on each flask to facilitate the delivery and removal of medium, cells, or gases, and also permit multiple sampling of loaded microcarriers during experiments [122]. The impellors within each flask enable cell-seeded constructs to be suspended in dynamic culture, while also facilitating oxygen and nutrient transfer in a 3-D environment [121]. Overall, spinner flask systems offer more precise control over operating parameters such as nutrient content, pH, and pO_2, as compared to conventional 2-D plating techniques [121].

2.12 Microcarrier Approaches in Adipose Tissue Engineering

Microcarriers, or microspheres, have been extensively investigated as a means of encapsulating cells or growth factors, and were originally developed for use in the production of viral vaccines and mammalian cell line-sourced biologicals [128, 129]. Recent tissue-engineering strategies have employed microcarriers as scaffolds to support anchorage-dependent cells in dynamic culturing environments [6, 125, 130]. Overall, during culture, these spherical microparticles are seeded with an appropriate cell source, suspended in culturing medium, and subjected to a low-shear, stirred environment achieved by spinner flasks or other dynamic bioreactor systems [122].

From a scaffold design perspective, microcarriers provide a high surface area to volume ratio as compared to conventional 2-D plates, resulting in significantly less incubator space and materials required to yield the same cell numbers *in vitro* [125]. Through adjusting microcarrier composition, surface topography, porosity, charge density, and/or size, cell responses may be controlled, thereby mediating the desired regeneration [15, 130, 131]. Moreover, enzymatic release of the cells from the microcarriers may not be required, depending on the substrate selected as the base material [124, 132].

Microcarriers hold promise as injectable cell delivery vehicles for the repair of small-volume and/or irregularly-shaped subcutaneous defects, through the potential to directly inject

cell-loaded microcarriers following dynamic cell expansion *in vitro* [125]. Overall, microcarrier design and selection are critical to achieve the desired regenerative response. For the repair of larger-volume or shape-specific defects, composite approaches have employed microcarriers as an intermediary scaffold. In brief, cell-loaded and/or growth-factor loaded microcarriers have shown promise when encapsulated within hydrogels or incorporated within porous scaffolds [15, 133, 134].

Due to the great potential of the overall microcarrier approach, microcarriers are central to many tissue-engineering approaches to date. A variety of commercially-available microcarriers have been developed. Most beads employ a composite approach, involving a synthetic core enrobed in a naturally-derived material to promote cell attachment. Cytodex 1 and Cytodex 2 (Amersham, Biosciences, Sweden) microcarriers, and Hillex (SoloHill, USA) microcarriers employ modified dextran as a base material [135-137], whereas Cytodex 3 (Amersham Biosciences, Sweden) microcarriers contain a modified dextran core with a denatured porcine-derived collagen coated surface [135, 138, 139]. Additionally, Cytopore 1 (Amersham Biosciences, Sweden) microcarriers fabricated from surface-modified crosslinked cotton cellulose and Cytoline 2 (Amersham Biosciences, Sweden) microcarriers based on poly(ethylene) and silica are available [126, 130, 140].

To better mimic the native ECM, commercially-available microcarriers based on naturally-derived materials are also available and have shown promise. The CultiSpher G and CultiSpher S lines (Percell Biolitica, Sweden) are commercially-available porcine-derived crosslinked gelatin microcarriers, while Cellagen (MP Biomedicals, USA) microcarriers are fabricated from porcine-derived crosslinked collagen type I [130, 141]. In a study by Rubin *et al.* (2007), hASCs were cultured on Cellagen microcarriers in a spinner flask system and upon induction, the hASCs successfully differentiated into adipocytes [141].

Microcarriers developed in the laboratory for the dynamic culture of ASCs have employed a wide range of synthetic and naturally-derived materials. Many research groups have focused on developing PLA- and PLGA-based microcarriers modified with RGD or TGF-β to promote ASC attachment and/or growth [124, 142-144]. Other studies employing microcarriers for the dynamic culture of ASCs have investigated RGD-peptide modified alginate microcarriers [145], small intestinal submucosa particulates [103], and powderized forms of adipose ECM-derived materials [28, 146].

Interestingly, limited research has investigated the design of custom, tissue-specific microcarriers, engineered to mimic the native ECM from which the seeded cells are sourced. Based on the literature, this methodology may induce a tissue-specific and/or cell-specific response in the seeded population(s). No methodology to date incorporates the composition of a fully decellularized tissue in combination with a tailored scaffold microgeometry, more specifically as spherical microcarriers. Most similarly, Choi *et al.* (2009) described extracting the lipid portion of adipose tissue and using the resulting tissue-derived gel as an injectable product, or as a base material for producing scaffolds [146]. However, DAT provides a more purified form of the adipose matrix, and coupled with its adipo-inductive potential, presents an attractive base material for the development of cell-specific and/or tissue-specific microcarriers for use in adipose tissue engineering.

2.13 Summary

Adipose tissue is recognized far beyond its role in energy storage as a complex endocrine organ. The repair of subcutaneous soft-tissue defects remains a clinical problem, with current treatments relying largely on autologous tissue transfer that requires the creation of extensive donor site defects. Adipose tissue engineering aims to regenerate functional and stable adipose tissue, largely through seeding scaffolds with adipose-derived stem cells and subjecting the

constructs to a controlled microenvironment. Static 2-D culturing negatively impacts cellular behavior, in terms of both proliferation and differentiation. However, dynamic 3-D systems, such as spinner flasks, offer promising alternatives with significant advantages, and commonly employ microcarriers as cell-culture substrates. While microcarriers fabricated from a variety of synthetic and naturally-derived materials have been investigated, the optimal bead composition and architecture to facilitate rapid cell expansion with maintenance of the stem cell capacity is unknown. To date, no research has described the development of a tissue-specific microcarrier based on fully decellularized tissue. As the basis for this thesis, decellularized adipose tissue is a promising adipogenic material that may provide the ideal base material for developing adipogenic, tissue-specific microcarriers for use in adipose tissue-engineering applications.

Chapter 3

Design and characterization of tissue-specific extracellular matrix-derived microcarriers for adipose tissue engineering

***Large portions of this chapter have been submitted to Acta Biomaterialia, Elsevier:**
Turner AE, Flynn LE. (2010) Design and characterization of tissue-specific extracellular matrix-derived microcarriers.

3.1 Introduction

Adipose tissue engineering holds promise for the regeneration of functional and stable tissue, as a means to treat a variety of clinical conditions and disorders [12, 147]. *In vitro* and *in vivo* research points to the ability of cell-seeded three-dimensional (3-D) scaffolds (or cellular support structures), intended to mimic the native extracellular matrix (ECM), to contribute to the regenerative response [6, 9, 82]. Overall, unseeded scaffolds have demonstrated limited success to date in the long-term correction of soft tissue defects. The ability to rapidly expand cell populations *in vitro,* through clinically-translatable methods, must be established before cell-based strategies may be realized on a broad scale [8].

Microcarriers, or microspheres, have been extensively investigated in tissue-engineering strategies, as a means of encapsulating cells or growth factors [128]. More recently, microcarriers have been applied in tissue-engineering research as cell culture substrates, intended to support anchorage-dependent cell attachment and proliferation in a variety of culturing environments [6, 125, 130]. During microcarrier culture, seeded cells adhere to spherical microparticles suspended in growth medium, and are typically subjected to low-shear stirring in dynamic culturing systems [122]. Toward the goal of achieving significant cellular expansion, microcarriers possess an attractive scaffold geometry based on their high surface area to volume ratio, as compared to conventional two-dimensional (2-D) plating techniques on tissue culture polystyrene (TCPS). Moreover, conditions in microcarrier culturing environments such as pH, pO_2, and nutrient

delivery, may be more precisely controlled relative to static culturing [121]. Studies have demonstrated that the dynamic 3-D environment achieved by using microcarriers within stirred systems promotes cells to retain a more native morphology and phenotype, and to produce a matrix that more closely resembles the ECM *in vivo* [139].

Clinically speaking, microcarriers hold great promise as a minimally-invasive product for the repair of small-volume and/or irregularly shaped defects, given their potential direct injectability following cell seeding and dynamic culture [128]. For the repair of larger-volume or shape-specific defects, composite approaches have investigated microcarriers within hydrogels [15, 133, 134] or macroporous scaffolds [89, 148].

In vivo, the ECM functions to provide structural and mechanical support for residing cellular components, and also modulates a wide range of cell- and tissue-specific behaviors via cell-matrix communication and/or endocrine signaling. Therefore, the scaffold selection and design directly impacts the overall success of a regenerative approach. Many studies, as outlined in Chapter 2, have investigated the development of synthetic and/or naturally-derived microcarrier scaffolds, fabricated from materials including poly(lactic acid) (PLA) [132, 142], poly(lactic-co-glycolic acid) (PLGA) [124, 143, 149], dextran [135], alginate [145], gelatin [150], and collagen [127, 141]. However, little research has investigated the development of a custom-designed tissue-specific microcarrier, intended to modulate a cell- and/or tissue-specific response.

Decellularization protocols have been successfully established for a broad range of human tissues including the dermis [106, 107], intestine [108, 109], bladder [110], liver [111], pericardium [112], arteries [113, 114], heart valves [115, 116], nerves [117], skeletal muscle [118], placenta [119], and more recently, adipose tissue [14]. These strategies aim to remove antigenic components, while preserving the native structure and composition of the ECM as well

as possible, to yield naturally-derived matrix materials. These decellularized tissues represent a promising base material for the design of tissue-specific microcarriers.

Decellularized adipose tissue (DAT) has shown particular promise as a naturally-derived biomaterial, providing a microenvironment supportive of adipogenesis [14]. Established detergent-free protocols for the decellularization of human fat enable the removal of cellular components and debris, nucleic acids, and lipids from the matrix, while preserving the native proteinaceous structure, including the basement membrane composition, rich in collagen IV and laminin [14]. Intact DAT-based scaffolds have been shown to induce the expression of the master regulator adipogenic genes peroxisome proliferator activated receptor γ (PPARγ) and CCAAT/enhancer binding protein α (C/EBPα), in seeded adipose-derived stem cells (ASCs) *in vitro*, without the need for exogenous differentiation factors [14]. This research highlights the ability of the ECM to mediate cell response, and supports the use of tissue-specific scaffolds designed to mimic the native environment from which the cells are sourced.

To date, no methodology exists that incorporates the composition of a fully decellularized tissue within a tailored scaffold microgeometry, in the form of spherical engineered microcarriers. As DAT provides a highly purified form of the adipose matrix, the fabrication of DAT-based microcarriers could provide an adipogenic scaffold approximating the native matrix in composition, while ensuring the removal of most cellular components. As a result, the first objective of the research presented in this chapter was to develop methods for the fabrication of porous matrix-derived microcarriers from DAT using non-cytotoxic materials. Protocols were developed for the solubilization of DAT to facilitate microcarrier fabrication, and three crosslinking agents were investigated for the stabilization of the DAT-based microcarriers.

Upon establishing reproducible methods for DAT-based microcarrier fabrication, the microcarriers were thoroughly characterized and evaluated for their suitability as an injectable

anchorage-dependent cell culture substrate. Overall, the DAT-based microcarriers, in parallel with gelatin-based microcarriers developed as a control, were evaluated under optical microscopy, fluorescence microscopy, and scanning electron microscopy. Microcarrier diameter, size distribution, and porosity were determined. Stability and swelling behaviors of the microcarriers were measured over a 28-day period, based on changes in diameter and protein release over time. Finally, sterility and injectability of the microcarriers were assessed.

3.2 Materials and Methods

3.2.1 Materials

All chemicals were used as received and purchased from Sigma-Aldrich Canada Ltd. (Oakville, ON, Canada) unless otherwise stated.

3.2.2 Procurement of Adipose Tissue

Freshly excised breast or subcutaneous abdominal adipose tissue samples were obtained from female patients undergoing reduction mammoplasty or abdominoplasty procedures at the Kingston General Hospital and Hotel Dieu Hospital in Kingston, ON, Canada. Upon harvesting, the adipose tissue samples were immersed in 100 mL of sterile divalent cation-free phosphate buffered saline (PBS) on ice and transported to the laboratory within 45 minutes of harvesting. Patient age, weight, and height, in addition to the anatomical location from which the tissue was sourced (breast versus abdomen), were recorded. Research ethics board approval from Queen's University was obtained for this research (REB No. CHEM-002-07).

3.2.3 Decellularization of Adipose Tissue

Upon arrival to the laboratory, each adipose tissue sample was transferred into a 250 mL sealable plastic container. Cauterized portions of the tissue were excised and discarded, and for larger samples, the tissue was divided into sections approximately 20-25 grams in mass. Tissue

decellularization was achieved through following an established detergent-free protocol [14]. Overall, tissue samples were immersed in a series of decellularization solutions delivered systematically over a five-day period (Table 3.1). All solutions (100 mL working volume) were supplemented with 1 % antibiotic/antimycotic (ABAM) solution (Invitrogen, Burlington, ON, Canada) and 0.27 mM phenylmethylsulfonylfluoride (PMSF) solution (a protease inhibitor). Unless otherwise stated, all treatments were conducted at 37°C under constant agitation on an Excella^{TM} 24 Benchtop Incubator (New Brunswick Scientific, Edison, NJ, USA) at 150 RPM.

Table 3.1: Detergent-free 5-day protocol for the decellularization of adipose tissue [14].

Day	Processing Steps
1	- Freeze-thaw 3 times in Solution A (Freezing Buffer Solution) - Incubate for 16 hours (overnight) in Enzymatic Digestion Solution 1
2	- Polar solvent extraction in 99% isopropanol
3	- Polar solvent extraction in 99% isopropanol
4	- Rinse 3 times (30 minutes each) in Sorenson's Phosphate Buffer (SPB) Rinse (Rinsing Buffer Solution) - Incubate for 6 hours in Enzymatic Digestion Solution 1 - Rinse 3 times (30 minutes each) in SPB Rinse (Rinsing Buffer Solution) - Incubate for 16 hours (overnight) in Enzymatic Digestion Solution 2
5	- Rinse 3 times (30 minutes each) in SPB Rinse (Rinsing Buffer Solution) - Polar solvent extraction in 99% isopropanol (8 hours) - Rinse 3 times (30 minutes each) in SPB Rinse (Rinsing Buffer Solution)

Initially, 20-25 gram portions of adipose tissue were immersed in Solution A (a hypotonic tris-ethylenediaminetetraacetic acid (EDTA) buffer at pH 8.0) and frozen for 30 minutes at -80ºC. Once frozen, the tissue was incubated under constant agitation until entirely thawed. All fluid was drained and replaced with fresh Solution A. This freeze-thaw cycle was repeated twice, for a total of three cycles. The tissue was then immersed in Enzymatic Digestion Solution 1 (0.25 % trypsin and 0.1 % EDTA (Gibco®, Invitrogen, Burlington, ON, Canada)) and incubated under constant agitation for 16 hours. During the next 48 hours, the tissue was immersed in 99.9% isopropanol. Fresh isopropanol was provided every 8 hours, and the tissue

was gently massaged between each solvent change. Following polar solvent extraction, the tissue was rinsed three times (30 minutes each) in SPB rinse solution (8 g/L NaCl, 200 mg/L KCl, 1 g/L Na_2HPO_4, and 200 mg/L KH_2PO_4 (pH 8.0)) prior to a second digestion with Enzymatic Digestion Solution 1 for 6 hours. The tissue was then subjected to three 30-minute additional SPB rinses, and immersed in Enzymatic Digestion Solution 2 containing DNase (15000 U Type II from bovine pancreas), RNase (12.5 mg Type III A from bovine pancreas), and Lipase (2000 U Type VI-S from porcine pancreas) for 16 hours. Finally, the tissue was rinsed three times (30 minutes each) in SPB rinse solution, extracted in isopropanol for 8 hours, and subjected to three 30-minute rinses in SPB Rinse. The resulting DAT was stored in 70% ethanol at 4ºC.

3.2.4 Solubilization of Decellularized Adipose Tissue

To permit the fabrication of DAT-based microcarriers, protocols were developed and optimized for the solubilization of DAT using an acid/pepsin digestion approach. Varying concentrations of pepsin (1-100 mg pepsin/g tissue) and volumetric ratios of 0.5 M acetic acid (0.1-10.0 g tissue/mL acetic acid) were investigated, with the aim of effectively solubilizing DAT within a minimum volume of acetic acid, thereby maximizing the total protein concentration within the solubilized DAT solution.

Prior to digestion, each DAT sample was decontaminated within a 50 mL sterile centrifuge tube by three 30-minute rinses in 70% (v/v) aqueous ethanol solution at room temperature under constant agitation (55 RPM). Following decontamination, the DAT was aseptically rehydrated using three washes (30 minutes each) of sterile divalent cation-free PBS. Using sterile scissors and working within a sterile tissue culture dish, the hydrated DAT was divided into sections of approximately 1 cm^3 to increase the overall tissue surface area. Finally, the lightly minced DAT was aseptically compressed using a sterile scoopula within a 50 mL sterile centrifuge tube, and the excess PBS was removed by aspiration and/or pipetting with a 5

mL serological pipette. Following this physical dehydration step, the minced DAT was suspended in an equal volume of 0.5 M acetic acid, and incubated at 37°C under constant agitation (150 RPM) to achieve acid perfusion throughout the tissue. The acid-treated DAT was recompressed aseptically, and the excess acetic acid was removed by aspiration or pipetting.

To develop an optimized protocol, pepsin concentrations of 1 mg, 10 mg, 50 mg, and 100 mg of pepsin/g of DAT (wet weight) were investigated for their ability to solubilize the DAT. For each concentration, a sterile pepsin digest solution was prepared by combining the pepsin (1064 units/mg protein) with 0.5 M acetic acid, such that the acid was provided at a concentration of 10 mL acetic acid/g DAT (wet weight). Prior to digestion, the pepsin digest solutions were filtered through 0.22 μm pore size Millex GP Syringe Driven Filter Units (Millipore Express PES Membrane, Millipore, Carrigtwohill, Ireland).

Each pepsin concentration was investigated in triplicate, by incubating the samples for 20 hours at 37ºC under constant agitation (150 RPM). Also included in this study was an acid-treated DAT sample as a control (no pepsin added) and a DAT sample suspended in 70% (v/v) aqueous ethanol as a blank (no acid-treatment). Following digestion, all samples were visually assessed to determine the overall degree of solubilization.

Upon selecting an optimized pepsin concentration, digestion protocols were further refined to reduce the volume of acetic acid required. Pepsin slurries were prepared ranging from 0.1-10 mL of acetic acid/g tissue, and assessed for their ability to successfully solubilize the tissue. Following digestion, the pepsin was inactivated by raising the solution pH above 8.0 via drop-wise addition of 10 M sodium hydroxide solution, and insoluble proteins and residual pepsin were removed by centrifugation (15,000 x *g*, 30 minutes, 4ºC).

For the production of larger volumes of solubilized DAT for use in the microcarrier fabrication experiments, DAT samples obtained from breast and abdominal adipose tissues sourced from multiple patients (n=5) varying in age and body mass index (BMI) were pooled, thereby yielding collective DAT samples of 20-40 grams (wet weight). Overall, DAT solubilization involved decontamination, acid-treatment, pepsin digestion, and purification. After processing, solubilized DAT (DATsol) was stored at 4ºC.

3.2.5 Protein Quantification of Solubilized DAT

Total protein content of solubilized DAT was determined using the Bio-Rad protein assay (Bio-Rad Laboratories, Inc., Hercules, CA, USA) according to the manufacturer's instructions. As sodium hydroxide is known to interfere with this assay, DAT samples selected for protein measurement were assayed immediately following pepsin digestion and centrifugation. Solubilized DAT samples were measured in triplicate (n=3, N=3), and compared to an albumin standard curve with concentrations of 0 μg/mL, 10 μg/mL, 20 μg/mL, 40 μg/mL, 60 μg/mL, and 80 μg/mL. All standards were prepared via serial dilution of 1.42 mg/mL bovine albumin standard stock solution, and measured in duplicate (n=2, N=3). In preparation for absorbance analysis, each sample or standard solution was pipetted at a volume of 160 μL/well into a 96-well TCPS plate. To each loaded well, 40 μL of Coomassie® Brilliant Blue G-250 dye solution was then added and mixed thoroughly by pipetting up and down. The plate was incubated for 5 minutes at room temperature prior to measuring the absorbance at 595 nm using a Synergy™ HT multi-detection microplate reader and KC4™ data analysis software (Bio-Tek Instruments, Inc., Winooski, VT, USA). Absorbances of DATsol samples were compared to the albumin standard curve generated, so as to calculate the total protein content in units of μg/mL for each sample.

3.2.6 Microcarrier Fabrication

3.2.6.1 Composite Microcarrier Fabrication

Sterile, composite DAT/alginate microcarriers were fabricated using a custom-designed and assembled apparatus employing an air-jet droplet technique (Figure 3.1). Based on the methods of Tsai *et al.* (1998) that employed solubilized collagen from rat tails [151], solubilized DAT was combined with sterile-filtered sodium alginate (alginic acid sodium salt from brown algae, Sigma A0682) solutions (ranging in concentration from 1.0 - 4.0% (w/v)) in varying volumetric ratios (3:2 and 4:3 parts DAT to alginate). The resulting solubilized DAT/alginate mixtures were loaded into disposable 6 mL BD (Becton, Dickinson and Company, USA) syringes and added drop-wise to 40 mL of 1.5% (w/v) calcium chloride solution (pH 7.2) on a magnetic stir plate, using a blunt-ended, 21-gauge Punctur-Guard® winged intravenous infusion set (ICU Medical, Inc., Vernon, CT) at a distance of 50 ± 5 mm using a PHD 2000 Infusion syringe pump (Harvard Apparatus Inc., South Natick, MA, USA) in the presence of a compressed nitrogen jet to help reduce droplet size. The solubilized DAT/alginate solution flow rates were varied (0.10 - 0.45 mL/minute) depending on the DAT/alginate ratio, as was the nitrogen gas pressure (5, 10, and 15 psi), to obtain spherical microparticles of controlled sizes.

To develop a 3-D control, gelatin was selected as a base material for microcarrier fabrication, as it represents an alternative denatured collagenous material. Gelatin solutions ranging in concentration (10-200 mg/mL) were prepared using Type B gelatin from bovine skin and deionized water, and assayed for total protein content using the Bio-Rad protein assay following the methods previously described. Gelatin/alginate composite microcarriers were fabricated using similar methods as those described for the production of DAT/alginate composite microcarriers. Gelatin solutions of 10 mg/mL, 20 mg/mL, and 50 mg/mL, were prepared and combined in varying volumetric ratios (3:2 and 4:3 parts gelatin to alginate) with sodium alginate

solutions ranging in concentration from 1-4% (w/v). These gelatin/alginate solutions were added drop-wise to 40 mL of sterile 1.5% calcium chloride solution on a magnetic stir plate at varying flow rates (0.10-0.45 mL/minute) and disruptive nitrogen gas pressures (5, 10, and 15 psi) to yield gelatin/alginate composite microcarriers.

3.2.6.2 Crosslinking of Composite Microcarriers

For the non-cytotoxic stabilization of the DAT-phase within the composite DAT/alginate microcarriers, photosensitizing dyes were investigated as potential photochemical crosslinkers. Specifically, rose bengal and riboflavin were selected and assessed for their ability to effectively stabilize the DAT-based microcarriers, as compared to glutaraldehyde.

Rose bengal was combined with deionized water under dark conditions in 15 mL centrifuge tubes to yield 0.01% (w/v) rose bengal photosensitizing solution [93]. Composite DAT/alginate microcarriers were photosensitized by immersion in an equal volume of rose bengal solution for 30 minutes under dark conditions at room temperature, with constant agitation (50 RPM). Following crosslinking, residual rose bengal was removed by repeated washes with deionized water, and photochemical crosslinking was performed through microcarrier exposure to visible light (20W/12V Halogen JC Type Bulb positioned 15 cm above the samples) for 2 hours, 4 hours, and 8 hours.

Riboflavin 5′-monophosphate sodium salt dihydrate and deionized water were combined to prepare 0.1% (w/v) riboflavin photosensitizing solution in 15 mL centrifuge tubes under dark conditions [98]. DAT/alginate composite microcarriers were immersed in an equal volume of riboflavin solution for 10 minutes under dark conditions at room temperature with constant agitation (50 RPM), followed by repeated rinsing with deionized water to remove residual riboflavin. Photochemical crosslinking was induced with an EXFO Lite high-intensity long-wave lamp (320-480 nm filter), at a relative intensity of 5 mW/cm^2 for 600 and 900 seconds.

For both photochemical crosslinking agents, comparable protocols as those described for the DAT-based microcarriers were followed to stabilize the gelatin phase within the gelatin/alginate composite microcarriers. Additionally, all sample preparation and crosslinking steps were performed under sterile conditions to permit future use of microcarriers in cell culture.

In addition to photochemical crosslinking, glutaraldehyde was selected as a control, based on its established efficacy for the stabilization of collagenous materials [96, 152]. DAT/alginate microcarriers were thoroughly rinsed with divalent cation-free PBS and immersed in 0.1% (v/v) glutaraldehyde solution for 20 hours at room temperature under constant gentle agitation (50 RPM) [127]. Following crosslinking treatment, the DAT/alginate microcarriers were repeatedly rinsed with sterile deionized water to remove residual glutaraldehyde. In parallel, glutaraldehyde was also used to stabilize gelatin/alginate composite microcarriers. Again, all crosslinking steps were performed following aseptic technique to minimize potential microcarrier contamination.

3.2.6.3 Sodium Alginate Extraction

Overall, composite microcarriers stabilized by glutaraldehyde, rose bengal, and riboflavin, were each treated with sodium citrate to liquefy the alginate phase within the microcarriers, thereby permitting alginate extraction (Figure 3.1). Each microcarrier sample was immersed in an equal volume of sterile 50 mM sodium citrate solution and gently agitated by hand. Three sodium citrate treatment periods of 10 minutes, 15 minutes, and 20 minutes were investigated for their ability to effectively permit alginate extraction from the microcarriers. After sodium citrate treatment, the resulting DAT-based microcarriers were rinsed repeatedly with divalent cation-free PBS and stored at 4ºC. Composite gelatin/alginate microcarriers were also subjected to comparable sodium citrate treatments to yield gelatin-based microcarriers.

3.2.6.4 Summary

Overall, DAT- and gelatin-based microcarriers were fabricated through the drop-wise addition of DAT/alginate and gelatin/alginate solutions, respectively, to calcium chloride to crosslink the alginate phase within the composite microparticles. Following this, the collagenous phase within the particles was stabilized by non-cytotoxic photochemical crosslinking or by glutaraldehyde, as a control. Finally, the alginate phase within the microcarriers was liquefied and extracted through calcium ion chelation by sodium citrate, and repeated rinsing with divalent cation-free PBS. Figure 3.1 illustrates the overall methodology by which the microcarriers were produced.

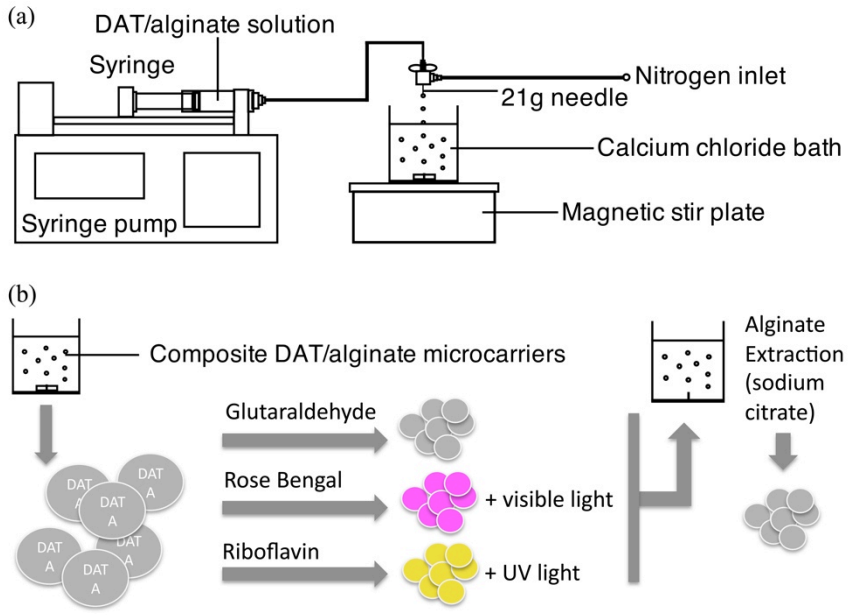

Figure 3.1: Overview of microcarrier fabrication.
(a) Composite microcarrier apparatus schematic. (b) Crosslinking and alginate extraction methodology.

3.2.7 Microcarrier Characterization

3.2.7.1 Scanning Electron Microscopy and Optical Microscopy

Scanning electron microscopy (SEM) was performed to examine the microcarrier architectures pre- and post-sodium citrate treatment. Microcarriers were also flash-frozen with

liquid nitrogen to enable individual microcarriers to be fractured, and the internal microarchitecture was imaged under SEM. Each microcarrier formulation was dried using supercritical CO_2, mounted onto an aluminum microscopy stud via adhesive carbon tape, pulse-coated with gold for 20 minutes, and observed under a JEOL JSM-840 microscope (working distance 15 mm, accelerating voltage 10 kV). Optical microscopy was also employed to visualize individual microcarriers before and after alginate extraction using a Zeiss Invertoskop 40C optical microscope and Axiovision Release 4.7.2 software (Carl Zeiss, Germany).

3.2.7.2 Alginate Fluorescence

Alginate extraction was further probed by fabricating microcarriers from solubilized DAT with sodium alginate solution pre-treated with a fluorescent dye [153], and the resulting microcarriers were observed before and after sodium citrate treatment under fluorescence microscopy. A 3% (w/v) sodium alginate solution was prepared and the pH was adjusted to 11.0 via drop-wise addition of 10 M NaOH. Fluorescein 5(6)-isothiocyanate (FITC) mixed isomers were dissolved in dimethylsulfoxide (DMSO) at a concentration of 1 mg/mL, and added to the alginate solution at a concentration of 0.025 mg FITC/mL. The mixture was agitated for 1 hour (150 RPM) at 40ºC, and then ammonium chloride (NH_4Cl) was added (50 mM final concentration). The FITC-infused alginate was used to fabricate composite DAT/alginate microcarriers using the previously described methods, with extensive rinsing in deionized water prior to visualization. Control DAT-based microcarriers without sodium citrate treatment, as well as pure alginate microcarriers with sodium citrate treatment, were fabricated to confirm the stability and specificity of the labeling over the time frame of the study. The microcarriers were imaged using a Zeiss AxioImager.M1 fluorescence microscope and Axiovision Release 4.7 software (Carl Zeiss, Germany).

3.2.7.3 Microcarrier Diameter and Size Distribution

Selected microcarrier formulations (3:2 and 4:3 parts solubilized DAT and 3% (w/v) alginate) were fabricated and crosslinked by i) glutaraldehyde, ii) rose bengal, or iii) riboflavin as previously described, and the alginate was extracted. From each formulation, microcarriers (n = 100) were selected at random and immersed in 5 mL of Ringer's simulated physiological fluid (8.6 mg/mL NaCl, 0.3 mg/mL KCl, 0.33 mg/mL $CaCl_2$) in individual 15 mL centrifuge tubes. Each sample was incubated under constant agitation (37°C, 55 RPM) for 28 days and photographed at time points of 0, 24, 48, and 72 hours, and 7, 14, 21, and 28 days using a Canon Powershot A640 AiAf 10.0 megapixel digital camera (macro setting) positioned at a height of 13.0 ± 0.1 cm above each sample. Mean diameters and size distributions of samples at each time point were determined from digital photographs using ImageJ (National Institute of Health, Bethesda, MD, USA) image analysis software. In brief, the Feret's diameters (n=100) were determined using ImageJ for each microcarrier formulation, and in turn used to calculate the mean diameter and respective standard deviation for each formulation, at each time point.

3.2.7.4 *In Vitro* Microcarrier Protein Release

In vitro protein release from microcarriers over time was assessed using the Bio-Rad Protein Assay, as previously described. A mass of 1,000 mg (wet weight) of each microcarrier formulation was suspended in 5 mL of Ringer's fluid within individual 15 mL centrifuge tubes. Samples were incubated at 37°C under constant agitation for 28 days (55 RPM). The Ringer's fluid was assayed for total protein content (n=1, N=3) after 24, 48, and 72 hours, and 7, 14, 21, and 28 days, with Ringer's fluid being replaced at each time point.

3.2.7.5 Microcarrier Swelling Behavior

To assess swelling behavior, microcarriers (n=100) of each 3:2 DAT/alginate and 4:3 DAT/alginate microcarrier formulation were randomly selected after alginate extraction, super-

critically dried, photographed, and weighed (dry weight, W_D). Each dried sample was incubated under constant agitation in 5 mL of Ringer's fluid (37°C, 55 RPM) for 24 hours, the fluid removed by pipette to prevent sample loss, and the microcarriers were blotted with filter paper prior to re-photographing and re-weighing (wet weight, W_W). This process was repeated at time points of 48 and 72 hours, 7, 14, 21, and 28 days.

Mean sample diameters (n=100) were determined using ImageJ software as previously described, and sample swelling ratios for each formulation were calculated as follows;

$$Swelling\ Ratio = \frac{\left(W_W - W_D\right)}{W_D}$$

3.2.7.6 Microcarrier Porosity

Approximations of DAT- and gelatin-based microcarrier percent porosity were determined through liquid displacement by comparing the volume displaced by a microcarrier sample before and after sodium alginate extraction. Composite DAT/alginate microcarriers (n~500) were immersed in 5 mL of deionized water and the change in volume was immediately recorded (ΔV_1) in triplicate (N=3). This process was repeated for the same microcarrier sample post-alginate extraction (ΔV_2). The mean difference in volume between the two samples was used as a measure of percent porosity for the DAT-based microcarriers, using the expression;

$$\%\ porosity = \left(\frac{\Delta V_1 - \Delta V_2}{\Delta V_1}\right) \cdot 100$$

Composite gelatin/alginate and gelatin-based microcarriers were similarly assessed in triplicate before and after alginate extraction (n~500, N=3) to estimate the percent porosity.

3.2.7.7 Microcarrier Sterility

Microcarrier sterility was confirmed by adding 10 mg (wet weight) of DAT-based microcarriers into each of 3 wells within a 6-well tissue culture plate and providing 3 mL of

DMEM:Ham's F12 nutrient mixture to each microcarrier-loaded well. This process was repeated for the gelatin-based microcarriers and the plate was incubated for 7 days (37°C, 5% CO_2) with DMEM:Ham's F12 being changed every 2-3 days. Following 7 days, the medium and beads were assessed using optical microscopy to detect signs of contamination. Conventional streaking of the medium following 7 days of culture was also performed in triplicate on nutrient agar-coated tissue culture plates, and examined following 3 days of incubation (37°C, 5% CO_2).

3.2.7.8 Microcarrier Injectability

Injectability of the DAT-based microcarriers was evaluated using a 1 mL BD (Becton, Dickinson and Company, USA) syringe equipped with hypodermic needles of different gauges. A quantity of 100 mg of microcarriers were suspended in 0.5 mL of PBS and tested for the ability to pass through needles ranging in gauge from 18 to 21. The beads were examined by optical microscopy, both before and after injection, to assess any damage or dimensional changes.

Upon identifying the smallest needle gauge capable of passing microcarriers without imparting structural damage, a second injection experiment was performed. A 250 mg sample of DAT-based microcarriers in a minimal volume of PBS was collected by filtration through a Whatman type I qualitative filter paper, and loaded into a 1 mL syringe equipped with an 18-gauge needle. Microcarriers before and after extrusion were imaged under SEM.

3.2.8 Statistical Analysis

As appropriate, data are expressed as means ± standard deviations (SDs). Statistical analyses were performed with the software program OriginPro 8.0 (OriginLab Corp., Northampton, MA, USA) to compare microcarrier diameter and protein release over time and between the different microcarrier formulations, by one-way ANOVA with a Tukey's post-hoc comparison of means. All differences were considered statistically significant at $p < 0.05$.

3.3 Results

3.3.1 Decellularization and Solubilization of Adipose Tissue

Immediately after harvesting, the adipose tissue appeared yellow in overall color due to the lipid-filled mature adipocytes comprising the majority of the tissue volume. Upon completion of the 5-day detergent-free decellularization protocol, the tissue appeared loose, white, and highly hydrated (Figure 3.2). Approximately 80-90% of the total mass of the hydrated DAT samples in PBS was attributed to the fluid phase.

Optimization of the acid/pepsin digestion protocols for solubilizing DAT showed that a pepsin concentration of 50 mg of pepsin/g DAT (wet weight) was sufficient to solubilize the DAT. Lower concentrations resulted in inefficient digestion, while there was no significant benefit determined for higher levels of the enzyme, which would be associated with a higher cost. Therefore, this concentration was selected for use in the fabrication of the DAT-based microcarriers. The initial volume of 10 mL of 0.5 M acetic acid/g DAT (wet weight) was lowered and optimized to a volume of 0.1 mL acetic acid/g DAT (wet weight) and used in the microcarrier fabrication. Overall, the developed solubilization protocols used a 500 mg pepsin/mL 0.5 M acetic acid digest solution, coupled with a 20-hour digestion period. The resulting solubilized DAT appeared yellow in color and slightly viscous (Figure 3.2), and could be easily extruded by syringe pump through a 21-gauge needle, to permit composite microcarrier fabrication.

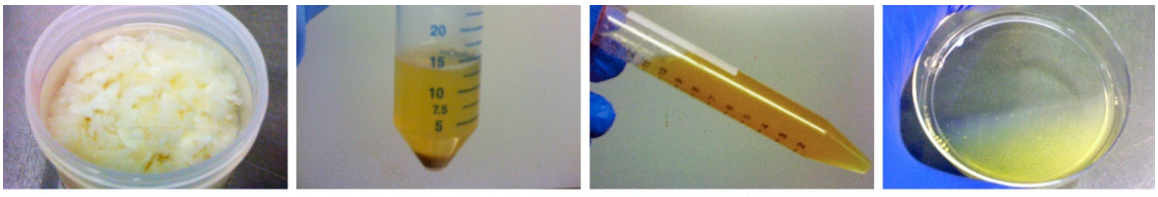

(a) (b) (c) (d)

Figure 3.2: Solubilization of decellularized adipose tissue.
(a) Decellularized adipose tissue (DAT). (b) DAT following 20-hour acid/pepsin digestion and centrifugation. (c) Solubilized DAT after the removal of residual pepsin and insoluble protein. (d) Viscous solubilized DAT ready for use in microcarrier fabrication.

Quantitatively, the total protein content of the DAT solutions prepared using the optimized solubilization protocol was determined to range from approximately 2-4 mg/mL in concentration. A sample calibration curve employed to calculate the relative total protein content to sample absorbance is shown in Appendix A. Solubilized DAT stored at 4°C was visually observed to be stable for at least 14 days, as confirmed by its use in the later fabrication of stable microcarriers.

3.3.2 Microcarrier Fabrication

In designing and assembling the spherical microparticle fabrication apparatus, all selected parts were either purchased as pre-sterilized disposables, or were reusable through autoclaving prior to each use. To permit the disruptive nitrogen jet to flow as desired over the needle during droplet extrusion, custom stainless steel tees were machined and evaluated during preliminary microcarrier fabrication, until an optimal design was achieved (Figure 3.3). Microcarrier fabrication using the apparatus developed, yielded spherical microdroplets, with the resulting microcarrier morphologies and diameters achieved remaining largely dependent on the solution extrusion flow rate and/or the disruptive nitrogen jet pressure.

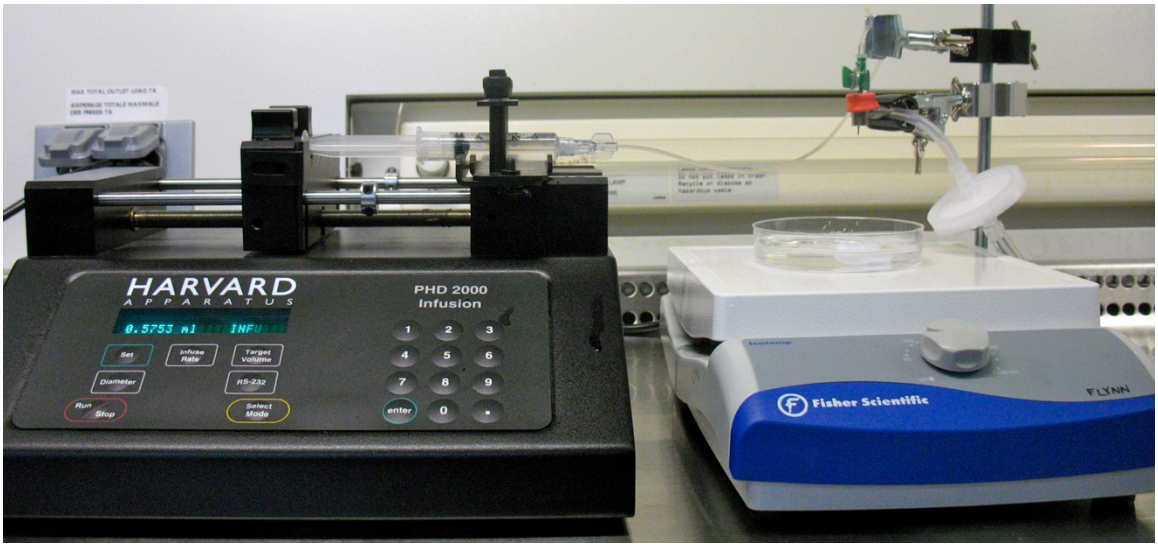

Figure 3.3: Custom-designed apparatus for the fabrication of sterile microparticles.

The concentration of the sodium alginate solutions, and the different volumetric ratios of solubilized DAT (or gelatin) to sodium alginate employed also impacted the overall ease of fabrication and the resulting microcarrier size, morphology, and stability. Initial microcarrier fabrication trials indicated that a minimum sodium alginate solution concentration of 1% (w/v) was required to facilitate adequate droplet gelation upon addition to the calcium chloride solution, with a minimum concentration of 3% (w/v) required to avoid non-spherical particle formation. Sodium alginate solution concentrations of 4% (w/v) combined with the solubilized DAT proved too viscous to permit microdroplet formation. Therefore, 3% (w/v) sodium alginate solution was selected for further investigation. Specifically, solubilized DAT (2-4 mg/mL total protein, as measured with the BioRad assay) and 50 mg/mL gelatin solutions were combined with 3% (w/v) sodium alginate solution in volumetric ratios of 3:2 and 4:3 parts collagenous material to alginate, and used to prepare composite microcarriers. Depending on the solution extrusion rate (0.10-0.45 mL/minute) and nitrogen jet pressure applied (5-15 psi), spherical composite DAT/alginate and gelatin/alginate microcarriers ranging in diameter from 750-2000 μm were obtained, with optimized conditions of 0.25 mL/minute and 5 psi selected to ensure consistency, uniformity, and reproducibility of the microcarriers produced.

Initial stabilization of 3:2 and 4:3 DAT/alginate microcarriers by the crosslinking agents glutaraldehyde, rose bengal, and riboflavin was confirmed by the persistence of the beads following alginate extraction with sodium citrate for 15 minutes, to yield DAT-based microcarriers with minimal residual alginate (Figure 3.4).

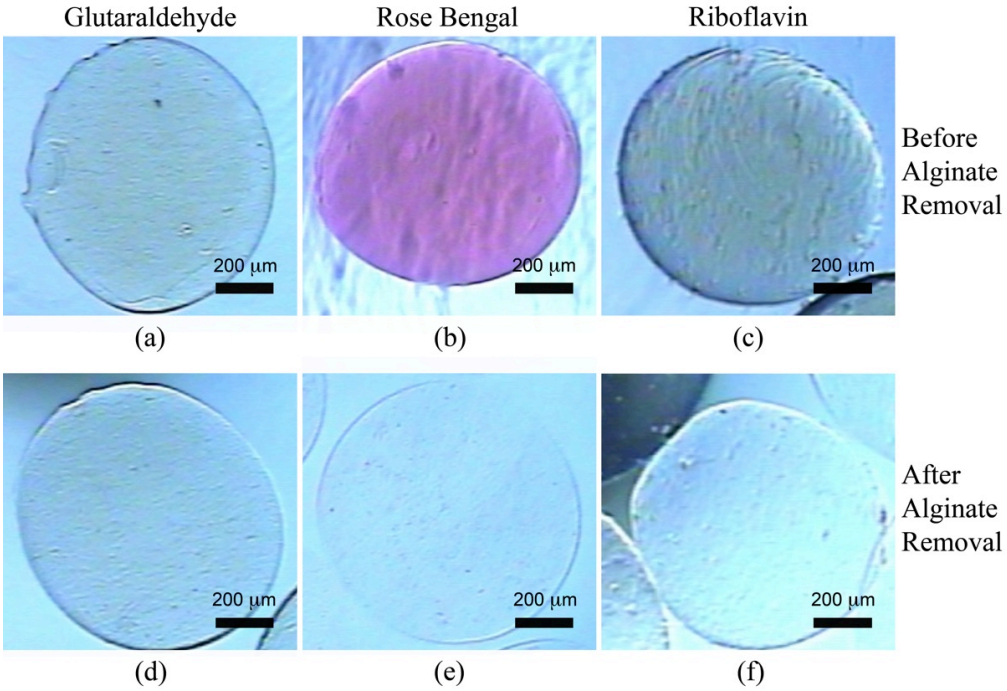

Figure 3.4: Representative DAT-based microcarriers before and after alginate extraction.
Prepared using a 3:2 DAT/alginate ratio, and viewed under optical microscopy, original mag. 20x. Glutaraldehyde, GTA; Rose bengal, RB; Riboflavin, Rib. (a) GTA DAT/alginate. (b) RB DAT/alginate. (c) Rib DAT/alginate. (d) GTA DAT. (e) RB DAT. (f) Rib DAT.

Qualitatively, the DAT-based microcarriers were spherical, colorless, and translucent in appearance, and were structurally robust enough to withstand routine manipulation with serological pipettes and tweezers. Optical microscopy confirmed adequate alginate removal from all formulations, with an alginate core evident if sodium citrate rinsing was < 10 min (Figure 3.5).

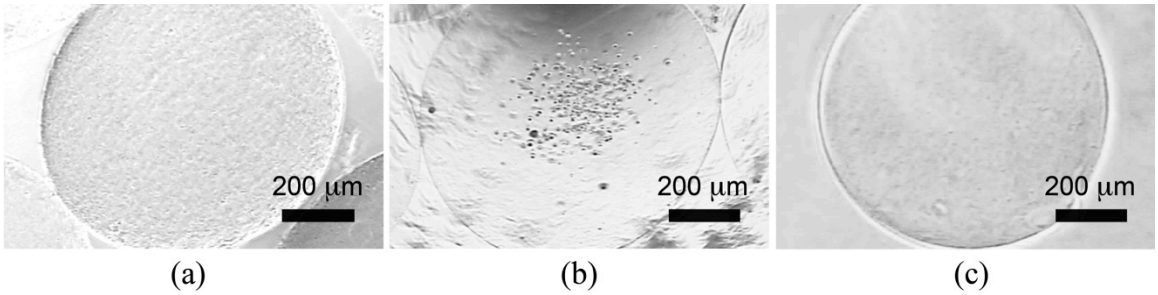

Figure 3.5: Representative DAT-based microcarriers.
Original mag. 20x. (a) DAT/alginate composite microcarrier post-RB crosslinking. (b) Visible alginate core during sodium citrate treatment. (c) DAT-based microcarrier post-alginate extraction.

Gelatin-based microcarriers (3:2 and 4:3 gelatin/alginate volumetric ratios) were also successfully stabilized by crosslinking with glutaraldehyde, rose bengal, and riboflavin, and were comparable in appearance and microstructure under optical microscopy and SEM after alginate extraction, supporting their use as a control for characterizing the DAT-based microcarriers.

Representative SEM images revealed a porous surface microarchitecture devoid of alginate for the DAT- and gelatin-based microcarriers, whereas microcarriers subjected to sodium citrate treatments < 10 minutes demonstrated residual alginate that appeared crystalline in microstructure under SEM (Figure 3.6). Representative SEM imaging of microcarriers flash-frozen and fractured post-alginate extraction revealed an inner porous and somewhat fibrous microstructure (Figure 3.6). Examination of the microcarriers fabricated with FITC-labeled sodium alginate solution pre- and post-sodium citrate treatment confirmed the efficacy of the alginate extraction protocols, as no appreciable fluorescence following sodium citrate treatments of > 15 minutes was apparent (Figure 3.6).

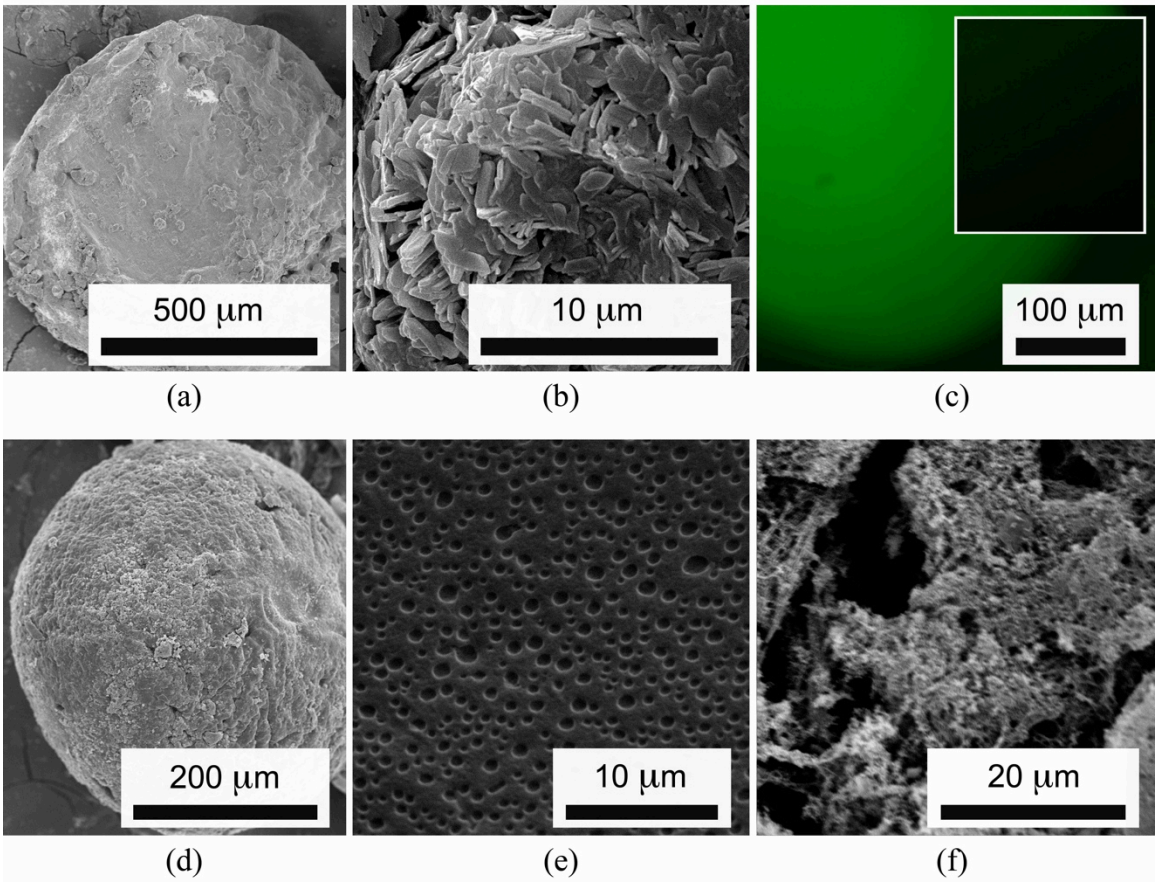

Figure 3.6: Representative images of DAT microcarriers produced.
(a) Composite DAT/alginate microcarrier under SEM. (b) Surface alginate under SEM. (c) Composite microcarrier with FITC-labeled alginate under fluorescence microscopy, insert shows microcarrier post-sodium citrate treatment. (d) Post-alginate extraction microcarrier. (e) Porous surface architecture. (f) Inner microstructure of fractured DAT microcarrier.

3.3.3 Microcarrier Diameter and Size Distribution

Following alginate extraction, the overall mean diameter for the DAT-based microcarriers was 934 ± 51 μm, while the overall mean diameter for the gelatin-based microcarriers was 967 ± 99 μm. Figure 3.7 compares the mean diameters for each DAT- and gelatin-based specific microcarrier formulation investigated.

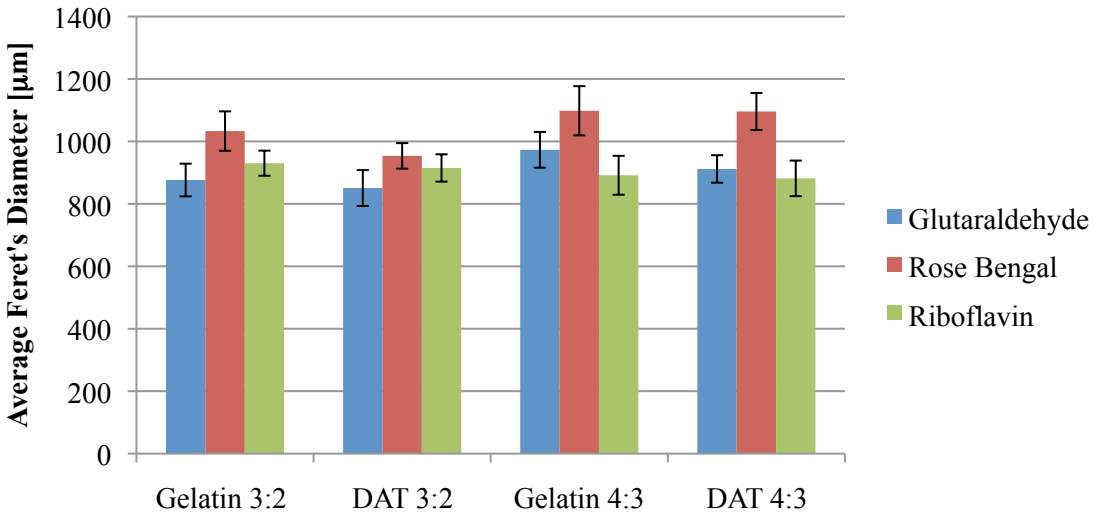

Figure 3.7: Microcarrier mean diameters (*n*=100) immediately after fabrication.
All data are expressed as the mean ± SD.

Overall, formulations crosslinked using rose bengal were found to have greater mean diameter values at time=0 than those formulations crosslinked with glutaraldehyde or riboflavin. For the DAT-based microcarriers assessed, the mean diameter of the 3:2 rose bengal-crosslinked microcarriers was found to be 954 ± 41 μm, while the mean diameters of the DAT-based microcarriers crosslinked by glutaraldehyde and riboflavin were 851 ± 58 μm and 915 ± 44 μm, respectively. DAT-based microcarriers formulated using a 4:3 volumetric ratio of DAT to alginate were found to have mean diameters of 1096 ± 59 μm, 912 ± 44 μm, and 882 ± 57 μm, for microcarriers crosslinked with rose bengal, glutaraldehyde, and riboflavin, respectively. Statistically speaking, all mean diameters at t=0 for the DAT-based microcarriers produced were significantly different from one another. For the gelatin-based microcarriers fabricated as a control, the rose bengal-crosslinked microcarriers also demonstrated greater mean diameter values than microcarriers stabilized using glutaraldehyde or riboflavin. Overall, the mean diameters recorded at t=0 remained between 850-1100 μm for all formulations investigated.

Microcarrier size distributions obtained by image analyses indicated that all microcarrier formulations demonstrated limited polydispersity, without employing sieves. Figure 3.8 shows a representative size distribution for a 3:2 rose bengal-crosslinked DAT-based microcarrier sample (n=100).

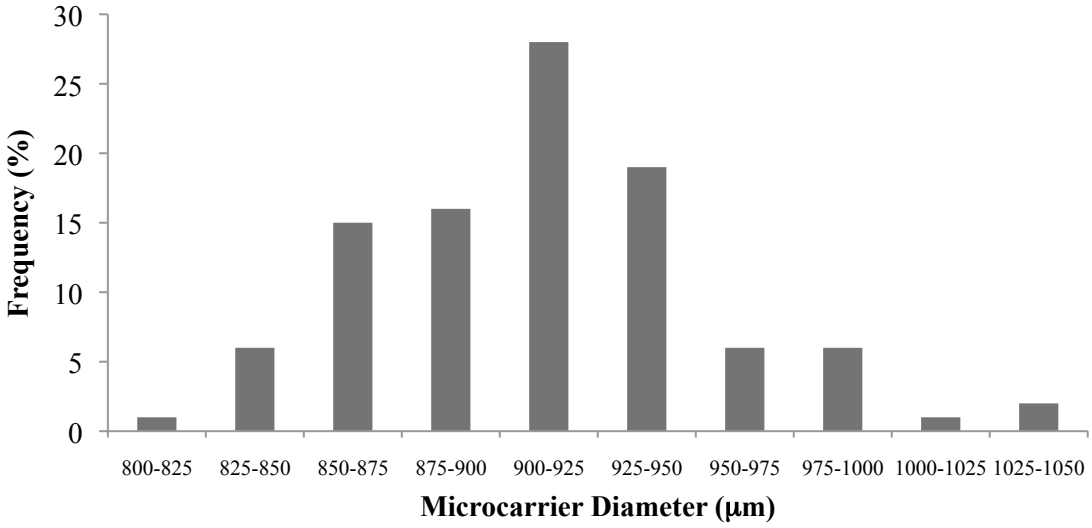

Figure 3.8: Representative size distribution.
For DAT-based microcarriers (n=100) crosslinked with rose bengal and fabricated using a DAT to alginate volumetric ratio of 3:2.

3.3.4 Microcarrier Stability and Swelling Behavior

To assess the *in vitro* stability of the glutaraldehyde-, rose bengal-, and riboflavin-crosslinked DAT-based microcarriers in a simulated physiological environment under constant agitation (37°C, 50 RPM) for 28 days, the mean diameter as a function of time for each DAT-based microcarrier formulation was determined and plotted as shown in Figure 3.9.

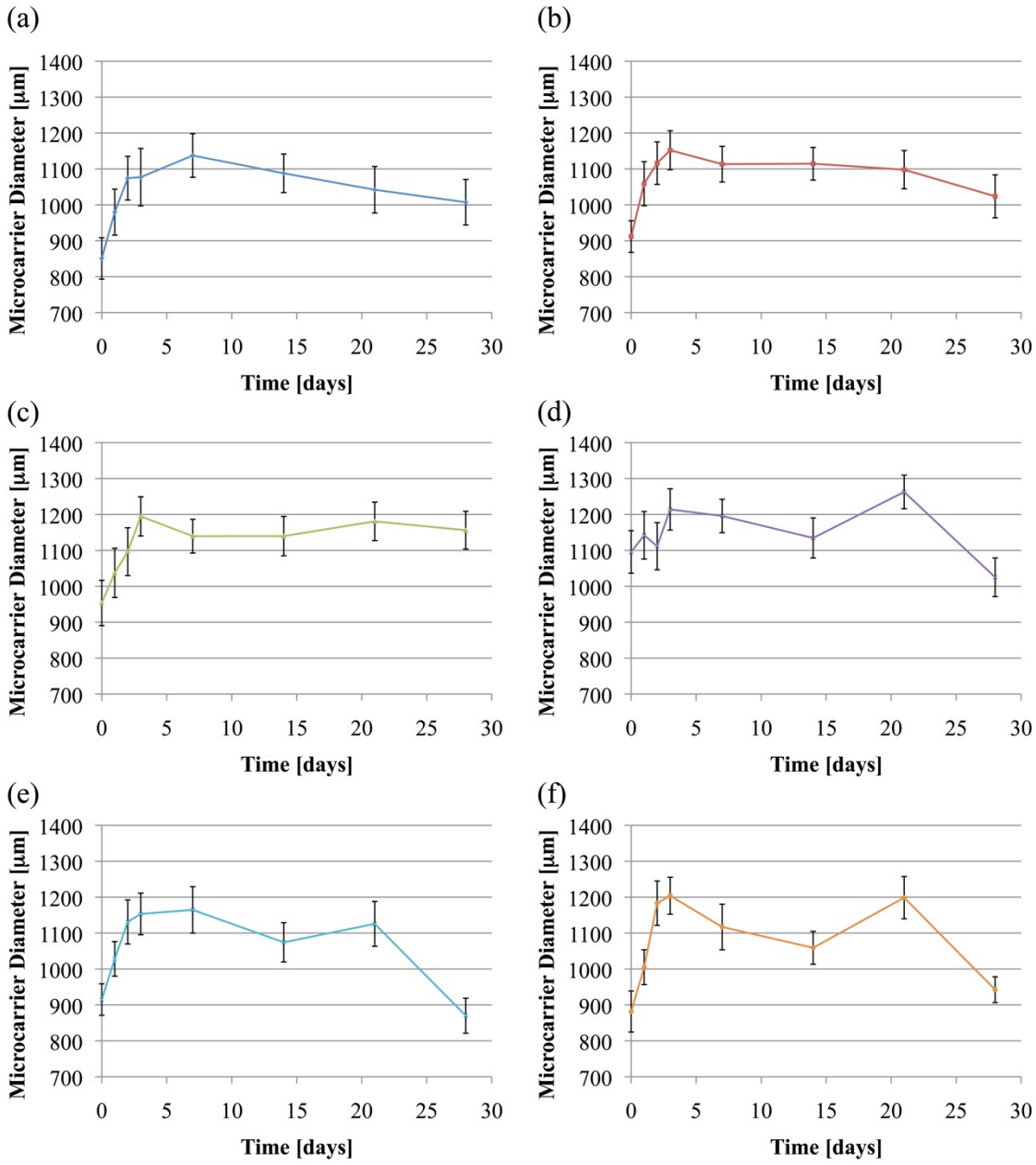

Figure 3.9: DAT-based microcarrier stability as a function of diameter over 28 days. Glutaraldehyde, GTA; Rose bengal, RB; Riboflavin, Rib. All data are expressed as the mean ± SD at each time point (n=100). (a) 3:2 GTA. (b) 4:3 GTA. (c) 3:2 RB. (d) 4:3 RB. (e) 3:2 Rib. (f) 4:3 Rib.

Analyses of the mean DAT-based microcarrier diameters as a function of time indicated that rose bengal-crosslinked DAT-based microcarriers, with a 3:2 volumetric ratio of solubilized

DAT to 3% (w/v) sodium alginate solution, demonstrated fewer significant changes in mean diameter over time than the riboflavin-crosslinked microcarriers. Furthermore, the 3:2 rose bengal-crosslinked DAT-based microcarriers had comparable changes in mean diameter to those microcarriers crosslinked with conventional glutaraldehyde as a control, without the associated cytotoxicity concerns of glutaraldehyde. Similarly, comparing the mean gelatin-based microcarrier diameters over time indicated that gelatin-based microcarriers crosslinked with rose bengal demonstrated fewer significant changes in diameter over 28 days, as compared to gelatin-based microcarriers crosslinked with riboflavin.

Differences in protein release for each formulation over time, as well as between different microcarrier formulations at each time point, were found to be statistically insignificant. Minimal protein release was observed from all formulations over the 28-day period, with protein release from each DAT-based microcarrier formulation remaining below 15 μg/mL under all conditions. Protein release from the 3:2 rose bengal-crosslinked microcarriers remained below 10 μg/mL at each time point (Figure 3.10).

In vitro protein release from the gelatin-based microcarrier formulations was also investigated in parallel with the DAT-based microcarriers over the 28-day stability study. For all conditions, protein released at each time point for all gelatin-based microcarrier formulations remained below 25 μg/mL, with the protein release from 3:2 gelatin-based microcarriers crosslinked with rose bengal remaining below 20 μg/mL at all time points.

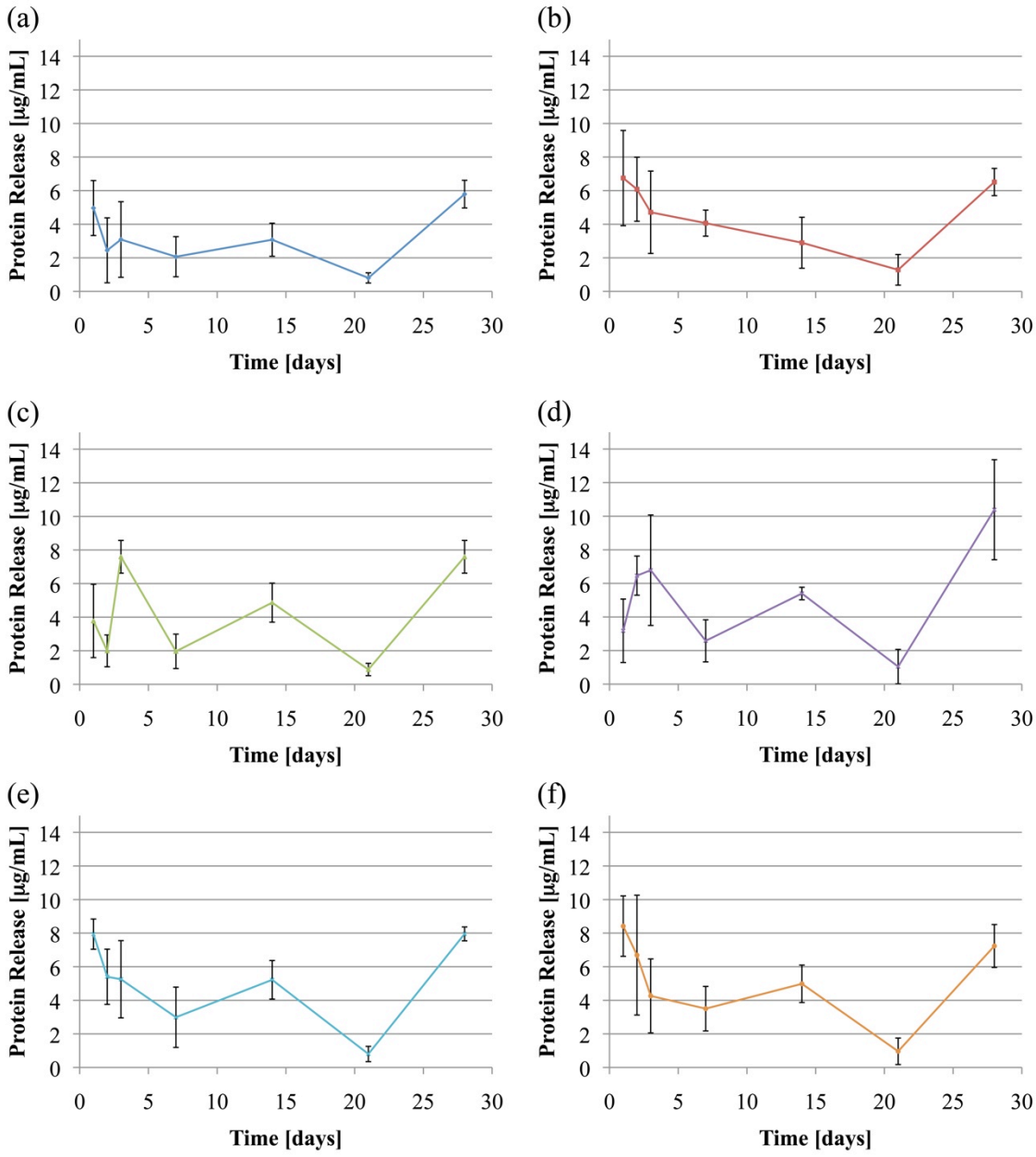

Figure 3.10: *In vitro* protein release from DAT-based microcarriers over 28-days.
Glutaraldehyde, GTA; Rose bengal, RB; Riboflavin, Rib. All data are expressed as the mean ± SD at each time point. (a) 3:2 GTA. (b) 4:3 GTA. (c) 3:2 RB. (d) 4:3 RB. (e) 3:2 Rib. (f) 4:3 Rib.

Microcarriers dehydrated by supercritical drying prior to equilibration in Ringer's fluid for diameter and protein release analyses over 28 days demonstrated no significant changes in the mean microcarrier diameters beyond 72 hours. Therefore, it was assumed that equilibrium swelling had been reached within 72 hours, and the weight of each microcarrier formulation at t=72 hours was used to calculate the weight-based swelling ratios (Table 3.2).

Table 3.2: Weight-based swelling ratios for microcarrier formulations investigated.

Crosslinking Agent	Microcarrier Formulation	Swelling Ratio (t=72 hours)	Microcarrier Formulation	Swelling Ratio (t=72 hours)
Glutaraldehyde	3:2 DAT/alginate	12	3:2 Gelatin/alginate	20
	4:3 DAT/alginate	15	4:3 Gelatin/alginate	13
Rose Bengal	3:2 DAT/alginate	**9**	3:2 Gelatin/alginate	19
	4:3 DAT/alginate	15	4:3 Gelatin/alginate	13
Riboflavin	3:2 DAT/alginate	14	3:2 Gelatin/alginate	14
	4:3 DAT/alginate	12	4:3 Gelatin/alginate	11

While the calculated swelling ratios for each formulation represent approximated values due to intrinsic experimental variability, it is noteworthy that the 3:2 rose bengal-crosslinked formulation demonstrated the lowest swelling ratio. Furthermore, pre-drying of the microcarriers did not significantly impact the final mean microcarrier diameter values after 28 days, or protein release from microcarriers observed over 28 days in a simulated physiological environment. Overall, protein release for all rehydrated DAT-based microcarriers remained below 15 μg/mL at all time points, and for those DAT-based microcarriers fabricated using a 3:2 volumetric ratio and crosslinked by rose bengal, protein release at all time points remained below 10 μg/mL. For the rehydrated gelatin-based microcarriers, all protein release over 28 days remained below 25 μg/mL.

3.3.5 Microcarrier Porosity

As 3:2 DAT/alginate microcarriers crosslinked by rose bengal were determined to be more stable than the riboflavin-crosslinked microcarriers, and comparable in stability to the

glutaraldehyde-crosslinked microcarriers yet non-cytotoxic, this formulation was selected for further characterization. As measured by liquid displacement, these 3:2 rose-bengal crosslinked DAT-based microcarriers were shown to have a porosity of 29 ± 4%. Similarly, gelatin-based microcarrier porosity, as approximated by liquid displacement, was found to be 28 ± 9%.

3.3.6 Microcarrier Sterility and Injectability

Sterility using the described fabrication protocols was confirmed for all samples. Macroscopically, no changes in medium color or odor were observed, and there was no evidence of bacterial, fungal or yeast contamination on microcarrier surfaces under optical microscopy. During injection testing, the microcarriers were successfully passed through an 18-gauge needle, without impacting structural integrity, size, or shape. SEM imaging of representative DAT-based microcarriers pre- and post-extrusion from the 18-gauge needle are shown in Figure 3.11.

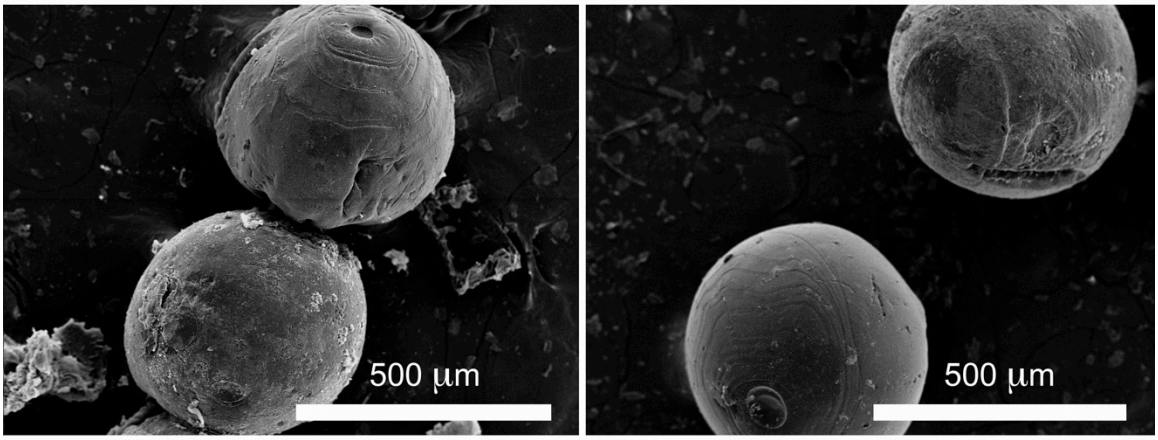

Figure 3.11: Representative SEM images of 3:2 RB-crosslinked DAT-based microcarriers. (a) before extrusion and (b) after extrusion, from an 18-gauge hypodermic needle. Samples were dried before SEM imaging resulting in comparable shrinkage of all microcarriers.

Higher needle gauges investigated (up to 21-gauge) showed indications of some structural and/or morphological damage to the extruded microcarriers.

3.4 Discussion

The DAT solubilization and microcarrier fabrication protocols developed in this work produced stable, non-cytotoxically crosslinked, porous matrix-derived microcarriers, ultimately yielding novel sterile and injectable tissue-engineering scaffolds. These methods could be extended to produce microcarriers from matrices derived from other native tissue sources, thereby creating a range of customized microcarriers tailored toward individual cell types, eliciting tissue and/or lineage-specific regenerative responses. Any tissue that can be effectively decellularized has the potential to be processed in this manner. Expanding the concept of tissue-specific ECM-derived microcarriers could initiate the production of many potentially clinically-translatable treatments for a wide range of diseases, from diabetes to cancer.

In general, microcarriers may be designed to incorporate specific material and surface properties, ultimately contributing to the regenerative response [130]. The use of biodegradable synthetic and/or naturally-derived materials has the advantage of eliminating the need to enzymatically extract the cells following culture [132]. As a result, these types of microcarriers have become central to many tissue-engineering approaches, being directly incorporated within the overall regeneration strategies. The material properties modulate the cell response, similarly to the native ECM *in vivo* [154]. Microcarriers capable of mediating cell responses in a more controlled manner have been developed through adjusting properties including chemical composition, surface topography, size, charge density, and/or porosity [15, 130, 131].

To this end, synthetic biopolymers have advantages in terms of controlled composition and tunability, avoiding the batch-to-batch variations that can be associated with naturally-derived materials [147]. Many groups have focused on the development of porous PLA- and PLGA-based microcarriers modified with RGD or TGF-β_1 to promote cell attachment and growth combined with biodegradability *in vivo* [124, 142-144, 155]. A number of commercially-available

microcarrier substrates have also been developed using synthetic and/or composite materials including chemically-modified dextran (Cytodex 1 and Cytodex 2, Amersham Biosciences, Sweden; Hillex, SoloHill, USA) [135-137], denatured collagen-coated dextran (Cytodex 3, Amersham Biosciences, Sweden) [135, 138, 139], denatured collagen-coated plastic (PlasticPlus, SoloHill, USA) [135, 156], surface-modified cross-linked cotton cellulose (Cytopore 1, Amersham Biosciences, Sweden) [126], and poly(ethylene)/silica (Cytoline 2, Amersham Biosciences, Sweden) [130, 140]. However, despite large flexibility in material design, and convenient availability of the synthetic base materials, the incorporation of bioactive and/or naturally-derived molecules is necessary to facilitate more normal cell-matrix interactions, which are key to mediating cell behavior [128].

Materials obtained from natural tissues are attractive for use in fabricating tissue-engineering scaffolds, based on their inherent similarities to the native ECM [7]. *In vivo*, the ECM is comprised of a complex mixture of proteinaceous fibers interwoven with glycoproteins and proteoglycans [119]. The ECM is dynamic and multifunctional, not only imparting structural integrity to tissues, but also modulating cell migration, morphology, apoptosis, and cytokine secretion, amongst other responses [157]. Adhesion of cells to the ECM is essential for normal cell development, growth, and differentiation, in addition to achieving tissue maintenance and organization [158]. Variations in relative amounts of ECM macromolecules and their organization give rise to specific tissue characteristics [61], and the incorporation of naturally-derived ECM materials within tissue-engineering scaffolds, as a means to recapitulate the native environment, can significantly contribute to the overall regenerative response [104].

Toward this goal, microcarriers fabricated from a variety of naturally-derived materials have been developed for use as cell culture substrates within tissue-engineering strategies [7, 89, 128]. A number of commercially-available microcarriers have been prepared from crosslinked

porcine gelatin (Cultispher G and Cultispher S, Percell Biolitica, Sweden) and crosslinked bovine collagen type I (Cellagen, MP Biomedicals, USA), yielding promising results in short-term seeding and cell culturing studies [130, 141]. However, these xenogenically-sourced collagenous microcarriers are not yet approved for clinical use. Microcarriers fabricated in the laboratory have employed a wide range of naturally-derived materials including RGD-peptide modified alginate [145], modified chitosan [159, 160], bFGF-loaded gelatin [148], small intestinal submucosa [103], and ECM-derived gels [146]. Chaubey *et al.* (2008) investigated the impact of varying collagen type I and laminin concentrations on bone marrow-derived mesenchymal stem cells, showing that cell behavior and/or fate could be directly affected by altering laminin densities [73]. However, only varying degrees of success have been achieved, with the 'ideal' biomaterials for tissue-engineering microcarriers for each application remaining to be established [128].

In developing the microcarrier fabrication protocols, alternatives to the acid/pepsin solubilization of the DAT were explored to permit the fabrication of DAT into uniform microspheres. In one approach, samples of DAT were flash frozen with nitrogen, ground into a powder using a custom ball mill, and lyophilized, to produce a fine powderized form of DAT. This powderized DAT was in turn rehydrated with deionized water, to yield a DAT-based slurry. The polydispersity of the DAT particles, combined with their aggregation in solution, prohibited stable bead formation. In the final approach, combining breast and abdominal adipose tissues sourced from multiple patients reduced the variability of the isolated matrices, thereby yielding a more consistent range in the total protein content between batches, and allowing for the fabrication of more reproducible microcarriers. It is anticipated that this reduced variability in scaffold composition will also be beneficial in terms of obtaining a more uniform cell response.

Protocols investigating the stability of uncrosslinked microcarriers and films fabricated from solubilized DAT proved largely unstable beyond 72 hours. Therefore, a method for

stabilizing the DAT phase via crosslinking was required. Glutaraldehyde is commonly employed as a highly effective chemical crosslinking agent for collagenous materials, but it is relatively cytotoxic, raising concerns with clinical applicability [161]. Therefore, the effective crosslinking of DAT via less initially cytotoxic photochemical crosslinkers was a primary focus of this work. Many photosensitive dyes, such as rose bengal, are effective for crosslinking collagen [91] and are currently approved for specific clinical applications [99]. In this study, the stabilization of the DAT-based microcarriers was confirmed over a 28-day period. Microcarriers were subjected to agitation speeds greater than 45 RPM, to assess the ability of DAT-based microcarriers to withstand long-term culture in spinner flasks or other dynamic culture systems under typical operating conditions [150, 162, 163]. Additionally, microcarriers were immersed in a simulated physiological environment, and maintained at body temperature (37°C) during agitation, to model short-term microcarrier stability. Based on measured changes in mean diameter over time, DAT-based microcarriers crosslinked with rose bengal demonstrated comparable stability to those crosslinked with glutaraldehyde.

Overall, of the two non-cytotoxic photochemical crosslinkers investigated, rose bengal was found to yield more stable microcarriers, with respect to changes in microcarrier diameter over time. Protein release measurements from all microcarrier formulations over 28 days indicated no significant microcarrier degradation, confirming microcarrier stability within this simulated physiological environment. Additionally, photochemically-crosslinked microcarriers stored at 4°C in Ringer's buffer were visually observed to be stable for at least 6 months. Swelling behavior also indicated no significant impact on DAT-based microcarrier stability or size as a result of initially drying the microcarriers for storage at room temperature. The ability to easily rehydrate the DAT-based microcarriers has significant logistical advantages for employing

these scaffolds in a clinical setting. Specifically, DAT-based microcarriers could be fabricated at a centralized location and dehydrated prior to distribution, potentially extending shelf life.

Confirmation of effective alginate removal from composite microcarriers following crosslinking of the DAT phase was another focus of this work, as alginate may inhibit cell attachment [164], and could thereby influence cell proliferation and/or differentiation. Results clearly confirmed the efficacy of the finalized alginate extraction protocols. The porous microstructure achieved, as observed via SEM imaging and estimated by liquid displacement, may be beneficial in facilitating cell attachment during culture, as well as nutrient delivery within the dynamic system.

The methods in the current study were developed with a view to the clinical applicability of the overall approach. More specifically, sterility investigations confirmed the absence of bacterial, fungal, and/or yeast contamination without the use of antibiotics or antimycotics. In addition, 18-gauge needles, which are commonly used in the clinic, were shown to permit microcarrier injectability in this study. Overall, the potential exists for DAT-based microcarriers to be delivered subcutaneously by injection in a clinical setting.

Subsequent studies discussed in Chapter 4 concentrate on probing the cell response to DAT-based microcarriers, with particular focus on assessing the potential for DAT-based microcarriers to contribute to ASC commitment along the adipogenic lineage. The ability for DAT-based microcarriers to support ASC proliferation and differentiation could translate to a clinically-relevant, tissue-specific, injectable product for the treatment of small-scale soft tissue defects, or potentially be applied as a cell delivery vehicle in composite larger-volume constructs, for use in a wide range of soft tissue repair strategies.

Chapter 4

Proliferation and differentiation of adipose-derived stem cells on decellularized adipose tissue-based microcarriers

4.1 Introduction

The development of a minimally-invasive adipose tissue regenerative approach, capable of restoring function and appearance to damaged subcutaneous tissues, while minimizing the potential for immune response *in vivo*, would greatly enhance clinical outcomes in reconstructive and cosmetic surgeries [6]. To date, a variety of injectable constructs, including microcarriers, have been investigated for use in adipose tissue-engineering strategies, as reviewed in Chapter 2.

Clinical approaches for the repair of soft tissue defects have focused largely on the temporary restoration of volume, rather than on the regeneration of functional and stable tissues [34]. Injectable products for small-volume augmentation procedures have employed a range of synthetic and naturally-derived materials including poly(lactic acid) (PLA), poly(tetrafluoroethylene) (PTFE), collagen, hyaluronic acid, and autologous fat and dermal tissues [11]. However, significant disadvantages exist for each approach, with long-term subcutaneous defect repair remaining an unsolved problem [9].

With the objective of regenerating functional adipose tissue, numerous tissue-engineering studies have investigated a variety of cell-seeded scaffold-based strategies [6, 9, 82]. From the perspective of injectable delivery, great promise lies in the use of microcarriers as scaffolds, given their potential role as not only a three-dimensional (3-D) dynamic cell culture substrate, but also as a directly injectable cell delivery vehicle [128]. A number of approaches to date have investigated microcarriers fabricated from materials such as poly(lactic-co-glycolic acid) (PLGA), dextran, alginate, gelatin, and collagen, for use in the dynamic culture of adipose-

derived stem cells (ASCs) [124, 127, 135, 141, 143, 145, 149, 150, 165, 166]. Varying degrees of success have been demonstrated during these short-term studies. Promisingly, the microcarriers investigated have shown potential for the support of ASC proliferation, and *in vitro* adipogenic differentiation upon induction with exogenous differentiation factors. In particular, work by Rubin *et al.* (2007) investigating ASC response to CultiSpher G commercially-available microcarriers made from crosslinked porcine-derived gelatin indicated significant ASC expansion within a spinner flask environment [141]. However, the microcarrier approaches to date have not resulted in the appreciable formation of stable adipose tissue *in vivo*, and significant challenges in obtaining clinical approval for xenogenic products, such as the CultiSpher line, restrict their use to *in vitro* applications [6]. Moreover, limited work has investigated the development of a tissue-specific microcarrier for use in adipose tissue engineering that could modulate the cell response exhibited by seeded ASCs such that adipogenesis is enhanced.

ASCs represent an abundant and highly proliferative multipotent stem cell population that can be isolated from otherwise discarded tissues [7]. Interestingly, ASCs have been shown to suppress histocompatibility antigen expression *in vitro*, potentially reducing the *in vivo* immunogenic response, and rendering both autologous or allogenic sources as promising for clinical use [35]. Moreover, adipose tissue-engineering research points to the ability of ASC-seeded scaffolds to positively contribute to the adipogenic response [167]. Therefore, the ability to obtain primary ASCs on a clinically-relevant scale through *in vitro* expansion methods, such as seeded microcarriers, is essential to facilitate the widespread therapeutic use of ASCs [8, 120-122].

Conventional culturing techniques depend largely on the expansion of cells in a 2-D environment on tissue culture poly(styrene) (TCPS) [168]. However, there are significant disadvantages to this approach, including altered cell morphology, the decreased differentiative

capacity of ASCs following multiple passages *in vitro*, and the differences in the extracellular matrix (ECM) secreted by 2-D cultured ASCs relative to the complex 3-D matrix of native tissues [38, 139, 169]. *In vivo*, ASCs organize ECM proteins to form the natural adipose tissue scaffold, or matrix [169]. In response, the ECM environment plays a critical role in mediating normal cellular behavior and tissue organization [59].

Through designing tissue-specific, custom-fabricated microcarriers, engineered to mimic the native adipose ECM, a highly adipogenic microscaffold may be achievable. Methods have been successfully developed, as described in Chapter 3, for the fabrication of tissue-specific microcarriers from decellularized adipose tissue (DAT). The third chapter described the design and characterization of these DAT-based microcarriers, produced in the laboratory using non-cytotoxic reagents.

DAT-based materials may provide ideal scaffolds for adipose tissue engineering. While the decellularization process is effective at removing cellular components, nucleic acids, and lipids from the tissues, the native adipose matrix (or scaffold) is well preserved, including the endogenous structural protein composition and architecture [14]. Promisingly, DAT has demonstrated inductive capabilities for the expression of the key genes that regulate adipogenesis, peroxisome proliferator activated receptor γ (PPARγ) and CCAAT/enhancer binding protein α (C/EBPα) [14]. This research highlights the ability of the ECM to mediate the cell response, and points to the potential of implementing tissue- and/or cell-specific matrices. Overall, employing a DAT-sourced scaffold could potentially promote a stronger adipogenic response in seeded or host-derived ASCs.

To date, no work has investigated the response of ASCs on fully decellularized tissues combined with a tailored scaffold microgeometry, more specifically, microcarriers. The first

objective of the work described in this chapter was to develop seeding protocols and operating parameters for the dynamic culture of human ASCs (hASCs) on DAT-based microcarriers within a CELLSPIN (Integra Biosciences, Chur, Switzerland) spinner flask system. Three different dynamic culturing protocols were designed, performed, and evaluated, using fluorescence cell imaging and quantification of total double stranded (ds) deoxyribonucleic acid (DNA), to assess the proliferation of hASCs on DAT-based microcarriers over time.

Following initial seeding studies, a dynamic *in vitro* culturing study investigating the proliferation and the adipogenic differentiation of hASCs on DAT-based microcarriers within the CELLSPIN system was conducted. Prior to inducing differentiation, the hASCs proliferated for 14 days on the DAT-based microcarriers, and the total dsDNA content was measured to confirm an elevated cell count. The adipogenic differentiation of the hASCs on the DAT-based microcarriers was then characterized over a 14-day period via intracellular lipid visualization and quantification of glycerol-3-phosphate dehydrogenase (GPDH) activity, an enzyme involved in triacylglycerol synthesis that is up-regulated during adipogenesis.

4.2 Materials and Methods

4.2.1 Materials

All chemicals were purchased from Sigma-Aldrich Canada Ltd. (Oakville, ON, Canada) unless otherwise stated, and were used as received.

4.2.2 Procurement of Adipose Tissue

Freshly-excised breast or subcutaneous abdominal adipose tissue samples were obtained from female patients undergoing elective reduction mammoplasty or abdominoplasty at either the Kingston General Hospital or the Hotel Dieu Hospital in Kingston, ON, Canada. Within 45 minutes of harvesting, the human adipose tissue samples were transported to the laboratory on ice

in a sterile transport solution comprised of divalent cation-free phosphate buffered saline (PBS) (Fisher Scientific, Ontario, Canada) with 20 mg/mL bovine serum albumin (BSA). Patient age, weight, and height were recorded for each sample, in addition to the original anatomical location from which the tissue was sourced (breast versus abdomen). The required research ethics board approval from Queen's University was obtained for this research (REB No. CHEM-002-07).

4.2.3 Isolation and 2-D Culture of Human Adipose-Derived Stem Cells

Human ASCs were isolated from the adipose tissue samples within 2 hours of their procurement, according to established methods [119]. Approximately 10 g of adipose tissue was finely minced, and excess fibrous tissue, blood vessels, and cauterized portions were discarded. A collagenase digest solution was prepared by combining and sterile-filtering 3 mM glucose, 2 mg/mL collagenase type II, and 25 mM HEPES in Kreb's Ringer Buffer (KRB) solution through a 0.22 μm pore Millex GP Syringe Driven Filter Unit (Millipore Express PES Membrane, Millipore, Carrigtwohill, Ireland). This filtrate was combined with 35% sterile BSA solution to achieve a concentration of 20 mg/mL, and warmed to 37°C before being added to the minced adipose tissue in a sterile 50 mL centrifuge tube. Finally, the tissue was permitted to digest for 45 minutes at 37°C under agitation (100 RPM).

Following digestion, the sample was filtered through a 250-μm pore stainless steel filter into a new 50 mL centrifuge tube, and permitted to gravity separate for 5 minutes. The resulting upper layer comprised of buoyant mature adipocytes was removed by aspiration, to yield the bottom layer containing the adipose-derived stem cell (ASC) population within the stromal vascular fraction (SVF). The collagenase was inactivated by adding an equal volume of Dulbecco's Modified Eagle's Medium and Ham's F-12 (DMEM:Ham's F-12) nutrient mixture supplemented with 10% fetal bovine serum (FBS) and 1% Pen/Strep (100 U/mL penicillin and 0.1 mg/mL streptomycin). Next, the sample was centrifuged at 1200 x *g* for 5 minutes, and the

supernatant was discarded. The remaining cell pellet was resuspended in 20 mL of erythrocyte lysing buffer (0.154 M ammonium chloride, 10 mM potassium bicarbonate, and 0.1 mM ethylenediaminetetraacetic acid (EDTA) in sterile deionized water) and agitated gently by hand for 10 minutes at room temperature. The sample was recentrifuged at 1200 x *g* for 5 minutes, the supernatant discarded, and the cell pellet resuspended in 20 mL of complete medium (DMEM:Ham's F-12 supplemented with 10% FBS and 1% Pen/Strep). This cell suspension was filtered through a 100-μm pore size nylon mesh, centrifuged at 1200 x *g* for 5 minutes, the supernatant discarded, and the cell pellet again resuspended in 20 mL of complete medium. Following an additional wash in complete medium, the cell pellet was finally suspended in complete medium and used to seed T-75 tissue culture polystyrene (TCPS) flasks (Corning, NY, USA) at a density of approximately 2 x 10^6 cells/flask. Complete medium was added to yield 15 mL medium/flask.

The seeded flasks were incubated at 37°C and 5% CO_2 for 24 hours to permit cell attachment, after which the medium was aspirated and the growth surface rinsed with sterile divalent cation-free PBS to remove cellular debris and unattached cells. During 2-D static culture, each T-75 flask was provided with fresh complete medium at a working volume of 15 mL every 2-3 days until the proliferating hASCs reached 80% confluence. At this time, the hASCs were passaged by trypsin-release using 0.25% trypsin/0.1% EDTA (Gibco®, Invitrogen, Burlington, ON, Canada), and replated at an approximate density of 2 x 10^6 cells/flask. For the purposes of the seeding experiments and differentiation studies, passage 2 (P2) hASCs were employed.

4.2.4 Decellularization of Adipose Tissue

Samples of adipose tissue were subjected to a detergent-free decellularization protocol, as detailed in Chapter 3 [14]. Adipose tissue samples were cut into 20-25 gram sections, and processed using a 5-day protocol incorporating mechanical disruption, polar solvent extraction in

isopropanol, and enzymatic digestion (trypsin/EDTA, DNase, RNase, and lipase). All decellularization solutions were supplemented with 1% antibiotic/antimycotic (ABAM) (Invitrogen, Burlington, ON, Canada) and 0.27 mM phenylmethylsulfonylfluoride (PMSF) solution, and incubated under constant agitation during processing (37°C, 150 RPM). The resulting decellularized adipose tissue (DAT) was stored in 70% (v/v) aqueous ethanol at 4ºC.

4.2.5 Solubilization of Decellularized Adipose Tissue

As detailed in Chapter 3, DAT samples sourced from multiple patients ($n=5$) and ranging in mass, were pooled to reduce batch variability. Each collective DAT sample (20-40 g) was decontaminated with three 30-minute rinses in 70% (v/v) aqueous ethanol at room temperature under constant agitation (55 RPM). Following decontamination, the DAT was aseptically rehydrated by three 30-minute sterile washes in PBS, and excess fluid was removed by aspiration. The DAT was then incubated in sterile 0.5 M acetic acid for 30 minutes at 37°C under constant agitation (150 RPM). Excess fluid from the acid-treated DAT was removed by aspiration and a 500 mg/mL pepsin/acetic acid slurry was added to the tissue at a concentration of 0.1 mL/g DAT (wet weight). Finally, the DAT was digested for 20 hours at 37ºC under constant agitation (150 RPM), and the pepsin was inactivated by drop-wise addition of 10 M sodium hydroxide (NaOH). Insoluble proteins and residual pepsin were removed by centrifugation (15,000 x *g*, 30 minutes, 4ºC) and the solubilized DAT was stored sterilely at 4ºC.

4.2.6 Microcarrier Fabrication

DAT-based microcarriers were fabricated according to the optimized protocol described in the previous study, using a volumetric ratio of 3 parts solubilized DAT to 2 parts 3% (w/v) sodium alginate solution, and stabilized through rose bengal photochemical crosslinking.

Composite DAT/alginate microcarriers were produced using an aseptic air-jet droplet

technique. Solubilized DAT (DATsol) was combined with sterile 3% (w/v) sodium alginate solution in a 3:2 v/v ratio and thoroughly mixed by agitation (150 RPM, 5 minutes) at 37ºC. The resulting DATsol/alginate mixture was added drop-wise to sterile 1.5% (w/v) calcium chloride solution using a blunt-ended, 21-gauge Punctur-Guard® winged intravenous infusion set (ICU Medical, Inc., Vernon, CT, USA) and a PHD 2000 Infusion syringe pump (Harvard Apparatus Inc., South Natick, MA, USA), at a rate of 0.25-0.30 mL/min in the presence of a compressed nitrogen jet (5 psi) to reduce the droplet size.

The composite microcarriers were stabilized by non-cytotoxic crosslinking using rose bengal photosensitizing solution and visible light exposure for 8 hours. The stabilized microcarriers were treated with 50 mM sodium citrate for 15 minutes, rinsed with divalent cation-free PBS, and stored at 4ºC. Sterile 50 mg/mL gelatin solution was prepared and gelatin-based porous microcarriers were fabricated using identical methods as for the DAT-based microcarriers.

4.2.7 Culturing System Preparation

To assess the cell response of hASCs on DAT-based microcarriers in a 3-D dynamic culturing environment, a CELLSPIN spinner flask system (Integra Biosciences, Chur, Switzerland), equipped with two 250 mL and two 500 mL volume spinner flasks, was employed (Figure 4.1). The CELLSPIN system permits low shear mixing via 2 glass pendula within each flask, magnetically driven by the stirring platform upon which the flasks rest. This platform is connected to a control unit that permits tight regulation over stirring speed and pause intervals during cell seeding and culturing. Additionally, the flask contents are easily sampled during experiments via serological pipettes.

In the culturing experiments described herein, two spinner flasks were designated for the dynamic culture of hASCs on DAT-based microcarriers, while the remaining two spinner flasks were used for the dynamic culture of hASCs on gelatin-based 3-D control microcarriers. The 500

mL spinner flasks were used for the dynamic culture of fluorescently-labeled hASCs under dark conditions, while the 250 mL volume spinner flasks were employed in the dynamic culture of unlabeled hASCs for DNA quantification or GPDH enzyme activity studies (Figure 4.1). Prior to each experiment, all spinner flasks were autoclaved for 30 minutes at 121ºC, and the 500 mL spinner flasks were wrapped in aluminum foil to achieve dark culturing conditions.

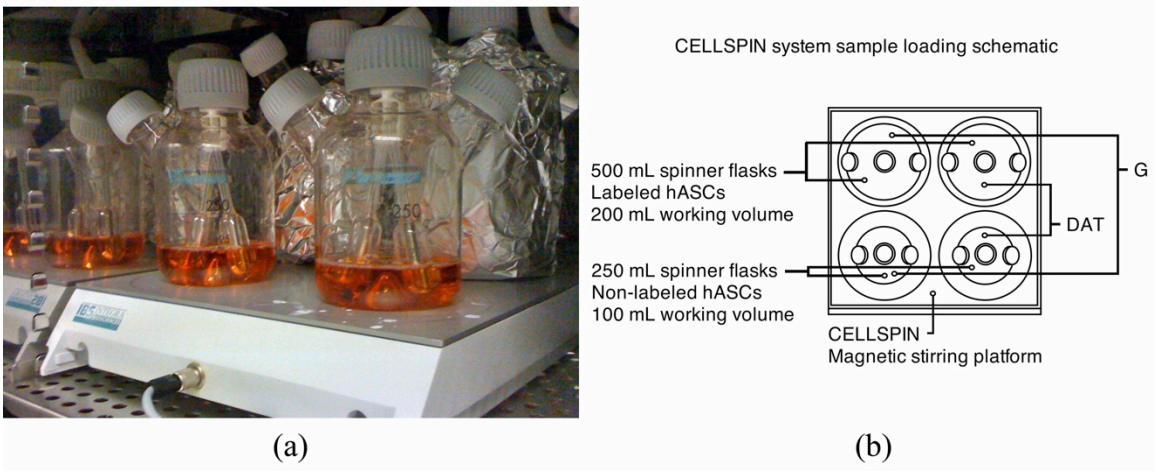

Figure 4.1: CELLSPIN dynamic culture system.
(a) Loaded spinner flasks on the magnetic stirring platform. (b) Sample distribution and layout employed during culturing experiments using the CELLSPIN system. DAT, decellularized adipose tissue; G, gelatin.

4.2.8 Microcarrier Preparation for Cell Culturing

In preparation for cell culture, the DAT- and gelatin-based microcarriers were rinsed once with serum-free DMEM:Ham's F-12 mixture prior to loading the microcarriers into the spinner flasks (Figure 4.1) and the static 3-D control plates. A mass of 1000 mg (wet weight, ~ 10 mL in volume) of DAT-based microcarriers were suspended in 20 mL of DMEM:Ham's F-12 supplemented with 1% Pen/Strep and transferred to the first 500 mL foil-wrapped spinner flask using a 25 mL serological pipette. To the same flask, the total volume was topped up to 200 mL using DMEM:Ham's F-12 supplemented with 1% Pen/Strep, and the flask was placed on the CELLSPIN platform within the incubator (37ºC, 5% CO_2). Similarly, for the gelatin-based microcarriers, 1000 mg (wet weight, ~ 10 mL in volume) of gelatin-based microcarriers were

suspended in 20 mL of DMEM:Ham's F-12 supplemented with 1% Pen/Strep, and transferred by pipette to the second 500 mL foil-wrapped spinner flask. This second flask was also topped up to a total working volume of 200 mL with DMEM:Ham's F-12 supplemented with 1% Pen/Strep and placed onto the CELLSPIN platform (37ºC, 5% CO_2).

The remaining microcarriers were rinsed once with DMEM:Ham's F-12 medium. In order to load the 250 mL spinner flasks with microcarriers, 500 mg (wet weight, ~ 5 mL in volume) of DAT-based microcarriers were suspended in 20 mL of DMEM:Ham's F-12 supplemented with 1% Pen/Strep and transferred into a 250 mL spinner flask using a 25 mL pipette. This spinner flask was topped up with 100 mL of DMEM:Ham's F-12 supplemented with 1% Pen/Strep and placed on the CELLSPIN platform (37ºC, 5% CO_2). Gelatin-based microcarriers were added to the second 250 mL spinner flask (500 mg microcarriers (~ 5 mL in volume)/100 mL medium) following the same methods. The four loaded spinner flasks were left stationary to permit microcarrier equilibration in medium for 3 hours (37ºC, 5% CO_2), after which the CELLSPIN impellor speed was set at 15 RPM for 1 hour.

In developing a static 3-D control, 6-well BD Falcon™ TCPS plates (Becton, Dickinson and Company, USA) were coated to exclude cell adherence by adding 2 mL of sterile-filtered 2% (w/v) agarose (type VII) solution in DMEM:Ham's F-12 (60ºC) to each well. Upon cooling, the agarose gelled to yield a surface non-conducive to ASC adhesion. In preparation for cell culture, DAT or gelatin microcarriers (n~100) were suspended in 5 mL of DMEM:Ham's F-12 supplemented with 1% Pen/Strep, and added in triplicate (N=3) to the wells of the agarose-coated plates. These microcarriers were equilibrated in serum-free medium for 3 hours (37ºC, 5% CO_2).

Following microcarrier equilibration in both the spinner flasks and the agarose-coated control plates, the microcarriers were permitted to gravity settle and the medium was carefully

removed using 5 mL serological pipettes. Complete medium was then added at volumes of 100 mL/250 mL spinner flask, 200 mL/500 mL spinner flask, and 5 mL/well of each agarose-coated 6-well plate. The spinner flasks and plates were maintained at 37ºC and 5% CO_2 and seeded with hASCs within 3 hours.

4.2.9 Cell Preparation

To permit cell tracking, P2 hASCs were fluorescently-labeled with CellTracker™ Green 5-chloromethylfluorescein diacetate (CMFDA) dye (Invitrogen, Burlington, ON, Canada) before seeding. CellTracker™ reagents are fluorescent chloromethyl derivatives that freely diffuse through cell membranes to react with intracellular components, thereby yielding fluorescent viable cells. In preparation, 10 mM CellTracker™ Green stock solution in DMSO was diluted using DMEM:Ham's F-12 to yield a 10 μM working solution. The culturing medium was aspirated from each T-75 flask before rinsing with sterile PBS, and the hASCs were trypsin-released, as previously described. Following centrifugation at 1200 x *g* for 5 minutes and aspiration of the supernatants, the cell pellets were resuspended in the CellTracker™ Green working solution (2 mL) and incubated at 37ºC, 5% CO_2 for 45 minutes. Next, the solutions were recentrifuged and the supernatants discarded before resuspending the cell pellets in complete medium and incubating for an additional 30 minutes (37ºC, 5% CO_2). Following incubation, the cells were counted using a haemocytometer with trypan blue exclusion to assess viability, centrifuged and resuspended in complete medium at the desired density (see following sections) to facilitate cell seeding on the microcarriers within the foil-wrapped spinner flasks. All work was conducted under minimal lighting conditions. P2 hASCs used to inoculate the 250 mL spinner flasks were also trypsin-released from the T-75 plates, but remained unlabeled to permit DNA quantification and enzymatic activity assaying, as detailed in the sections to follow.

4.2.10 Preliminary Cell Attachment Studies

To establish the initial seeding densities for the hASCs on the microcarriers, a series of preliminary cell attachment experiments were performed within the agarose-coated 6-well TCPS plates. More specifically, initial seeding densities of 200 hASCs/mg of microcarriers, 1,000 hASCs/mg of microcarriers, and 2,000 hASCs/mg of microcarriers were investigated. P2 hASCs were fluorescently labeled with CellTracker^{TM} Green as previously described, seeded onto microcarriers within each well at the selected density, and statically cultured for 6 hours (37ºC, 5% CO_2) to permit cell attachment. Beyond 6 hours, the plates were cultured under constant agitation on a rotomix (50 RPM) for a total culture period of 72 hours. Seeded DAT- and gelatin-based microcarrier samples (n=5) were viewed under a Zeiss AxioImager.M1 fluorescence microscope with Axiovision Release 4.7 software (Carl Zeiss, Inc., Germany) at 24 hours and 72 hours after seeding to qualitatively assess cell attachment at each seeding density.

4.2.11 Cell Seeding

Following the preliminary cell attachment studies described in the previous section, the most promising seeding density was applied within the larger-scale CELLSPIN spinner flask system, to assess the ability of the DAT- and gelatin-based microcarriers to support the proliferation and adipogenic differentiation of hASCs in a low shear, 3-D dynamic culturing environment. Overall, 3 dynamic seeding protocols were investigated (Table 4.1).

Following microcarrier equilibration, the first protocol employed an initial seeding density of 2,000 hASCs/mg of microcarriers. The 500 mL foil-wrapped spinner flasks were each seeded with 2 x 10^6 CellTracker^{TM} Green-labeled hASCs using a 5 mL serological pipette under minimal lighting conditions, while the 250 mL spinner flasks were each seeded with 1 x 10^6 unlabeled hASCs. Immediately following seeding, all spinner flasks were placed on the

CELLSPIN platform (37ºC, 5% CO_2) and subjected to 2 minutes of intermittent stirring (15 RPM) every 30 minutes for 6 hours. The system was then continuously stirred at 45 RPM.

The second seeding protocol involved an initial seeding density of 10,000 hASCs/mg of microcarriers. Each 500 mL spinner flask was seeded with 1 x 10^7 CellTracker™ Green-labeled hASCs under light-sensitive conditions, while each 250 mL spinner flask was seeded with 5 x 10^6 unlabeled hASCs. Following seeding, the spinner flasks were returned to the CELLSPIN platform (37ºC and 5% CO_2) and subjected to 2 minutes of stirring (15 RPM) every 30 minutes for 6 hours. The CELLSPIN system was then set to continuous stirring at 45 RPM.

The third seeding protocol involved an increased initial seeding density of 20,000 hASCs/mg of microcarriers, and a modified stirring regime. Each 500 mL spinner flask was seeded with 2 x 10^7 CellTracker™ Green-labeled hASCs under light-sensitive conditions, while each 250 mL spinner flask was seeded with 1 x 10^7 unlabeled hASCs. Upon seeding, the spinner flasks were returned to the CELLSPIN platform (37ºC and 5% CO_2) and subjected to 2 minutes of stirring (15 RPM) every 30 minutes for 3 hours. Following this, the system was operated statically (0 RPM) for 6 hours, and then for an additional 3 hours of intermittent stirring (2 minutes at 15 RPM every 30 minutes), totaling 12 hours. Finally, the platform was set to continuous stirring at 15 RPM. This protocol was also employed during the differentiation study.

Table 4.1: Culturing parameters selected for the dynamic spinner flask culture of hASCs.

Protocol	Initial Seeding Density	Dynamic Seeding Protocol	Dynamic Culture
1	2,000 hASCs/mg of microcarriers	- Intermittent stirring for 2 minutes at 15 RPM every 30 minutes for 6 hours	Continuous stirring at 45 RPM
2	10,000 hASCs/mg of microcarriers	- Intermittent stirring for 2 minutes at 15 RPM every 30 minutes for 6 hours	Continuous stirring at 45 RPM
3	20,000 hASCs/mg of microcarriers	- Intermittent stirring for 2 minutes at 15 RPM every 30 minutes for 3 hours - Static incubation for 6 hours - Intermittent stirring for 2 minutes at 15 RPM every 30 minutes for 3 hours	Continuous stirring at 15 RPM

Agarose-coated control plates containing equilibrated microcarriers were seeded in triplicate with the same densities of hASCs in parallel with the dynamic microcarrier seeding experiments. Microcarriers within the wells were seeded with CellTracker^{TM} Green-labeled hASCs to enable cell imaging, and unlabeled hASCs for subsequent DNA quantification. Similarly, for 2-D static controls, uncoated 6-well TCPS plates were seeded with labeled and unlabeled hASCs in triplicate, with a seeding density of 2.5×10^5 cells/well.

4.2.12 Proliferation Cell Culturing

Cell proliferation in the CELLSPIN system (37ºC, 5% CO_2) was investigated under continuous stirring conditions (Table 4.1). The spinner flasks were removed from the CELLSPIN platform and the microcarriers permitted to gravity settle for 1 minute. Three quarters of the existing medium volume were removed and replaced with fresh complete medium, using serological pipettes, before returning the spinner flasks to the CELLSPIN platform. The proliferation studies were conducted over a 14-day period, with sampling at 24 hours, 72 hours, 7 days, and 14 days after cell seeding. Both 3-D and 2-D seeded static controls, as previously defined, were run in parallel with the dynamic spinner flask seeding studies. The complete medium was changed every 2-3 days in all samples, which were incubated at 37ºC and 5% CO_2.

4.2.13 Adipogenic Differentiation Culturing

Cell differentiation in the incubated CELLSPIN system (37ºC, 5% CO_2) was investigated under continuous stirring at 15 RPM. Prior to inducing adipogenic differentiation, seeded hASCs were permitted to proliferate for 14 days, with fresh medium provided every 2-3 days. Following 14 days of cell culture in complete medium (DMEM:Ham's F-12 supplemented with 10% FBS and 1% Pen/Strep), adipogenic differentiation was induced according to established methods [14]. All spinner flasks were supplied with serum-free adipogenic differentiation medium

comprised of DMEM:Ham's F12 supplemented with 33 μM biotin, 17 μM pantothenate, 66 nM human insulin, 1 nM triiodothyronine, 10 μg/mL transferrin, 100 nM hydrocortisone, 100 U/mL penicillin, and 0.1 mg/mL streptomycin. For the first 72 hours only (days 14-17 of culture), the differentiation medium was supplemented with 1 μg/mL of troglitazone and 0.25 mM isobutylmethylxanthine (IBMX). Fresh differentiation medium was provided every 2-3 days, by replacing 75% of the total medium volume. Samples were taken for analysis at 72 hours, 7 days, and 14 days following the induction of adipogenic differentiation.

As controls, 6-well TCPS plates were seeded directly with hASCs at a density of 50,000 cells/well. All wells were rinsed with sterile divalent cation-free PBS 24 hours after seeding, and provided with fresh medium every 2-3 days. Following 14 days in proliferation medium, each seeded 6-well plate was divided into two subgroups. The first triplicate set was used as a negative (i.e. non-induced) control, and was therefore provided with complete medium for the remaining 14 days of culture (negative control). The second triplicate set was induced to differentiate and provided with adipogenic differentiation medium (as previously defined) for 14 days (positive control). The medium in all TCPS plates was changed in parallel with the spinner flasks, and sampled at identical time points for evaluation of the differentiative response.

4.2.14 Cell Attachment and Organization

To visually assess cellular attachment and organization of seeded hASCs on the DAT-based microcarriers, hASCs were fluorescently labeled with CellTracker™ Green before seeding. Microcarrier samples (n=10) were drawn using 25 mL serological pipettes and viewed under a Zeiss AxioImager.M1 fluorescence microscope with Axiovision Release 4.7 software (Carl Zeiss, Inc., Germany) at 24 hours and 72 hours after seeding. Gelatin-based microcarriers were also seeded with CellTracker™ Green-labeled hASCs and cultured under identical conditions to serve as 3-D dynamic positive controls.

4.2.15 DNA Quantification

The total double-stranded DNA content was used as a measure of the number of cells in each sample condition. The Quant-iT™ PicoGreen® dsDNA Kit (Molecular Probes®, Burlington, ON, Canada) was used to quantify the total dsDNA content on the DAT- and gelatin-based microcarrier samples at 24 hours, 72 hours, 7 days, and 14 days after seeding. The PicoGreen® dsDNA reagent is an ultrasensitive fluorescent nucleic acid stain that detects dsDNA in solution, while minimizing the fluorescence of ribonucleic acid (RNA) and single-stranded (ss) DNA.

In preparation for total dsDNA content quantification, 0.5 mL DAT-based microcarrier samples (n~100) were drawn in triplicate at each time point using 25 mL serological pipettes. Seeded gelatin-based microcarriers cultured under identical conditions were sampled as 3-D dynamic positive controls, and unseeded DAT- and gelatin-based microcarrier samples were included as negative controls (n~100, N=3). Each sample was transferred into an individual 1.5 mL microcentrifuge tube, allowed to settle, and the supernatant culturing medium was removed by pipetting. The samples were thoroughly rinsed with sterile divalent cation-free PBS and resuspended in 1 mL of 1X tris-EDTA (TE) working solution, prepared with sterile DNase-free water to dilute the concentrated 20X TE buffer (200 mM tris-HCl, 20 mM EDTA, pH 7.5) provided with the PicoGreen® dsDNA Kit. The DNase-free sterile water was prepared by adding 1 mL of diethylpyrocarbonate (DEPC) to 1 L of deionized water, stirring at room temperature for 1 hour and incubating at 37°C overnight, before autoclaving for 30 minutes at 121°C.

Following the addition of 1X TE solution, each microcarrier sample was homogenized using a sonic dismembrator (Model-100, Fisher Scientific, Toronto, ON, Canada) at a setting of 4 to achieve cell lysis using three 10-second bursts. Additionally, at each time point, hASCs cultured on i) static DAT- and gelatin-based microcarriers within agarose-coated 6-well TCPS plates, and ii) 2-D TCPS (6-well plates), were prepared as previously described, and assayed for

total dsDNA content. The hASCs grown in 2-D on TCPS were detached and lysed through aspirating the culture medium and rinsing each well with sterile divalent cation-free PBS, adding 1 mL of 1X TE to each well, and sonicating with three 5-second bursts. Following cell detachment and disruption, each 1 mL suspension was transferred into an individual 1.5 mL microcentrifuge tube (n=3, N=3).

After homogenization, all samples were centrifuged (12,000 x g, 5 minutes, 4°C) to obtain the cytosolic fraction that includes dsDNA. The supernatant from each sample was analyzed according to the manufacturer's instructions and compared to a standard dsDNA curve prepared from Lamda DNA, provided with the kit. A 2 μg/mL DNA standard working solution was prepared through a 50-fold dilution of 100 μg/mL Lamda DNA solution with 1X TE. This 2 μg/mL DNA standard working solution was diluted with 1X TE to obtain five DNA standards of 0 ng/mL, 1 ng/mL, 10 ng/mL, 100 ng/mL, and 500 ng/mL.

To load the samples for fluorescence measurement, 100 μL of each standard solution or sample supernatant was added to the individual wells of a black 96-well TCPS microplate (Becton, Dickinson and Company, USA). All samples and standards were prepared in triplicate (n=3, N=3). Under dark conditions, a 200-fold dilution of the PicoGreen® dsDNA reagent provided with the kit was prepared using 1X TE. Working quickly to prevent light exposure, 100 μL of the working solution was added to each loaded well and mixed via pipetting. The microplate was wrapped in aluminum foil and incubated at room temperature for 5 minutes. Finally, the sample fluorescence was measured using a Synergy™ HT multi-detection microplate reader (excitation 485 nm, emission 530 nm) with KC4™ (Bio-Tek Instruments, Inc., Winooski, VT, USA) software, and the total dsDNA content was calculated through comparison to the Lamda DNA standard curve.

4.2.16 Oil Red O Staining

Intracellular lipid accumulation within seeded hASCs was assessed qualitatively at 72 hours, 7 days, and 14 days following the induction of adipogenic differentiation. Before microcarrier seeding, P2 hASCs were labeled with CellTracker™ Green 5-chloromethylfluorescein diacetate (CMFDA) (Invitrogen, Burlington, Canada), as previously described. At each time point, DAT-based microcarriers (n=10, N=3) were sampled under dark conditions via 25 mL serological pipettes and fixed for 2 hours in 10% neutral buffered formalin and rinsed three times with divalent cation-free PBS. Seeded gelatin-based microcarriers (n=10, N=3) were also sampled, fixed, and rinsed thoroughly in PBS. 2-D control samples of undifferentiated (negative control) and adipogenically-induced (positive control) hASCs on TCPS were formalin-fixed for 30 minutes and rinsed three times with PBS.

Oil Red O stock solution was prepared in 99.9% isopropanol at a concentration of 3 g/L and incubated at room temperature for at least 2 hours. A mixture of 3 parts Oil Red O stock solution and 2 parts deionized water (v/v) was prepared and filtered through a Whatman type I qualitative filter paper and used within 30 minutes. Each sample was incubated at room temperature in 2 mL of the filtered Oil Red O solution for 5 minutes. Following staining, all samples were repeatedly rinsed in deionized water and incubated at room temperature for 2 minutes in 1 mL of hematoxylin counterstain. Finally, the hematoxylin was removed and the samples were rinsed three times in deionized water to remove residual counterstain. Optical microscopy was used to visually assess Oil Red O stained intracellular lipid droplets using a Zeiss Invertoskop 40C optical microscope and Axiovision Release 4.7.2 software (Carl Zeiss, Germany).

4.2.17 Glycerol-3-Phosphate Dehydrogenase Activity

As outlined in Chapter 2, GPDH is a key enzyme involved in triacylglycerol biosynthesis. Intracellular accumulation of lipids during adipogenic differentiation of hASCs corresponds to elevated GPDH activity. In this study, the cellular GPDH activity levels on the DAT-based microcarriers were measured at 72 hours, 7 days, and 14 days after the induction of adipogenic differentiation. Samples of DAT- and gelatin-based microcarriers (n~100) were obtained in triplicate with 25 mL serological pipettes at each time point and assayed for GPDH activity. To serve as 2-D controls, TCPS 6-well plates seeded in triplicate with non-induced hASCs (negative control) and adipogenically-induced differentiated hASCs (positive control) were also assayed.

To prepare the microcarrier samples for assaying, each aliquot of 100 microcarriers was placed in a separate 1.5 mL microcentrifuge tube. Residual culturing medium was removed by aseptic pipetting, and each sample was rinsed three times with PBS. Prior to homogenization, 1 mL of enzyme extracting reagent (5 mM Trizma base, 20 mM Tricine, 1 mM EDTA-2Na, pH 7.4) was added to each sample. A sonic dismembrator (Model-100, Fisher Scientific, Toronto, ON, Canada) at a setting of 4 was used to lyse the cells using three 5-second bursts for each sample. Following sonication, each sample was centrifuged (12,800 x g, 5 minutes, 4ºC) to obtain the cytosolic fraction in the supernatant that includes the intracellular GPDH protein.

The 2-D controls were prepared through aspirating the culturing medium from each well, rinsing three times with PBS, adding 1 mL of enzyme extracting reagent to each well, and disrupting the cells through three 5-second bursts at a setting of 4 using the sonic dismembrator. Following sonication, each seeded well was observed under an optical microscope to confirm cell detachment and lysis. The fluid from each well was pipetted into individual 1.5 mL microcentrifuge tubes and the samples were centrifuged (12,800 x g, 5 minutes, 4ºC).

Following centrifugation, each supernatant was assayed in triplicate for total cytosolic protein content, to normalize the measured GPDH activity levels. The Bio-Rad Protein Assay (Bio-Rad Laboratories, Inc., Hercules, CA) was used to determine the total protein content in each sample, as described in Chapter 3. To obtain protein measurements within the concentration range of the standard curve (0-80 μg/mL), samples were diluted accordingly with enzyme extracting reagent before analysis. A bovine albumin standard curve was prepared in enzyme extracting reagent via serial dilution to yield standard concentrations of 0 μg/mL, 10 μg/mL, 20 μg/mL, 40 μg/mL, 60 μg/mL and 80 μg/mL. To each well of a 96-well TCPS microplate, 160 μL of sample was mixed thoroughly with 40 μL of Bio-Rad Coomassie® Brilliant Blue G-250 dye solution using a multi-channel pipette. The microplate was incubated at room temperature for 5 minutes, following which the absorbance was measured at 595 nm using a Synergy™ HT multi-detection microplate reader and KC4™ (Bio-Tek Instruments, Inc., Winooski, VT, USA) data analysis software. Standards were measured in duplicate (n=1, N=2), and samples were measured in triplicate (n=3, N=3). Finally, the protein content within each sample was calculated through comparison to the albumin standard curve.

The GPDH Activity Measurement Kit from Kamiya Biomedical Corporation (Seattle, WA, USA) was used for the quantitative determination of the GPDH activity. As a precursor to triacylglycerol biosynthesis, GPDH reduces dihydroxyacetone phosphate (DHAP) to glycerol-3-phosphate using the coenzyme nicotinamide adenine dinucleotide (NAD). This GPDH assay includes a mixture of DHAP and NADH, which in the presence of GPDH from samples, yields glycerol-3-phosphate and NAD. The resulting decrease in NADH concentration versus time can be measured at 340 nm and used to calculate GPDH activity.

Following protein content determination, 50 μL of the isolated supernatant from each sample was added in duplicate to the wells of a fresh 96-well TCPS microplate. All samples were permitted to warm to room temperature. The GPDH substrate reagent was prepared by dissolving an aliquot provided with the kit in deionized water and warming it to 25ºC. A multi-channel pipette was then used to simultaneously add 100 μL of the GPDH substrate reagent to each sample in the 96-well microplate. Following thorough mixing via the multi-channel pipette, the absorbance of the samples was measured immediately at 340 nm over 10 minutes every 15 seconds at 25ºC using a Synergy™ HT multi-detection microplate reader and KC4™ (Bio-Tek Instruments, Inc., Winooski, VT, USA) software. By plotting absorbance data as a function of time, the change in absorbance (ΔOD/minute) was determined from the linear portion of the kinetic curve for each sample. The GPDH activity levels were then normalized to the total cytosolic protein content in each sample using the expression;

$$GPDH\ Activity\left[mU/mg\right] = \frac{\Delta OD_{avg} \cdot 0.4823 \cdot 0.5 \cdot 1000}{\left(\mathrm{Pr}_{avg}/1000\right)}$$

where 1 Unit of GPDH activity is defined as the activity required to consume 1 μmole of NADH/minute. Data is expressed in units of mU of GPDH activity/mg of total cytosolic protein.

4.2.18 Microcarrier Architecture

Following 28 days of dynamic culture, representative DAT-based microcarriers were examined under optical microscopy to qualitatively assess structural integrity. Additionally, samples of these DAT-based microcarriers were isolated by filtration through a Whatman type I qualitative filter paper to reassess injectability and clinical practicality of the DAT-based microcarriers after long-term culturing. A volume of 3 mL of the isolated DAT-based

microcarriers was loaded into a 5 mL syringe equipped with an 18-gauge hypodermic needle, and the microcarriers were passed through the syringe.

4.2.19 Statistical Analysis

Data are expressed as means ± standard deviations (SDs). All statistical analyses were performed with OriginPro 8.0 software (OriginLab Corp., Northampton, MA, USA) by one-way ANOVA with a Tukey's post-hoc comparison of the means. Differences were considered statistically significant at $p < 0.05$.

4.3 Results

4.3.1 Adipose-Derived Stem Cell Isolation and 2-D Culture

Cell isolation protocols, as shown below in Figure 4.2, yielded abundant populations of primary hASCs, varying in cell density depending on the tissue sample size and/or source.

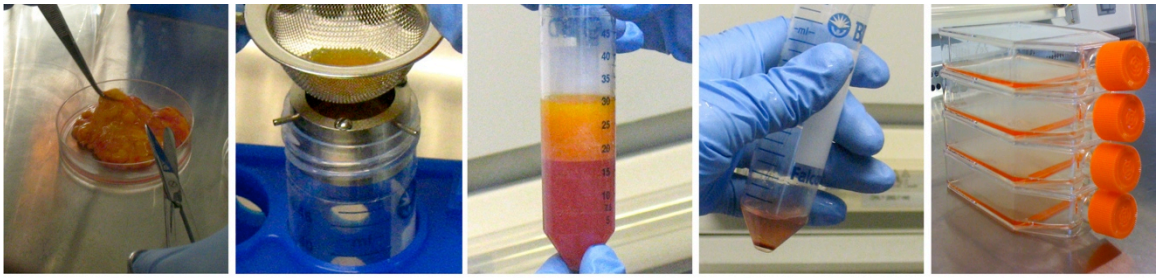

(a) (b) (c) (d) (e)

Figure 4.2: Adipose derived-stem cell isolation.
(a) Mincing freshly-isolated human adipose tissue. (b) Filtration of digested tissue. (c) Gravity separation to remove adipocyte fraction. (d) Centrifugation to obtain the SVF cell pellet containing the hASCs. (e) Plating hASCs onto TCPS.

Immediately following cell isolation, suspended hASCs appeared round and on the order of 10 μm or smaller in diameter. Within 24 hours after seeding onto TCPS, the hASCs adopted a fibroblast-like morphology and began to proliferate rapidly.

4.3.2 Tissue Preparation and Microcarrier Fabrication

Sections of adipose tissue were decellularized to yield the loose, white, and highly hydrated DAT (Figure 4.3). Upon completing the 5-day decellularization protocol on samples sourced from 5 different patients, the collective DAT sample was solubilized according to the optimized protocols developed in Chapter 3. The resulting DATsol appeared yellow/brown in color and was slightly viscous (Figure 4.3).

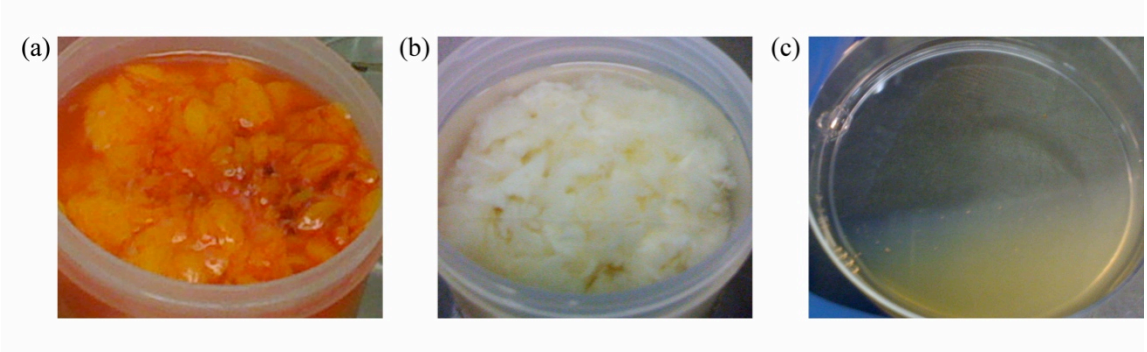

Figure 4.3: Tissue preparation.
(a) Freshly-excised human adipose tissue. (b) Decellularized adipose tissue (DAT) after the 5-day decellularization protocol. (c) Solubilized DAT.

Total protein quantification of DATsol determined using the Bio-Rad protein assay (as outlined in Chapter 3) indicated that all solubilized DAT samples ranged in total protein concentration from 2-4 mg/mL. Following preparation of solubilized DAT and gelatin solutions, porous DAT- and gelatin-based microcarriers were fabricated. In brief, the DAT-based microcarriers were prepared using a volumetric ratio of 3 parts DATsol and 2 parts 3% (w/v) sodium alginate solution, crosslinked with rose bengal and visible light, and alginate-extracted via sodium citrate treatment. As described in Chapter 3, the resulting DAT-based microcarriers appeared spherical in morphology, colorless, and translucent, while the gelatin-based microcarriers produced were similar in overall appearance (Figure 4.4).

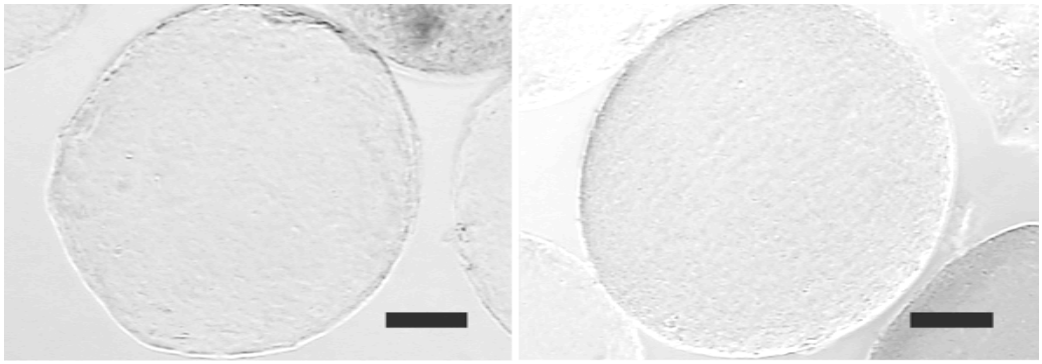

Figure 4.4: Representative microcarriers produced for 3-D hASC culture, original mag. 5x.
(a) DAT-based microcarrier. (b) Gelatin-based microcarrier. Scale bars = 200 μm.

4.3.3 Preliminary Cell Attachment

Preliminary hASC seeding onto DAT- and gelatin-based microcarriers was performed within agarose-coated 6-well plates and qualitatively assessed, as described in Section 4.2.10. Overall, the first seeding density of 200 hASCs/mg of microcarriers achieved limited cell attachment. Visualization under fluorescence microscopy confirmed the presence of cells and/or cellular debris within the sampled culturing medium. However, no cell attachment was observed on the microcarrriers following the 6-hour seeding period. Similarly, there was no appreciable cell attachment at 72 hours, following culturing under agitation (50 RPM). The second seeding density (1,000 hASCs/mg of microcarriers investigated) yielded similar results, with limited cell adherence following 72 hours in culture.

The third seeding density of 2,000 hASCs/mg of microcarriers resulted in low densities of hASC attachment to both the DAT- and the gelatin-based microcarriers, as assessed under fluorescence microscopy. Macroscopically, both the DAT- and the gelatin-based microcarriers appeared structurally intact, with no visible changes in overall morphology following 72 hours in culture in the agarose-coated 6-well plates under agitation (50 RPM). Individual microcarriers could be easily manipulated with tweezers to facilitate sample viewing during microscopy.

4.3.4 Dynamic Cell Attachment and Proliferation

Based on the results obtained during the preliminary attachment studies, an initial seeding density of 2,000 hASCs/mg of microcarriers was selected for investigation during the first dynamic culturing experiment within the CELLSPIN spinner flask system. Following 72 hours of dynamic culture (45 RPM), no detectable change in microcarrier size or morphology was observed, with both DAT- and gelatin-based hASC-seeded microcarriers maintaining their shape and structural integrity. However, limited cell attachment was achieved at this seeding density, as qualified under fluorescence microscopy and quantified via insignificant DNA content in samples measured at 24 hours and 72 hours after cell seeding. As a result, this first CELLSPIN culturing experiment was truncated following 72 hours of culture, and repeated with an increased initial cell seeding density of 10,000 hASCs/mg of microcarriers.

During this second dynamic attachment and proliferation study, the significant increase in seeding density yielded appreciable cell attachment following 72 hours of dynamic culture within the CELLSPIN system, as qualitatively determined by fluorescence microscopy (Figure 4.5). DNA content measured at 24 hours and 72 hours after cell seeding, although low in concentration, was detectable (Figure 4.6); therefore, dynamic cell culture was continued until 7 days after seeding, at which point cell attachment and total dsDNA content was reassessed.

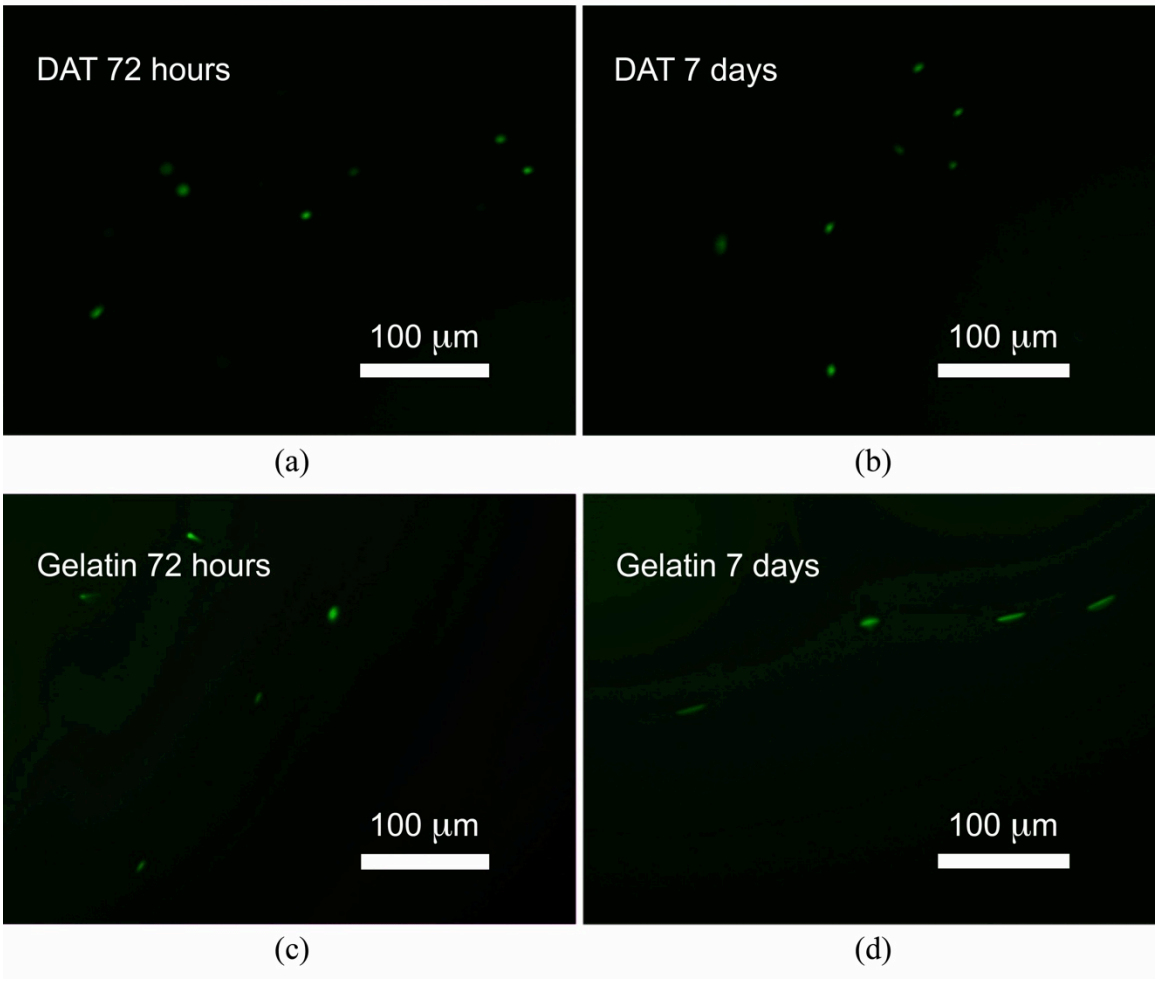

Figure 4.5: Dynamically-cultured hASCs on microcarriers.
Imaged under fluorescence microscopy (mag. 10x). (a) and (b) are representative images of seeded DAT-based microcarriers. (c) and (d) show seeded gelatin-based microcarriers. Initial seeding density = 10,000 hASCs/mg of microcarriers.

After seeding with an initial cell density of 10,000 hASCs/mg microcarriers, qualitative consideration of cell attachment (Figure 4.5) did not indicate a significant difference in cell number between the DAT- and gelatin-based microcarriers after 7 days of culture. To quantify the response, the DNA content levels were determined using the Quant-iT™ PicoGreen® dsDNA kit in comparison to a Lambda dsDNA standard curve (Appendix A).

All DNA content levels were calculated and expressed in ng/mL as means ± SD (Figure 4.6), and were statistically compared using a one-way ANOVA with a Tukey's post-hoc

comparison of the means ($p < 0.05$). Additionally, all DNA concentrations were normalized to the fluorescence levels measured in unseeded samples of DAT- and gelatin-based microcarriers.

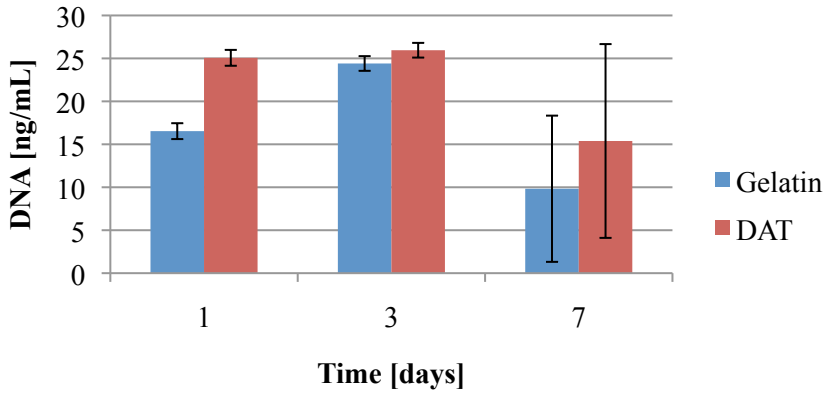

Figure 4.6: DNA quantification of DAT- and gelatin-based microcarriers.
At time points of 24 hours, 72 hours, and 7 days after cell seeding within the CELLSPIN system. Measured by fluorometric Quant-iT™ PicoGreen® dsDNA assaying (excitation 485 nm, emission 530 nm). Initial seeding density = 10,000 hASCs/mg of microcarriers. All data are expressed as means ± SD.

At 24 hours following cell seeding, the mean DNA content on the DAT-based microcarriers (25.67 ± 0.92 ng/mL), although not statistically higher, was greater in value than the mean DNA content on the seeded gelatin-based microcarriers (16.53 ± 0.92 ng/mL). At 72 hours following cell seeding, the mean DNA content on the DAT-based microcarriers (25.95 ± 0.86 ng/mL) was only slightly higher than that measured on the gelatin-based microcarriers (24.41 ± 0.86 ng/mL). At 7 days after seeding, the mean DNA content on the DAT-based microcarriers (15.39 ± 11.28 ng/mL) was higher than the mean DNA content on the gelatin-based microcarriers (9.83 ± 8.51 ng/mL), although again not statistically significant. Furthermore, no statistical differences were detected between the mean DNA content measurements when comparing differences between time points, with the means for all microcarrier samples remaining below 30 ng/mL at all time points. Therefore, a third proliferation study was conducted with an increased seeding density of 20,000 hASCs/mg of microcarriers, and a modified seeding protocol, incorporating a longer seeding period and reduced stirring speed.

This final attachment and proliferation study with hASCs seeded dynamically onto DAT- and gelatin-based microcarriers, and cultured in the CELLSPIN system, demonstrated enhanced cell attachment and a significant increase in DNA content at each time point for up to 14 days. Figure 4.7 illustrates hASCs adhered to DAT- and gelatin-based microcarriers at 72 hours, 7 days, and 14 days of dynamic culture in the CELLSPIN system (reduced stirring rate of 15 RPM).

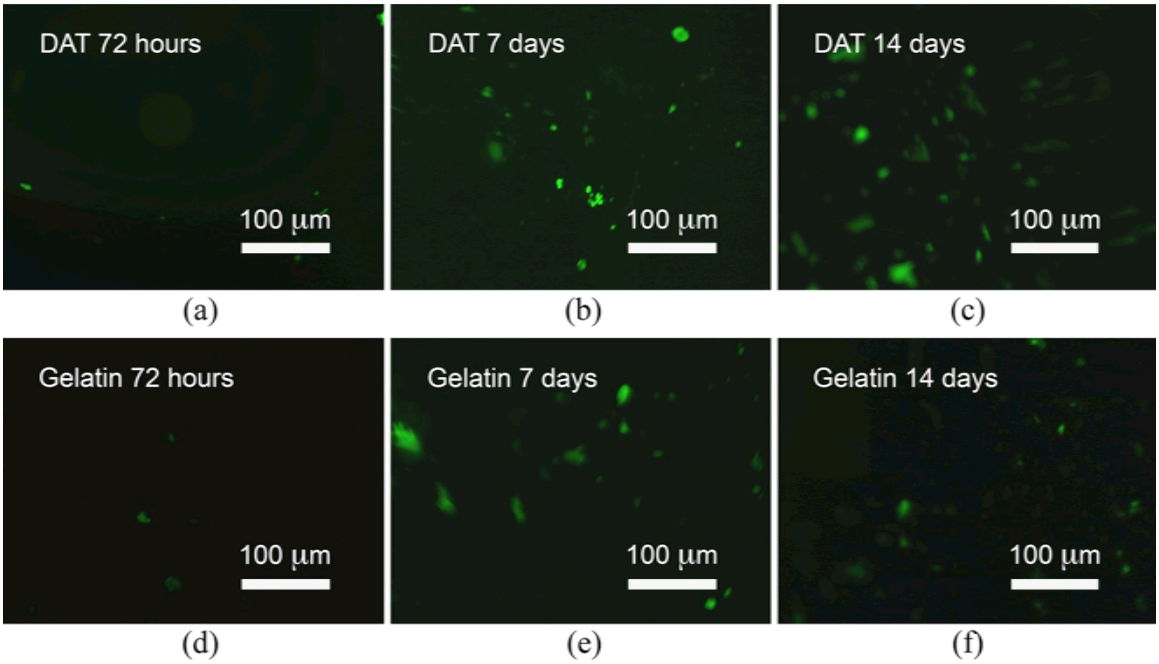

Figure 4.7: Dynamically-cultured hASCs on microcarriers.
Imaged under fluorescence microscopy (mag. 10x). (a), (b), and (c) are representative images of seeded DAT-based microcarriers at 72 hours, 7 days, and 14 days after seeding, while (d), (e), and (f) show gelatin-based microcarriers at 72 hours, 7 days, and 14 days after seeding.

As evidenced by Figure 4.7, the hASCs proliferating on microcarriers under dynamic culturing conditions appeared to adopt a more rounded cell morphology, as compared to the more fibroblast-like appearance of the hASCs (Figure 4.8) cultured under static conditions.

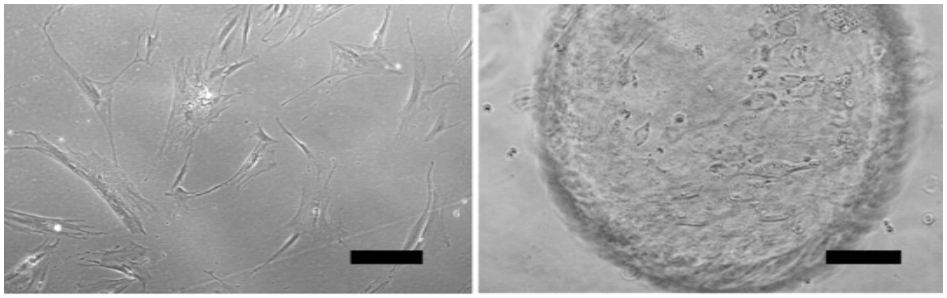

Figure 4.8: hASCs following 14 days of proliferation.
(a) 2-D TCPS and (b) statically-cultured DAT-based microcarriers, as viewed under optical microscopy (original mag. 10x). Scale bars = 200 μm.

DNA content on the dynamically-cultured microcarriers seeded with hASCs was significantly greater than DNA content measured for hASCs cultured statically on microcarriers or on TCPS (Figure 4.9).

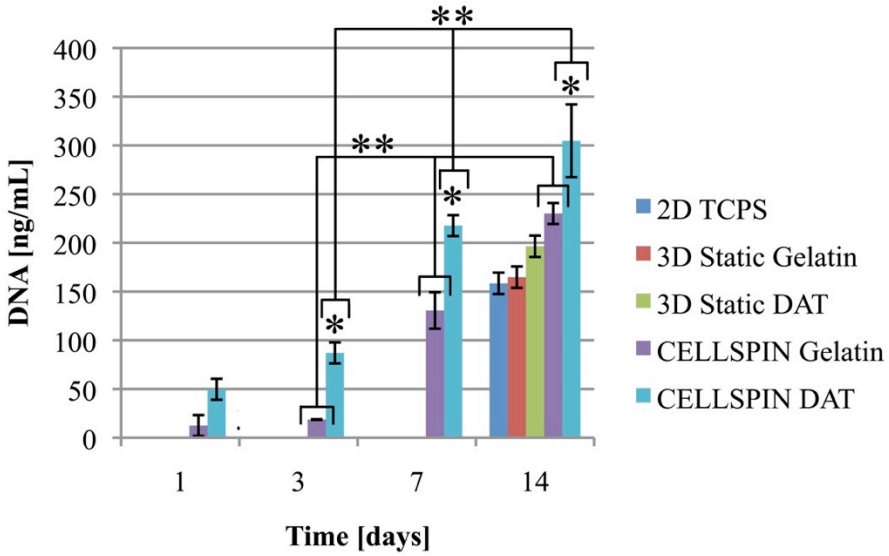

Figure 4.9: DNA quantification of DAT- and gelatin-based microcarriers.
Time points of 24 hours, 72 hours, 7 days, and 14 days after seeding microcarriers with hASCs, in addition to 2-D and 3-D static control plates at t=14 days. Determined from fluorometric PicoGreen® assaying (excitation 485 nm, emission 530 nm). Initial seeding density = 20,000 hASCs/mg of microcarriers. All data are expressed as means ± SD. Statistical significance was determined by one-way ANOVA with post-hoc Tukey's comparison of the means ($p < 0.05$); * = statistically different from other groups at time point, ** = statistically different between time points.

After 24 hours of culturing, the mean DNA content on the dynamically-cultured DAT-based microcarriers (49.75 ± 10.77 ng/mL) was higher in value than the mean DNA content on gelatin-based microcarriers (12.44 ± 10.77 ng/mL), but not statistically different.

Following 72 days of culturing, the mean DNA content on the dynamically-cultured DAT-based microcarriers (87.06 ± 10.77 ng/mL) was statistically higher than the DNA content on the dynamically-cultured gelatin-based microcarriers (18.66 ± 0.34 ng/mL). No significant difference was found between the mean DNA content on the DAT-based microcarriers after 72 hours of culture, as compared to 24 hours. Similarly, no significant difference was observed in DNA content on gelatin-based microcarriers from 24 hours to 72 hours.

After 7 days of culturing, the mean DNA content on the dynamically-cultured DAT-based microcarriers (217.66 ± 10.77 ng/mL) was statistically higher than on the dynamically-cultured gelatin-based microcarriers (130.60 ± 18.66 ng/mL). The mean DNA content on the dynamically-cultured DAT-based microcarriers after 7 days was statistically greater than at 24 hours (49.75 ± 10.77 ng/mL) and at 72 hours (87.06 ± 10.77 ng/mL), indicative of proliferation. Gelatin-based microcarriers also contained statistically higher DNA levels at 7 days (130.60 ± 18.66 ng/mL) as compared to gelatin-based microcarriers at 24 hours (12.44 ± 10.77 ng/mL) and 72 hours (18.66 ± 0.34 ng/mL).

After 14 days of culture, the mean DNA content was also measured for statically-cultured hASCs on DAT- and gelatin-based microcarriers within agarose-coated TCPS plates and for hASCs cultured statically on uncoated 2-D TCPS. The mean DNA content measured for seeded DAT-based microcarriers subjected to dynamic culture (304.73 ± 37.31 ng/mL) was significantly higher than the DNA content of sampled DAT-based microcarriers at all other time points, in addition to the gelatin-based microcarriers cultured for 14 days under dynamic conditions (230.10 ± 10.77 ng/mL). Seeded gelatin-based microcarriers demonstrated a significant increase in mean

DNA content at 14 days. The DNA content on the dynamically cultured DAT-based microcarriers at 14 days was statistically greater than all other investigated samples, including the 2-D seeded TCPS (158.43 ± 10.98 ng/mL) and the 3-D statically-cultured DAT-based microcarriers (196.45 ± 10.98 ng/mL) and gelatin-based microcarriers (164.77 ± 10.98 ng/mL). hASCs cultured statically on the microcarriers demonstrated no significant difference in mean DNA content as compared to TCPS cultures, emphasizing the critical role of the dynamic cell culturing environment in achieving increased cell proliferation.

4.3.5 Proliferation and Differentiation of Human Adipose-Derived Stem Cells

Based on the promising cell attachment and proliferation results obtained, the 28-day adipogenic differentiation study was conducted using the same seeding and culturing protocols. Effective hASC attachment was confirmed by elevated total dsDNA content levels on the microcarrier samples after 14 days of dynamic cell culture (Figure 4.10).

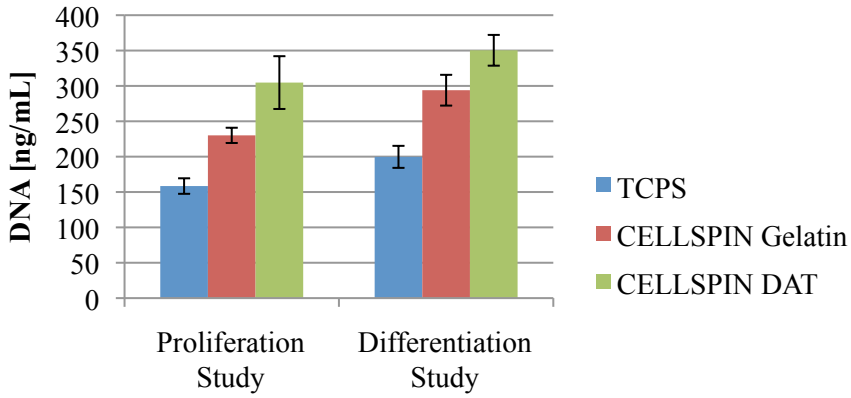

Figure 4.10: Total dsDNA content measured using the Quant iT™ PicoGreen® dsDNA kit.
At 14 days after cell seeding during the third proliferation study, and after 14 days of cell culture during the differentiation study. Data are expressed as means ± SD.

Upon initial inspection, it is apparent that both 14-day proliferation periods follow similar trends in total dsDNA content. Through performing a statistical comparison of the mean DNA

content levels between the two studies, it was found that no significant difference was observed between the two studies for TCPS DNA levels (158.43 ± 10.98 ng/mL and 199.71 ± 15.57 ng/mL), gelatin-based microcarrier DNA levels (230.10 ± 10.77 ng/mL and 293.94 ± 21.75 ng/mL), and DAT-based microcarriers (304.73 ± 37.31 ng/mL and 350.38 ± 21.75 ng/mL), although the mean DNA content values for all samples were higher than DNA levels observed during the third proliferation study. The observed differences may be due to patient variability, as the hASCs used for the 14-day proliferation study were sourced from a different patient (34 years in age, BMI=28.7) than the hASCs used for the differentiation study (20 years in age, BMI=25.2). Upon confirming the elevation of DNA levels within the spinner flasks after 14 days of culture, differentiation was induced as described in Section 4.2.13.

4.3.6 Oil Red O

Oil Red O staining was employed to visually assess intracellular lipid loading within the hASCs on the DAT- and gelatin-based microcarriers cultured dynamically in the CELLSPIN system for a total period of 28 days, with samples drawn at 72 hours, 7 days, and 14 days following the induction of differentiation. Figure 4.11 depicts the intracellular triacylglycerol droplets (stained red) accumulating within differentiating hASCs over time.

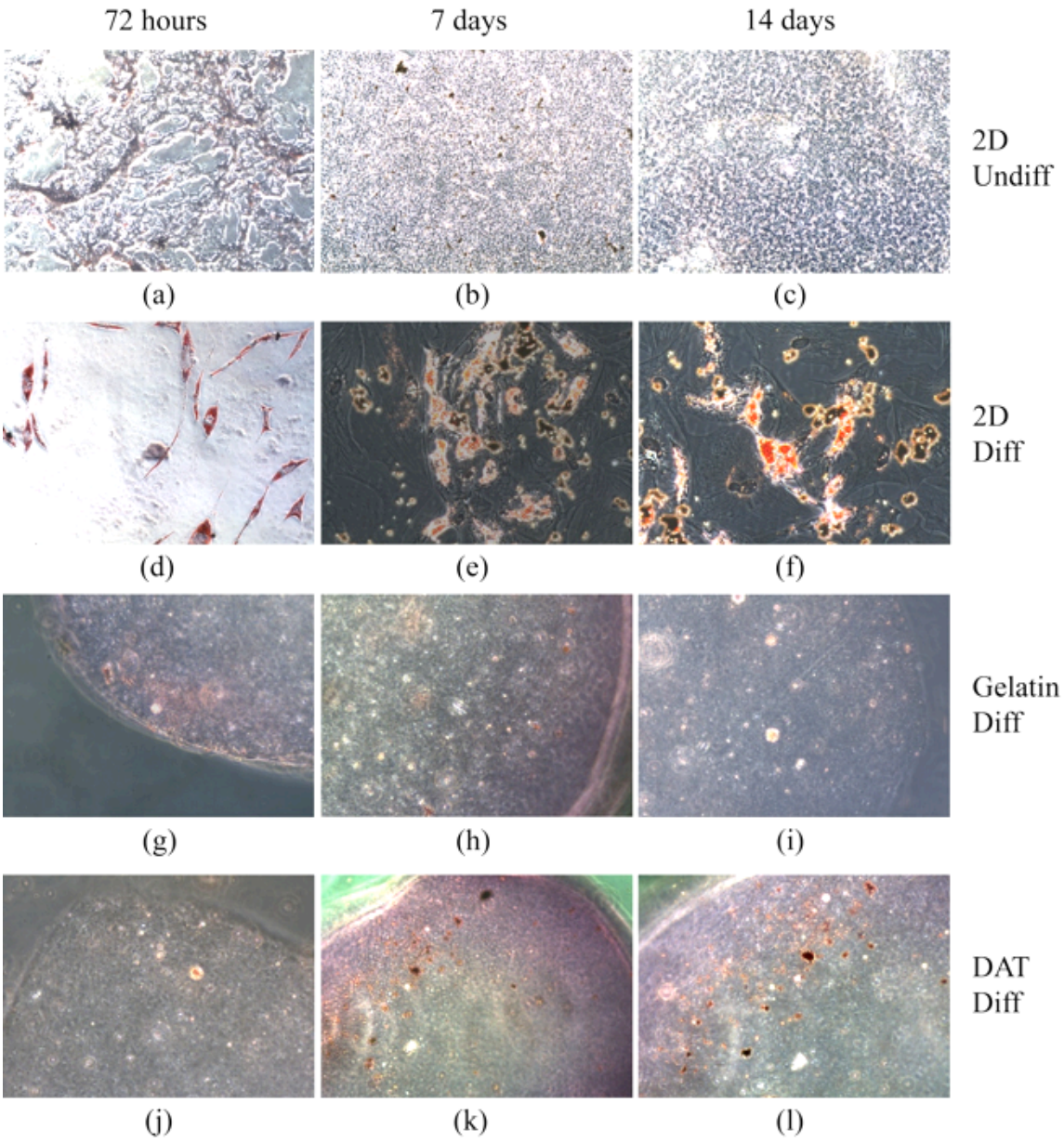

Figure 4.11: Oil Red O staining, original mag. 20x.
Images (a), (b) and (c) are non-induced (Undiff) hASCs; (d), (e), and (f) are induced (Diff) hASCs on TCPS; (g), (h), and (i) are differentiated hASC-seeded gelatin-based microcarriers; (j), (k), and (l) are differentiated hASC-seeded DAT-based microcarriers.

As evidenced in Figure 4.11, no significant lipid loading (as indicated by red droplet staining) was visible on the non-induced (undifferentiated) hASCs-seeded TCPS at any of the

times points following the induction of differentiation (72 hours, 7 days, and 14 days). Conversely, hASCs induced to adipogenically differentiate with adipogenic medium began to accumulate small intracellular lipid droplets as early as 72 hours after inducing differentiation. Qualitatively, lipid uptake increased between 72 hours and 7 days on TCPS. After 14 days of adipogenic differentiation, insignificant Oil Red O staining was observed in the induced-hASCs cultured on TCPS (n=2, N=3). This is attributed to gradual cell sloughing from the well surfaces over days 21-28.

Low levels of hASC Oil Red O staining were visible on the dynamically cultured gelatin-based microcarriers seeded with hASCs induced to adipogenically differentiate 14 days after cell seeding. Due to the reduced cell attachment and proliferation previously quantified, only isolated cells were visibly attached and actively accumulating lipid. In contrast, the hASCs induced to differentiate following 14 days of dynamic culture on the DAT-based microcarriers within the CELLSPIN system demonstrated a significant increase in Oil Red O staining over time. While few Oil Red O stained cells were detectable at 72 hours following differentiation induction, increased differentiation was observed at 7 days, with significant lipid loading after 14 days.

4.3.7 Glycerol-3-Phosphate Dehydrogenase Activity

To quantitatively assess adipogenesis in undifferentiated and differentiated hASCs cultured on 2-D TCPS, and differentiated hASCs cultured dynamically on DAT- and gelatin-based microcarriers, the mean GPDH activities were determined at 72 hours, 7 days, and 14 days after inducing adipogenic differentiation (Figure 4.12).

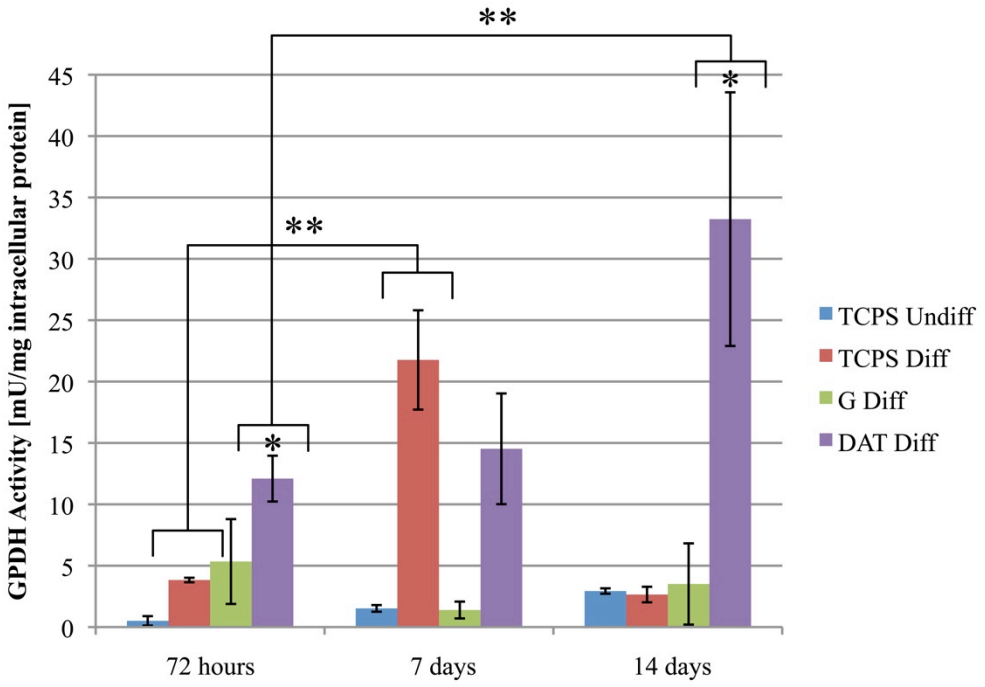

Figure 4.12: GPDH activity levels at 72 hours, 7 days, and 14 days after differentiation. Data are expressed as mean GPDH activities ± SD, in units of mU of GPDH activity level/mg of intracellular protein. Statistical significance was determined by one-way ANOVA with post-hoc Tukey's comparison of the means ($p < 0.05$); * = statistically different from other groups at time point, ** = statistically different between time points.

After 72 hours of differentiation, the mean GPDH activity for the DAT-based microcarriers (12.09 ± 1.86 mU/mg protein) was significantly greater than the mean GPDH activity for the gelatin-based microcarriers (5.34 ± 3.46 mU/mg protein), the differentiated hASCs on TCPS (3.83 ± 0.18 mU/mg protein), and the undifferentiated hASCs on TCPS (0.51 ± 0.39 mU/mg protein). No statistical significance was observed between the GPDH activities for the gelatin-based microcarriers and TCPS-cultured hASCs at 72 hours.

After 7 days of differentiation, the mean GPDH activity on the DAT-based microcarriers (14.52 ± 4.51 mU/mg protein) was greater in value, but not significant as compared to the DAT-based microcarrier GPDH activity at 72 hours (12.09 ± 1.86 mU/mg protein). Although no statistical difference was found between the DAT-based microcarrier GPDH activity and the

differentiated TCPS sample GPDH activity at 7 days (21.76 ± 4.04 mU/mg protein), the DAT-based microcarrier GPDH activity was significantly greater than the GPDH activity calculated for the gelatin-based microcarriers at 7 days (1.39 ± 0.69 mU/mg protein) and the undifferentiated hASCs grown on TCPS at 7 days (1.52 ± 0.27 mU/mg protein).

After 14 days of differentiation, the mean GPDH activity calculated for hASCs differentiated on DAT-based microcarriers (33.23 ± 10.33 mU/mg protein) was statistically greater than the mean GPDH activities for hASCs differentiated on gelatin-based microcarriers (3.51 ± 3.31 mU/mg protein), hASCs differentiated on TCPS (2.65 ± 0.63 mU/mg protein), and the undifferentiated hASCs on TCPS (2.94 ± 0.22 mU/mg protein). Furthermore, the GPDH activity at 14 days for the DAT-based microcarrier samples was significantly greater than the DAT-based microcarrier sample GPDH activities measured at 72 hours and 7 days.

Overall, the mean GPDH activity of hASCs dynamically cultured on DAT-based microcarriers significantly increased over 14 days following induction of adipogenic differentiation. The hASCs dynamically cultured on gelatin-based microcarriers did not exhibit a significant change in mean GPDH activity over the 14-day culturing period. hASCs induced to differentiate on TCPS exhibited a significant increase in GPDH activity at 7 days, but the activity decreased by day 14, potentially attributable to cell detachment and loss post-lipid loading.

4.3.8 Microcarrier Architecture Following Dynamic Culture

Qualitatively, the DAT- and gelatin-based microcarriers showed no significant change in morphology and retained their structural integrity over 28 days of dynamic culture in the CELLSPIN system, as confirmed under optical microscopy (Figure 4.13). Furthermore, DAT-based microcarriers were readily passed through a syringe with an 18-gauge hypodermic needle without negatively impacting microcarrier structure. Microcarriers could be extruded to form both monolayers of microcarriers, and larger volume constructs approximately 1 cm^3 in volume.

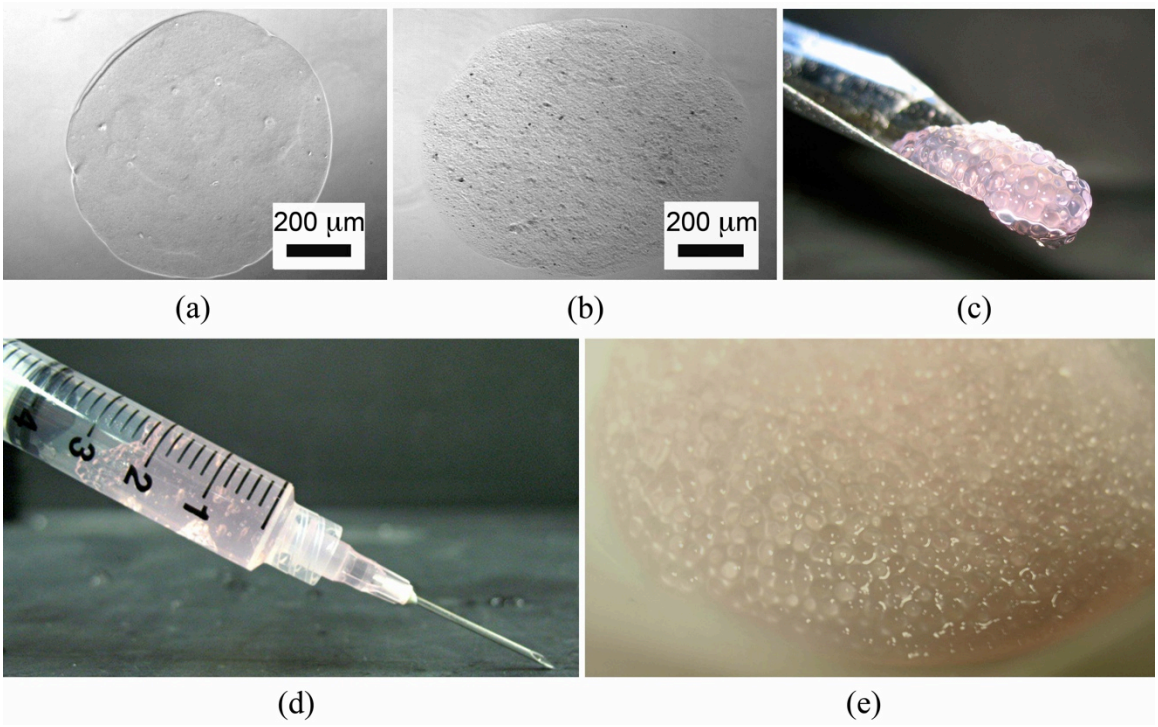

Figure 4.13: DAT-based microcarrier architecture and injectability.
(a) DAT-based microcarrier (before culture) and (b) after 28 days of dynamic culture, original mag. 5x. (c) Macroscopic DAT-based microcarriers (after dynamic culture). (d) Syringe loading with microcarriers. (e) Microcarriers post-extrusion through an 18-gauge hypodermic needle.

4.4 Discussion

The *in vitro* culturing experiments described in this chapter point to the ability of adipose-specific microcarriers to support hASC proliferation and to contribute significantly to the adipogenic response *in vitro*. More specifically, DAT-based microcarriers were shown to enhance ASC attachment and proliferation over 14 days of dynamic cell culture, as compared to gelatin-based microcarriers (3-D dynamic control) and statically cultured DAT- and gelatin-based microcarriers (3-D static controls). The dynamically cultured DAT-based microcarriers seeded with hASCs also demonstrated significantly greater adipogenic differentiation at 14 days of culture over gelatin-based microcarriers and 2-D plates.

Previous work in adipose tissue-engineering strategies supports a 3-D dynamic microcarrier approach over static and/or 2-D plating techniques for the culture of ASCs, as

evidenced by the growing body of work investigating the ability of microcarriers fabricated from PLGA and naturally-derived materials (collagen, modified alginate, small intestinal submucosa, and adipose tissue-derived gels) to support ASC expansion *in vitro*, and adipose tissue regeneration *in vivo* [59]. Research by Kang *et al.* (2008) evaluating macroporous PLGA-based microcarriers seeded with hASCs, and induced to adipogenically differentiate in spinner flasks, showed that PLGA microcarriers supported hASC proliferation and adipogenic differentiation [124]. These microcarriers displayed reduced apoptotic activity as compared to 2-D-cultured hASCs [124]. Furthermore, the regenerative response observed *in vivo* was greater for dynamically cultured hASCs on PLGA microcarriers, as compared to microcarriers mixed with hASCs cultured *in vitro* on 2-D plates prior to injection, pointing to the significant advantage of employing a 3-D and dynamic culturing strategy [124]. Commercially-available collagenous microcarriers (CultiSpher G) have also shown promise [141]. Dynamic seeding and culturing of hASCs on CultiSpher G microcarriers by Rubin *et al.* (2007) over several weeks yielded positive results for cell attachment, proliferation, and upon induction, adipogenic or osteogenic differentiation [141]. However, CultiSphers have not been approved for clinical use *in vivo*. Using a different microparticle material, Marra *et al.* (2007) investigated a composite approach, in which hASCs were dynamically cultured on small intestinal submucosa particles in spinner flasks prior to injection with FGF-2-loaded PLGA microspheres within mice for several weeks [103]. Results from this study, although short-term, also supported the potential for cell-seeded microcarriers to act as substrates for ASCs and yield a directly-injectable, cell-seeded scaffold.

Despite promising results, microcarrier approaches in adipose tissue engineering reveal little progress toward the development of an adipose tissue-specific microcarrier, custom-designed to modulate ASC behavior to achieve a highly adipogenic response. Research surrounding tissue-specific scaffold design is an emerging area that holds immense potential for

the development of inductive scaffolds capable of directing cell-response and/or fate towards a specific tissue of interest. During the culture of pluripotent or multipotent cells, subtle differences in the ECM composition may impact cell response in a lineage-specific manner [170]. While individual ECM components, including collagen, laminin, and fibronectin, have been isolated and are commercially-available, the native ECM provides many complex cues that are difficult to recreate from a bottom-up scaffold design approach [73, 170]. This was exemplified in work by Chaubey and Burg (2008), who probed the ability for collagen and laminin in different densities to modulate adipogenic differentiation of mouse BMSCs. Results indicated that a complex ECM substrate balance is required [73].

Therefore, there is much interest in utilizing decellularized tissues as naturally-derived scaffold base materials, as they preserve the composition and structure of the matrix of a specific tissue, while minimizing immunogenicity through the removal of most cellular and antigenic components [105]. Many tissue types have been successfully decellularized to date [105]. More importantly for adipose tissue engineering, protocols have recently been established for detergent-free decellularization of adipose tissue, yielding a well preserved and highly purified form of the adipose matrix (DAT) [14].

Previous work by Flynn (2010) investigating the cell response to intact DAT scaffolds highlighted the ability of DAT to induce adipogenic differentiation without the addition of exogenous growth factors [14]. Specifically, high expression levels of the master adipogenic regulator genes, PPARγ and C/EBPα, in conjunction with elevated GPDH activities, were observed in hASCs seeded onto DAT, as compared to hASCs cultured in 2-D monolayer culture or cell aggregate culture [14]. This adipo-inductive quality of DAT renders it a promising biomaterial for adipose tissue engineering. To this end, the work described in Chapter 3 focused

on utilizing DAT as a base material for the fabrication of a custom-designed, tissue-specific microcarrier for applications in adipose tissue engineering.

The research presented in this chapter focused on assessing the *in vitro* response of hASCs to DAT-based microcarriers. Initial work surrounded the development of preliminary seeding protocols for the *in vitro* culture of hASCs on DAT-based microcarriers within a simple model system. Upon investigating three different seeding densities in parallel, it was observed that only the highest initial seeding density (2,000 hASCs/mg of microcarriers) resulted in appreciable cell attachment after 72 hours in culture. This seeding density was selected for use within the larger-scale dynamic CELLSPIN spinner flask system to assess the dynamic response of hASCs to the microcarriers, given the significant advantages of dynamic culturing within spinner flasks cited in the literature [7, 121, 122, 124, 141].

During the first proliferation study within the CELLSPIN system, DAT-based microcarriers, in conjunction with gelatin-based microcarriers developed as a control, were seeded with 2,000 hASCs/mg of microcarriers, over a 6-hour period with intermittent stirring, after which the system was continuously stirred (45 RPM). Sampling at 24 hours and 72 hours qualitatively assessed cell attachment and quantitatively measured total dsDNA content. However, insignificant cell attachment and DNA content observed for both microcarrier formulations led to the truncation of this study after 72 hours. In the next experiment, a higher initial seeding density (10,000 hASCs/mg of microcarriers) was used in combination with identical seeding and stirring protocols in the second proliferation study. Cell imaging under fluorescence microscopy at 72 hours and 7 days revealed improved cell attachment as a result of the increased cell seeding density. However, DNA quantification indicated that concentrations were below 30 ng/mL at all time points, with no significant increase in DNA content observed over 7 days of dynamic cell culture.

In an effort to reduce shear and decrease the probability of undesired microcarrier collisions with the flask walls, the third proliferation study investigated a reduced continuous stirring speed (15 RPM), coupled with an increased initial seeding density of 20,000 hASCs/mg of microcarriers, as well as a slightly modified seeding protocol. Greater cell attachment was achieved through seeding the higher density of cells onto microcarriers over a 12-hour seeding period as opposed to only 6 hours, and the prolonged static period may have aided in achieving lasting cell attachment. Seeded microcarrier imaging and DNA content measurements confirmed a significant increase in cell attachment and perhaps more importantly, a statistically significant increase in DNA content over time for both the DAT- and the gelatin-based microcarriers, indicative of cell proliferation. Furthermore, the total DNA content measured on the DAT-based microcarriers was statistically greater following 14 days of dynamic culture than the DNA content detected on statically cultured DAT- and gelatin-based microcarriers seeded with hASCs, and on hASC-seeded TCPS. This work points to the advantage of expanding hASCs on DAT-based microcarriers in a 3-D dynamic culturing environment, as compared to conventional 2-D plating techniques and static microcarrier culturing.

In addition to obtaining significantly greater cell expansion, the CELLSPIN system greatly reduced the required incubator space to procure high cell numbers that would otherwise require many single-use 2-D flasks to yield comparable cell numbers. From a clinical perspective, the use of spinner flasks loaded with DAT-based microcarriers could potentially provide relevant numbers of ASCs on an injectable scaffold, while simultaneously reducing space and material costs linked to cell culture, requiring only an incubator and spinner flask system on site to rapidly expand autologously- and/or allogenically-sourced hASCs.

Based on the promising proliferation results obtained in this work, the seeding density of 20,000 hASCs/mg of microcarriers was used with the modified 12-hour seeding protocol and 15

RPM continuous stirring rate to evaluate adipogenic differentiation on DAT-based microcarriers. DNA levels followed a similar trend to those measured during the third proliferation study at 14 days, indicating consistency in cell response. For both studies, the DAT-based microcarriers contained the greatest DNA content, and the seeded TCPS samples contained the lowest.

Interestingly, all DNA content values measured during the proliferation period prior to inducing differentiation were greater than the DNA content values measured during the 14-day third proliferation study. This overall increase in DNA content observed between experiments could be due to the inherent error associated with the haemocytometer method used to count cells before seeding and sample preparation for assaying. However, consideration of the cell sourcing is also worthwhile, as the hASCs used for the 14-day proliferation study were sourced from a 34-year-old patient with a BMI of 28.7, whereas the hASCs that demonstrated an elevated proliferative capacity were sourced from a younger 20-year-old patient with a lower BMI of 25.2. This increased proliferative capacity is consistent with general trends in the literature with respect to the influence of donor age and BMI on the observed cell responses [171].

Cell imaging on the DAT- and gelatin-based microcarriers under fluorescence microscopy confirmed a rounded cell morphology for cells seeded on microcarriers and dynamically cultured within the CELLSPIN system. This rounded morphology may be more consistent with the appearance of ASCs *in vivo* [83]. Individual attached hASCs were randomly distributed over the surface of the microcarriers at early time points, with clusters of cells visible on the microcarrier surfaces following 14 days, potentially representing highly proliferative cell aggregates. Overall, greater cell numbers were qualitatively observed on DAT-based microcarriers as compared to gelatin-based microcarriers at each time point, which is consistent with the elevated DNA levels detected on the DAT-based microcarriers at each time point.

Following induction of adipogenic differentiation within the spinner flasks, the number of attached cells remained largely unchanged on the microcarriers, likely due to growth arrest prior to differentiation and the uptake of intracellular lipids. Oil Red O staining revealed significant lipid-loading within cells on the DAT-based microcarriers, but only a few detectable lipid droplets on the gelatin-based microcarriers, potentially related to the decreased cell number observed on the gelatin-based microcarriers at the end of the proliferation phase.

Differentiated hASCs on TCPS revealed the formation of intracellular lipid droplets at 72 hours and 7 days after inducing differentiation, however little positive Oil Red O staining was detectable after 14 days of differentiation (28 days of total culture) on TCPS. Detachment of cells and cellular debris was observed within the wells of the differentiated and undifferentiated 2-D control plates between days 21 and 28. The hASCs grown in 2-D may have sloughed off beyond 21 days of culture, explaining the lack of staining observed on the induced TCPS plates at 14 days of differentiation (28 days of total culture). As differentiating ASCs accumulate intracellular lipid, they will gradually detach from the surface as they achieve a more mature unilocular morphology, and mature adipocytes are routinely cultured in suspension.

The intracellular GPDH activity levels measured at 72 hours, 7 days, and 14 days after the induction of differentiation were normalized to the total intracellular protein concentration to facilitate comparative analyses. A significant increase in intracellular protein levels over time for non-induced hASCs cultured in 2-D was observed, which correlates to the absence of growth arrest in the proliferation medium. More importantly, the normalized GPDH activity levels yielded highly promising results. The mean GPDH activity value calculated at 14 days for the hASCs dynamically cultured on DAT-based microcarriers was greater than the activity values of all other samples at 14 days, pointing to the ability of DAT-based microcarriers to provide an adipogenic microenvironment for the differentiating hASCs.

Overall, DAT-based microcarriers seeded with hASCs were shown to significantly support adipogenic differentiation following induction, based on lipid loading and significantly elevated GPDH activity following 14 days of adipogenic culture. In contrast, gelatin-based microcarriers investigated were not shown to appreciably support adipogenic differentiation of seeded hASCs, indicating that the complex composition and/or architecture of the ECM are key modulating factors that need to be considered. Qualitative assessment of the DAT-based microcarriers after 28 days of dynamic cell culturing indicated that the beads were highly robust and stable. Moving toward clinical translatability, isolated DAT-based microcarriers were successfully extruded in a minimized fluid volume from an 18-gauge hypodermic needle to form a 1 cm^3 microcarrier aggregate. This needle gauge is within the size range commonly employed in the clinic [11], and varying construct shapes could be produced by extrusion into size-limited voids, pointing to the potential for hASC-seeded DAT-based microcarriers to repair small-volume soft tissue defects.

Chapter 5
Global Discussion

This thesis highlights the potential of cell-based strategies for adipose tissue engineering, and the powerful manner by which cell responses can be directed as a function of cell microenvironment. Overall, microcarriers prepared from solubilized decellularized adipose tissue (DAT) using non-cytotoxic reagents were found to significantly enhance the cell response of seeded hASCs cultured in a dynamic spinner flask environment. Interestingly, gelatin-based microcarriers comprised of denatured collagen were not shown to support appreciable adipogenic differentiation of seeded hASCs, when subjected to comparable fabrication methods and culturing conditions as the seeded DAT-based microcarriers. This data points to the complex advantages of using tissue-specific extracellular matrices (ECMs) derived from decellularized tissue as scaffold base materials for tissue engineering.

The ECM secreted by undifferentiated ASCs is predominantly comprised of collagen type I, which is found in high concentrations within the fibrous tissue fractions in adipose tissue [59]. As a result, solubilized DAT also represents a denatured collagenous material. However, utilizing this solubilized matrix as a base for the fabrication of microcarriers demonstrated a superior capacity in supporting the attachment, proliferation, and adipogenic differentiation of seeded hASCs when compared to gelatin. Many proteins and important cell-mediating growth factors are embedded within the highly-complex ECM found in tissues, present in different combinations and ratios depending on the specific tissue type and anatomical depot [25, 104]. It is possible that within solubilized DAT, the proteinaceous composition of the adipose matrix, rich in basement membrane (collagen type IV and laminin), is at least partially retained, thereby

preserving an environment that is favorable to ASCs and mature adipocytes which, *in vivo*, are responsible for secreting and organizing the native adipose matrix [59].

Previous work has indicated that intact DAT with a highly-preserved three-dimensional (3-D) architecture and composition is inductive of adipogenesis in seeded human ASCs (hASCs) [14]. In particular, glycerol-3-phosphate dehydrogenase (GPDH) enzymatic activity of cells cultured in intact DAT scaffolds has been shown to be significantly elevated as compared to cell aggregates devoid of exogenous matrix and two-dimensional (2-D) tissue culture controls [14]. The results in this thesis corroborate these previous findings, while also providing motivation for the further development of tissue-specific microcarriers as scaffolds for tissue engineering. Interestingly, studies investigating the GPDH activity levels of seeded hASCs on decellularized placental matrices at 14 days have demonstrated significantly lower GPDH activity levels, as compared to those measured for hASCs dynamically cultured on DAT-based microcarriers, as well as on intact DAT [172]. This points to the significant advantage of employing tissue-specific approaches, through incorporating the ECM derived specifically from the native matrix of the tissue of interest.

Therefore, this thesis suggests the potential to develop other tissue- or cell-specific microcarriers derived from decellularized ECM from which the cells of interest are sourced, such that the overall approach is tailored toward the regeneration of specific tissues. In theory, any tissue that can effectively be decellularized has the potential to be used as a base material for preparing microcarriers using the developed methods, and could in turn be seeded with cells sourced from the same type of tissue. This customized approach could potentially enhance the desired cell response by closely recapitulating the native cellular microenvironment. Moreover, it is possible that by seeding multipotent ASCs or MSCs onto different decellularized tissue-based microcarriers, the direction of cell fate could be significantly directed and controlled by the cell

scaffold. A matrix-based approach could reduce or potentially eliminate the requirement for costly stem-cell differentiation factors, including growth factors and hormones, which could have undesirable systemic side effects, providing further support for the clinical translatability of this general approach.

Studies to date investigating the development of tissue-specific scaffolds, although limited in number, support the use of decellularized tissues as inductive scaffolds when seeded with cells isolated from the same type of tissue as the matrix. This has been evidenced not only by the ability of DAT to direct hASC fate toward the adipogenic lineage without the addition of exogenous factors [14], but also in work by Sellaro *et al.* (2007), in which sinusoidal endothelial cells isolated from the liver and cultured on ECM substrates derived from the liver, demonstrated superior retention of the differentiated liver cell phenotype [173]. In contrast, sinusoidal endothelial cells cultured on ECM materials derived from the bladder and small intestinal submucosa (SIS) lost their specialized phenotype within 3 days [173].

From a materials perspective, the promising results of DAT-based scaffolds may be due to the preservation of the basement membrane (BM). However, the 3-D architecture and composition of the scaffold itself are also important considerations that are likely modulating the cell responses, as evidenced by the higher GPDH activity levels observed in the literature on intact DAT scaffolds, as compared to DAT-based microcarriers [14]. While the microcarriers produced in this thesis were microporous in terms of surface morphology, potentially enhancing cell attachment, the incorporation of a more macroporous geometry, coupled with an overall smaller microcarrier diameter, could potentially influence the cell organization, infiltration, and distribution. These cell-cell and cell-matrix interactions could significantly impact proliferation and adipogenesis in seeded hASCs, resulting in even higher GPDH activities upon induction of differentiation.

Committed preadipocytes must enter growth arrest before differentiating, which is often achieved by cell-cell contact inhibition [39]. Therefore, the seeding density relative to the surface area of the DAT-based microcarriers could play a critical role in modulating the cell response. During this work, the initial seeding densities were based on positive results reported in the literature [141], with a range investigated to more thoroughly assess the hASC proliferative capacity. However, microcarrier diameter is another factor that will impact this cell response. To date, microcarriers investigated for use in adipose tissue-engineering strategies have been as small as 50 μm in diameter [174], with commercially-available microcarriers ranging between 100-2500 μm, depending on the particular lineage of interest [125]. In a study by Choi *et al.* (2008), the effect of PLGA microsphere diameter on rabbit MSCs was assessed, and an optimal diameter of 100-150 μm described for adipogenic applications [149]. However, inconsistencies between dynamic culturing studies in the literature renders the selection of the 'ideal' cell number to microcarrier surface area ratio as challenging, and systematic experimentation with both cell seeding density and microcarrier diameter is required to further optimize the cell response to DAT-based microcarriers. Through achieving a more closely-packed cellular distribution on the microcarriers, cell-cell and paracrine effects could be harnessed more effectively to help achieve the desired cell behavior. Nevertheless, the results in this thesis present the first important step towards a tissue-specific cell expansion substrate, as well as an adipogenic, injectable cell delivery vehicle.

To the author's knowledge, this thesis presents the first incorporation of a fully-decellularized tissue into a microcarrier geometry, with the aim of developing a tissue- or cell-specific microscaffold. Most similarly, work by Choi *et al.* (2009) investigated the use of adipose tissue-derived gels prepared by removing the lipid fraction from adipose tissue, freeze-drying the tissue, and rehydrating the product to form a gel [146]. This material does not present as pure a

base matrix for scaffold fabrication from a cell perspective, as it is not fully decellularized. However, results assessing the cell response of seeded ASCs to the adipose-derived gel demonstrated promise, further supporting the notion of tissue-specific scaffold development.

Within this thesis, the ability to successfully stabilize DAT-based microcarriers using less cytotoxic photochemical crosslinking agents *in lieu* of conventional chemical crosslinkers, such as glutaraldehyde, has potentially important clinical implications such as decreased cytotoxicity and the reduced calcification of transplanted microcarriers. Toward the goal of clinical translatability, the DAT-based microcarriers produced in this research demonstrated excellent stability upon drying and rehydration, pointing to the possible off-the-shelf availability of this product. DAT-based microcarriers could be fabricated at a centralized location, and dehydrated prior to distribution. The significantly reduced space requirements for spinner flasks with microcarriers, relative to TCPS substrates with the equivalent surface area, could permit hASCs to be more readily expanded on site at the clinic, further supporting the practicality of this approach. Overall, MSC numbers yielded from human adipose tissue are significantly greater than from human bone marrow. However, to be applied on a clinically-relevant scale, it may not be possible to achieve the cell number required without *in vitro* cell expansion prior to therapeutic use.

Given the promise of DAT-based microcarriers to support hASC proliferation *in vitro*, these microcarriers may also provide a means by which to expand hASCs for approaches beyond adipose tissue-engineering applications. For instance, based on the multipotent potential of ASCs, DAT-based microcarriers could be used to expand ASCs to relevant numbers *in vitro*, and the cells could be enzymatically extracted and incorporated in a cartilage or bone tissue-engineering strategy. To this end, characterization of the ASCs following expansion on the DAT-based microcarriers would prove useful in confirming the retained multilineage capacity of the ASCs.

Promising results around injectability, coupled with the higher adipogenic response of ASCs cultured on DAT-based microcarriers, as well as the expected biodegradability and low immunogenicity of DAT and autologous or allogenic hASCs, supports the investigation of DAT-based microcarriers as an injectable product for the minimally-invasive repair of small-volume or irregularly-shaped subcutaneous soft tissue defects, particularly of the face.

For the repair of larger-volume or shape-specific defects, a variety of composite approaches could be employed, involving the incorporation of seeded DAT-based microcarriers within hydrogels, such as photochemically-crosslinked solubilized DAT-based gels, or within larger sections of intact DAT, to yield highly adipogenic products. The work described in this thesis presents the groundwork for numerous microcarrier- or scaffold-design approaches, and the results obtained indicate the promising route of tissue-specific scaffolds in the fields of tissue engineering and regenerative medicine. This work also points to the complex interdisciplinary nature of the field, requiring a balance of engineering science and medicine to ultimately achieve the long-term goal of developing a safe and reliable clinical product.

Chapter 6
Conclusions and Future Work

6.1 Summary and Conclusions

Current treatments of subcutaneous defects, resulting from tumor resections, trauma, and congenital abnormalities, demonstrate limited long-term success, and depend largely on autologous tissue grafting or synthetic filler materials, which predominantly restore volume rather than function [6-8, 34]. For the correction of small-volume defects, injectable fillers have been investigated as a minimally-invasive approach [1, 6, 11]. Specifically, a variety of gels and microcarriers have been assessed for their ability to act as both cell culture substrates and directly-injectable cell delivery vehicles, following cell seeding with regenerative populations and *in vitro* expansion [6]. Recent literature points to the promise of using microcarriers for adipose tissue engineering, including the dynamic culture of adipose-derived stem cells (ASCs) [103, 124, 141, 149, 174]. However, to date, limited research has been conducted toward the design of an adipose-derived, tissue-specific microcarrier.

In this work, methods were developed for the fabrication of injectable microcarriers from decellularized adipose tissue (DAT) via non-cytotoxic protocols, which were in turn evaluated for their ability to support the proliferation and adipogenic differentiation of hASCs in a dynamic spinner flask microenvironment. More specifically, DAT was solubilized by an acid/pepsin digestion and combined with alginate to produce composite DAT/alginate microcarriers, the collagenous phase was stabilized through crosslinking, and the alginate was extracted. Microcarrier diameter, size distribution, porosity, stability, and swelling behavior were characterized, in addition to evaluating microcarrier sterility and injectability. Gelatin-based microcarriers were prepared using comparable methods and were used as controls.

Stability studies investigated changes in mean diameter and protein release over time for different microcarrier formulations. The data indicated that the non-cytotoxic photosensitizing agent rose bengal effectively stabilized the DAT-based microcarriers, with comparable results to glutaraldehyde crosslinking, but with reduced toxicity concerns. Minimal protein release was observed from all DAT-based microcarriers in a simulated physiological environment (< 15 μg/mL at all time points) over a 1-month time frame. Furthermore, no significant impact was observed on average microcarrier diameter (934 ± 51 μm) or stability following drying with supercritical CO_2, storage, and rehydration, pointing to the potential for DAT-based microcarriers to be fabricated at a centralized location, dried, distributed, and rehydrated on demand in a clinical setting.

Alginate removal from all microcarrier formulations was confirmed by optical and scanning electron microscopy (SEM), in addition to fluorescent imaging of microcarriers prepared using pre-labeled alginate. Adequate extraction of the alginate, coupled with the microporous surface observed under SEM, may be beneficial in promoting cell attachment. The fabricated beads had an estimated percent porosity of 29 ± 4 %, based on liquid displacement. Microcarrier sterility using the developed fabrication approaches supported the use of DAT-based microcarriers in subsequent *in vitro* culturing studies.

The second phase of this thesis evaluated DAT-based microcarriers as a dynamic cell culture substrate for human ASCs (hASCs). The rose bengal-crosslinked DAT-based microcarriers, selected based on the previous characterization data, were seeded with hASCs and cultured in a dynamic spinner flask system. Total double-stranded DNA (dsDNA) content and fluorescence microscopy were used as measures of cell proliferation over time. The adipogenic response following the induction of differentiation through the use of medium supplemented with adipogenic factors, was assessed through Oil Red O intracellular lipid staining and measurements

of glycerol-3-phosphate dehydrogenase (GPDH) activity, a key enzyme involved in triacylglycerol biosynthesis [7, 30]. Results obtained from culturing studies indicated that the DAT-based microcarriers provided a more positive response in terms of both proliferation and adipogenic differentiation relative to not only the gelatin-based microcarriers subjected to identical conditions, but also to hASCs from the same source cultured using conventional two-dimensional (2-D) monolayer techniques. These findings corroborate previous work in the literature that indicates that DAT provides an inductive microenvironment for adipogenesis [14], and highlight the critical role of both the scaffold material and the culturing environment employed in modulating cell response. Moreover, the results obtained support the use of tissue- and/or cell-specific scaffold biomaterials seeded and cultured with autologous or allogenic cells and cultured in a dynamic, low-shear culture system.

To date, limited work has investigated the use of tissue- and/or cell-specific biomaterials, with the aim of regenerating a specific tissue or inducing a specific cell response. The research presented in this thesis demonstrates the investigation of the first, fully decellularized tissue-based spherical microcarrier approach to date. Furthermore, the developed methods could be applied to other decellularized tissues or matrix sources to fabricate cell- or tissue-specific scaffolds. This general approach could potentially better mimic the native extracellular condition found in the body, and thereby promote more normal cellular organization and behavior. Overall, DAT-based microcarriers have great potential for clinical use in a wide range of reconstructive and cosmetic applications.

6.2 Contributions

The most significant contributions of this thesis to the field were as follows;

- Designed, fabricated, and characterized a new microcarrier scaffold prepared from decellularized adipose tissue, using non-cytotoxic reagents, for use in adipose tissue engineering as either a cell expansion substrate or a novel injectable biomaterial for soft tissue augmentation. This work represents a critical first step towards a tissue-specific, engineered microcarrier approach.
- Developed seeding and culturing protocols for the dynamic culture of hASCs on DAT-based microcarriers.
- Successfully demonstrated that DAT-based microcarriers supported higher ASC proliferation and also induced a greater adipogenic response, relative to ASCs grown on gelatin-based microcarriers or 2-D tissue culture polystyrene (TCPS).

6.3 Future Work

Results obtained during this work indicate that DAT-based microcarriers hold significant promise. The dynamic expansion of ASCs *in vitro* for direct injectability *in vivo* could translate to a novel clinical repair strategy for small-volume subcutaneous defects. Therefore, a discussion of recommendations for future short- and long-term work is included herein.

i. Microcarrier Fabrication

To further enhance DAT-based microcarrier stability and favorability to seeded ASCs, methods established for the fabrication of DAT-based microcarriers could be further optimized. This could be done by incorporating a macroporous structure, higher total protein content, and more tightly-controlled droplet sizes. Therefore, the following steps are recommended;

- Enhance control over total protein content within solubilized DAT by developing drying techniques such as lyophilization, to yield enriched DAT solutions with a higher and more specific protein concentration.
- Improve microcarrier core stabilization through the incorporation of non-cytotoxic photosensitizers within the solubilized DAT solution prior to microcarrier fabrication.
- Modify fabrication protocols such that a macroporous microcarrier structure is achieved; further enhancing cellular attachment and enabling cell ingrowth.
- Investigate microfluidic platforms and/or spray nozzles by which to achieve more precise control over droplet morphology and/or size.

ii. Microcarrier Characterization

Preserving the proteinaceous structure of the native adipose matrix, while also minimizing undesirable interactions between the collagenous and alginate phases within the microcarriers during fabrication steps could further enhance cell attachment and lead to an overall heightened adipogenic response. Moreover, ensuring that the microcarriers mimic the material and mechanical properties of native fat could significantly improve patient comfort associated with the transplanted material. Therefore, further microcarrier characterization is recommended;

- Perform immunohistochemical staining, including collagen typing, on sectioned DAT-based microcarriers to confirm the presence and distribution of the extracellular matrix (ECM) components within the beads, including collagen type IV and laminin.
- Measure the zeta potential of alginate microcarriers, DAT/alginate composite microcarriers, and alginate-extracted DAT-based microcarriers at fabrication conditions to characterize potential protein-alginate interactions.

- Determine the mechanical properties of DAT-based microcarriers, in a hydrated state under simulated physiological conditions, to assess the differences in microcarrier properties as compared to native adipose tissue and intact DAT.

iii. Microcarrier Adipogenic Potential *In Vitro*

While the *in vitro* work conducted in this thesis supported the capacity for DAT-based microcarriers to support the dynamic proliferation and adipogenic differentiation of hASCs in a spinner flask environment, considerable work is required to further optimize the overall approach from both a system design and characterization perspective. Through investigating the following recommendations, significant advances could be made in the current understanding of dynamic culturing microenvironments and their ability to modulate cell responses;

- Evaluate the impact of DAT-based microcarriers on the hASC response, as compared to micronized DAT particles prepared by freeze drying and grinding (cryo-milling), or other methods.
- Systematically evaluate the effect(s) of DAT-based microcarrier diameter (50-1000 μm) on the observed cell response, and further optimize cell seeding densities and dynamic seeding protocols. Expansion could be improved by reducing the bead diameter and increasing the seeding density, to promote desirable cell-cell interactions and effects modulated by paracrine factors.
- Assess the hASC response to DAT-based microcarriers dynamically cultured under i) normoxic (20-21%) and ii) hypoxic (1-5%) conditions. It is hypothesized that cell expansion could be significantly increased, as oxygen tension is a known mediator of mesenchymal stem cell (MSC) proliferation, with significantly reduced doubling times observed under hypoxic conditions [175].

- Assess the gene expression profile over time in adipogenically-induced and non-induced hASCs dynamically cultured on DAT-based microcarriers through end-point RT-PCR, to determine if DAT-based microcarriers can induce adipogenic differentiation without the addition of exogenous differentiation factors. Key genes include early stem cell markers (Stro-1, CD90 and CD34) and adipogenic genes (LPL, Glut-4, PPARγ, and C/EBPα).
- Measure the secretion of adipokines and metabolic glucose uptake by hASCs dynamically cultured on DAT-based microcarriers, as compared to 2-D-cultured hASCs.
- Characterize the cell-surface immunophenotype of hASCs dynamically cultured on DAT-based microcarriers using flow cytometry, as compared to hASCs cultured using a 2-D monolayer approach.
- Fabricate microcarriers from other decellularized tissues, such as the dermis, and seed with hASCs to probe the ability of DAT-based microcarriers to specifically direct cell fate.

iv. Microcarrier Adipogenic Potential *In Vivo*

Ultimately, the ability to predictably regenerate stable adipose tissue *in vivo* to provide long-term solutions to the clinical problem of subcutaneous soft tissue defect repair is the true measure of success for DAT-based microcarriers as an adipose tissue-engineering strategy. Despite attentions paid to incorporating clinical translatability into the overall approach in this work, the ability for DAT-based microcarriers to successfully induce fat formation must be tested in an animal model to further assess the regenerative response. A recommended model is proposed herein. Furthermore, consideration must be given to the defect size that may be treated with an injectable product, as compared to a larger-volume construct. Therefore, future work

investigating the regenerative *in vivo* response of injected DAT-based microcarriers in composite scaffolding approaches for large-volume soft tissue augmentation is recommended;

- Assess the biocompatibility of the unseeded DAT-based microcarriers in an immunocompetent, subcutaneous mouse model at 72 h, 7 days, 14 days, and 28 days.
- Subcutaneously inject nude mice with i) unseeded DAT-based microcarriers, ii) dynamically cultured hASC-seeded DAT-based microcarriers, and iii) statically-cultured hASCs combined with unseeded DAT-based microcarriers, and evaluate the regenerative response through histological and immunohistochemical staining and quantification of key adipogenic genes (LPL, PPARγ, and C/EBPα) at 3 and 8 weeks after transplantation.
- Combine seeded microcarriers with intact DAT scaffolds, after dynamically expanding hASCs on DAT-based microcarriers *in vitro*. Assess the *in vivo* regenerative response in terms of tissue organization and gene expression in a subcutaneous nude mouse model, as compared to directly injected cell-seeded DAT-based microcarriers at 3, 6, and 12 months after transplantation.

References

[1] Patrick CW. Tissue engineering strategies for adipose tissue repair. The Anatomical Record 2001;263:361-6.

[2] Hong L, Peptan I, Colpan A, Daw J. Adipose Tissue Engineering by Human Adipose-Derived Stromal Cells. Cells Tissues Organs 2006;183:133-40.

[3] American Society of Plastic Surgery. 2000/2008/2009 National Plastic Surgery Statistics. 2009.

[4] Hemmrich K, Vonheimburg D, Rendchen R, Dibartolo C, Milella E, Pallua N. Implantation of preadipocyte-loaded hyaluronic acid-based scaffolds into nude mice to evaluate potential for soft tissue engineering. Biomaterials 2005;26:7025-37.

[5] Cho S, Kim S, Wonrhie J, Micho H, Yongchoi C, Kim B. Engineering of volume-stable adipose tissues. Biomaterials 2005;26:3577-85.

[6] Bauer-Kreisel P, Goepferich A, Blunk T. Cell-delivery therapeutics for adipose tissue regeneration. Advanced Drug Delivery Reviews 2010;62:798-813.

[7] Choi JH, Gimble JM, Lee K, Marra KG, Rubin JP, Yoo JJ, et al. Adipose Tissue Engineering for Soft Tissue Regeneration. Tissue Engineering Part B: Reviews 2010;16:413-26.

[8] Beahm E, Walton R, Patrickjr C. Progress in adipose tissue construct development. Clinics in Plastic Surgery 2003;30:547-58.

[9] Flynn L, Woodhouse KA. Adipose tissue engineering with cells in engineered matrices. Organogenesis 2008;4:228-35.

[10] Torio-Padron N, Baerlecken N, Momeni A, Stark GB, Borges J. Engineering of Adipose Tissue by Injection of Human Preadipocytes in Fibrin. Aesthetic Plastic Surgery 2007;31:285-93.

[11] Klein AW, Elson ML. The history of substances for soft tissue augmentation. Dermatologic Surgery 2000;26:1096-105.

[12] Langer R, Vacanti JP. Tissue engineering. Science 1993;260:920-6.

[13] Zuk P, Zhu M, Ashjian P, De Ugarte D, Huang J. Human Adipose Tissue Is a Source of Multipotent Stem Cells. Molecular Biology of the Cell 2002;13:4279-95.

[14] Flynn LE. The use of decellularized adipose tissue to provide an inductive microenvironment for the adipogenic differentiation of human adipose-derived stem cells. Biomaterials 2010;31:4715-24.

[15] Gomillion C, Burg K. Stem cells and adipose tissue engineering. Biomaterials 2006;27:6052-63.

[16] Trayhurn P, Beattie JH. Physiological role of adipose tissue: white adipose tissue as an endocrine and secretory organ. Proceedings of the Nutrition Society 2001;60:11.

[17] MacDougald O, Mandrup S. Adipogenesis: forces that tip the scales. Trends in Endocrinology & Metabolism 2002;13:5-11.

[18] Hausman D, DiGirolamo M, Bartness T, Hausman G. The biology of white adipocyte proliferation. Obesity Reviews 2001;2:239-54.

[19] Singla P, Bardoloi A, Parkash AA. Metabolic effects of obesity: A review. World Journal of Diabetes 2010;1:76-88.

[20] Cinti S. The adipose organ. Prostaglandins, Leukotrienes and Essential Fatty Acids 2005;73:9-15.

[21] Crandall D, Hausman G, Kral J. A Review of the Microcirculation of Adipose Tissue: Anatomic, Metabolic, and Angiogenic Perspectives. Microcirculation 1997;4:211-32.

[22] Cinti S. Transdifferentiation properties of adipocytes in the adipose organ. American Journal of Physiology Endocrinology and Metabolism 2009;297:977-86.
[23] Arbuthnott E. Brown adipose tissue: structure and function. Proceedings of the Nutrition Society 2007;48:177-82.
[24] Garlid KD, Jabůrek M, Jezek P. The mechanism of proton transport mediated by mitochondrial uncoupling proteins. Federation of European Biochemical Societies Letters 1998;438:10-4.
[25] Rada T, Reis R, Gomes M. Adipose Tissue-Derived Stem Cells and Their Application in Bone and Cartilage Tissue Engineering. Tissue Engineering Part B: Reviews 2009;15:113-25.
[26] Christiaens V, Lijnen HR. Angiogenesis and development of adipose tissue. Molecular and Cellular Endocrinology 2010;318:2-9.
[27] Lijnen HR. Angiogenesis and obesity. Cardiovascular Research 2008;78:286-93.
[28] Choi JS, Yang H-J, Kim BS, Kim JD, Lee S-H, Lee EK, et al. Fabrication of Porous Extracellular Matrix (ECM) Scaffolds from Human Adipose Tissue. Tissue Engineering Part C: Methods 2009;15:1-10.
[29] Shenaq S, Yuksel E. New research in breast reconstruction: Adipose tissue engineering. Clinics in Plastic Surgery 2002;29:111-25.
[30] Ailhaud G, Grimaldi P, Negrel R. Cellular and Molecular Aspects of Adipose Tissue Development. Annual Reviews in Nutrition 1992;12:207-33.
[31] Jurgens WJFM, Oedayrajsingh-Varma MJ, Helder MN, Zandiehdoulabi B, Schouten TE, Kuik DJ, et al. Effect of tissue-harvesting site on yield of stem cells derived from adipose tissue: implications for cell-based therapies. Cell and Tissue Research 2008;332:415-26.
[32] Gimble J, Guilak F. Adipose-derived adult stem cells: isolation, characterization, and differentiation potential. Cytotherapy 2003;5:362-9.
[33] Gimble JM, Katz AJ, Bunnell BA. Adipose-Derived Stem Cells for Regenerative Medicine. Circulation Research 2007;100:1249-60.
[34] Patrick C. Adipose tissue engineering: The future of breast and soft tissue reconstruction following tumor resection. Seminars in Surgical Oncology 2000;19:302-11.
[35] Kiess W, Petzold S, Topfer M, Garten A, Bluher S, Kapellen T, et al. Adipocytes and adipose tissue. Best Practice & Research Clinical Endocrinology & Metabolism 2008;22:135-53.
[36] Rosen E, Spiegelman B. Molecular Regulation of Adipogenesis. Annual Reviews in Cell and Developmental Biology 2000;16:145-71.
[37] Wood R. Vitamin D and adipogenesis: new molecular insights. Nutrition Reviews 2008;66:40-6.
[38] Mitchell J, McIntosh K, Zvonic S, Garrett S, Floyd Z, Kloster A, et al. Immunophenotype of Human Adipose-Derived Cells: Temporal Changes in Stromal-Associated and Stem Cell–Associated Markers. Stem Cells 2005;24:376-85.
[39] Gregoire F. Adipocyte Differentiation: From Fibroblast to Endocrine Cell. Experimental Biology and Medicine 2001;226:997-1002.
[40] Gregoire F, Smas C, Sul H. Understanding Adipocyte Differentiation. Physiological Reviews 1998;78:783-809.
[41] Mandrup S, Lane M. Regulating adipogenesis. Journal of Biological Chemistry 1997;272:5367-70.
[42] Rosen ED, Walkey CJ, Puigserver P, Spiegelman BM. Transcriptional regulation of adipogenesis. Genes and Development 2000;14:1293-307.

[43] Holst D, Grimaldi P. New factors in the regulation of adipose differentiation and metabolism. Current Opinion in Lipidology 2002;13:241-5.
[44] Ayalasumuano J. Adipogenic genes on induction and stabilization of commitment to adipose conversion. Biochemical and Biophysical Research Communications 2008;374:720-4.
[45] Soukas A. Distinct Transcriptional Profiles of Adipogenesis in Vivo and in Vitro. Journal of Biological Chemistry 2001;276:34167-74.
[46] Stephens JM, Morrison RF, Wu Z, Farmer SR. PPARgamma ligand-dependent induction of STAT1, STAT5A, and STAT5B during adipogenesis. Biochemical and Biophysical Research Communications 1999;262:216-22.
[47] Novakofski J. Adipogenesis: Usefulness of in vitro and in vivo experimental models. Journal of Animal Science 2004;82:905-15.
[48] Kelly DJ, Jacobs CR. The role of mechanical signals in regulating chondrogenesis and osteogenesis of mesenchymal stem cells. Birth Defects Research: Part C 2010;90:75-85.
[49] Cao Y. Angiogenesis modulates adipogenesis and obesity. Journal of Clinical Investigation 2007;117:2362-8.
[50] Yao R, Zhang R, Yan Y, Wang X. In Vitro Angiogenesis of 3D Tissue Engineered Adipose Tissue. Journal of Bioactive and Compatible Polymers 2009;24:5-24.
[51] Kolditz C-I, Langin D. Adipose tissue lipolysis. Current Opinion in Clinical Nutrition and Metabolic Care 2010;13:377-81.
[52] Vernon R, Denis R, Sørensen A. Signals of adiposity. Domestic Animal Endocrinology 2001;21:197-214.
[53] Cornelius P, MacDougald O, Lane M. Regulation of Adipocyte Development. Annual Reviews in Nutrition 1994;14:99-129.
[54] Large V, Peroni O, Letexier D, Ray H, Beylot M. Metabolism of lipids in human white adipocyte. Diabetes Metabolism 2004;30:294-309.
[55] Kershaw EE, Flier JS. Adipose tissue as an endocrine organ. The Journal of Clinical Endocrinology & Metabolism 2004;89:2548-56.
[56] Ailhaud G. Adipose tissue as a secretory organ: from adipogenesis to the metabolic syndrome. Comptes Rendus Biologies 2006;329:570-7.
[57] Hauner H. Secretory factors from human adipose tissue and their functional role. Proceedings of the Nutrition Society 2005;64:163-9.
[58] Ahima R, Flier J. Leptin. Annual Reviews in Physiology 2000;62:413-37.
[59] Mariman ECM, Wang P. Adipocyte extracellular matrix composition, dynamics and role in obesity. Cellular and Molecular Life Sciences 2010;67:1277-92.
[60] Badylak SF. The extracellular matrix as a scaffold for tissue reconstruction. Cell & Developmental Biology 2002;13:377-83.
[61] Nakajima I, Yamaguchi T, Ozutsumi K, Aso H. Adipose tissue extracellular matrix: newly organized by adipocytes during differentiation. Ontogeny 1998;63:193-200.
[62] Kleinman HK, Philp D, Hoffman MP. Role of the extracellular matrix in morphogenesis. Current Opinions in Biotechnology 2003;14:526-32.
[63] Stillaert F, Blondeel P, Abberton K, Thompson E. Adipose Tissue Induction in Vivo. Advances in Experimental Medicine and Biology 2006;585:403-12.
[64] Gelse K. Collagens—structure, function, and biosynthesis. Advanced Drug Delivery Reviews 2003;55:1531-46.
[65] Patino M, Neiders M, Andreana S, Noble B. Collagen: An Overview. Implant Dentistry 2002;11:280-4.

[66] Ottani V, Raspanti M, Ruggeri A. Collagen structure and functional implications. Micron 2001;32:251-60.
[67] Hudson B, Reeders S, Tryggvason K. Type IV collagen: structure, gene organization, and role in human diseases. Journal of Biological Chemistry 1993;268:26033-6.
[68] Timpl R, Wiedemann H, Delden V, Furthmayr H, Kuhn K. A network model for the organization of type IV collagen molecules in basement membranes. European Journal of Biochemistry 1981;120:203-11.
[69] Martin GR, Timpl R. Laminin and other basement membrane components. Annual Review of Cell Biology 1987;3:57-85.
[70] Badylak SF. Regenerative medicine and developmental biology: the role of the extracellular matrix. Anatomical Record (Part B: New Anatomist) 2005;287:36-41.
[71] Engel J. Laminins and other strange proteins. Biochemistry 1992;31:10643-51.
[72] Tzu J, Marinkovich M. Bridging structure with function: Structural, regulatory, and developmental role of laminins. The International Journal of Biochemistry & Cell Biology 2008;40:199-214.
[73] Chaubey A, Burg KJL. Extracellular Matrix Components as Modulators of Adult Stem Cell Differentiation in an Adipose System. Journal of Bioactive and Compatible Polymers 2008;23:20-37.
[74] Patrick CW. Breast Tissue Engineering. Annual Review of Biomedical Engineering 2004;6:109-30.
[75] De Ugarte D, Ashjian P, Elbarbary A, Hedrick M. Future of Fat as Raw Material for Tissue Regeneration. Annals of Plastic Surgery 2003;50:215-9.
[76] Heimburg D, Hemmrich K, Zachariah S, Staiger H, Pallua N. Oxygen consumption in undifferentiated versus differentiated adipogenic mesenchymal precursor cells. Respiratory Physiology & Neurobiology 2005;146:107-16.
[77] Walton RL, Beahm EK, Wu L. De novo adipose formation in a vascularized engineered construct. Microsurgery 2004;24:378-84.
[78] Fernandez E, Mackley C. Soft tissue augmentation: a review. Journal of Drugs in Dermatology 2006;5:630-41.
[79] Borenstein JT, Weinberg EJ, Orrick BK, Sundback C, Kaazempur-Mofrad MR, Vacanti JP. Microfabrication of Three-Dimensional Engineered Scaffolds. Tissue Engineering 2007;13:1837-44.
[80] Sturm LP, Cooter RD, Mutimer KL, Graham JC, Maddern GJ. A systematic review of permanent and semipermanent dermal fillers for HIV-associated facial lipoatrophy. AIDS Patient Care STDS 2009;23:699-714.
[81] Rehfeldt F, Engler AJ, Eckhardt A, Ahmed F, Discher DE. Cell responses to the mechanochemical microenvironment - implications for regenerative medicine and drug delivery. Advanced Drug Delivery Reviews 2007;59:1329-39.
[82] Place ES, George JH, Williams CK, Stevens MM. Synthetic polymer scaffolds for tissue engineering. Chemical Society Reviews 2009;38:1139-51.
[83] Bunnell B, Flaat M, Gagliardi C, Patel B, Ripoll C. Adipose-derived stem cells: Isolation, expansion and differentiation. Methods 2008;45:115-20.
[84] Minguell J, Erices A, Conget P. Mesenchymal Stem Cells. Experimental Biology and Medicine 2001;226:507-20.
[85] Vashi A, Keramidaris E, Abberton K, Morrison W, Wilson J, Oconnor A, et al. Adipose differentiation of bone marrow-derived mesenchymal stem cells using Pluronic F-127 hydrogel in vitro. Biomaterials 2007;29:573-9.

[86] Zuk P, Zhu M, Mizuno H, Huang J, Futrell J. Multilineage Cells from Human Adipose Tissue: Implications for Cell-Based Therapies. Tissue Engineering 2001;7:211-28.
[87] Halbleib M. Tissue engineering of white adipose tissue using hyaluronic acid-based scaffolds. I: in vitro differentiation of human adipocyte precursor cells on scaffolds. Biomaterials 2003;24:3125-32.
[88] Borzacchiello A, Mayol L, Ramires P, Pastorello A, Bartolo C, Ambrosio L, et al. Structural and rheological characterization of hyaluronic acid-based scaffolds for adipose tissue engineering. Biomaterials 2007;28:4399-408.
[89] Mano JF, Silva GA, Azevedo HS, Malafaya PB, Sousa RA, Silva SS, et al. Natural origin biodegradable systems in tissue engineering and regenerative medicine: present status and some moving trends. Journal of the Royal Society Interface 2007;4:999-1030.
[90] Stenzel K, Miyata T, Rubin A. Collagen as a Biomaterial. Annual Reviews in Biophysics and Bioengineering 1974;3:231-53.
[91] Ibusuki S, Halbesma GJ, Randolph MA, Redmond RW, Kochevar IE, Gill TJ. Photochemically Cross-Linked Collagen Gels as Three-Dimensional Scaffolds for Tissue Engineering. Tissue Engineering 2007;13:1995-2001.
[92] Chan O, So K, Chan B. Fabrication of nano-fibrous collagen microspheres for protein delivery and effects of photochemical crosslinking on release kinetics. Journal of Controlled Release 2008;129:135-43.
[93] Chan BP, So K-F. Photochemical crosslinking improves the physicochemical properties of collagen scaffolds. Journal of Biomedical Materials Research 2005;75A:689-701.
[94] Bigi A, Cojazzi G, Panzavolta S, Roveri N, Rubini K. Stabilization of gelatin films by crosslinking with genipin. Biomaterials 2002;23:4827-32.
[95] Weadock K, Olson R, Silver F. Evaluation of Collagen Crosslinking Techniques. Artificial Cells, Blood Substitutes, & Biotechnology 1983;11:293-318.
[96] Bigi A, Cojazzi G, Panzavolta S, Rubini K, Roveri N. Mechanical and thermal properties of gelatin films at different degrees of glutaraldehyde crosslinking. Biomaterials 2001;22:763-8.
[97] Chan BP, Chan OCM, So K-F. Effects of photochemical crosslinking on the microstructure of collagen and a feasibility study on controlled protein release. Acta Biomaterialia 2008;4:1627-36.
[98] Wollensak G, Spoerl E. Collagen crosslinking of human and porcine sclera. Journal of Cataract & Refractive Surgery 2004;30:689-95.
[99] Rossoni RD, Junqueira JC, Santos ELS, Costa ACB, Jorge AOC. Comparison of the efficacy of Rose Bengal and erythrosin in photodynamic therapy against Enterobacteriaceae. Lasers in Medical Science 2010;25:581-6.
[100] Chen R-N, Ho H-O, Sheu M-T. Characterization of collagen matrices crosslinked using microbial transglutaminase. Biomaterials 2005;26:4229-35.
[101] Smidsrod O, Skjak-Braek G. Alginate as immobilization matrix for cells. Trends in Biotechnology 1990;8:71-8.
[102] Draget K, Skjåk-Bræk G, Smidsrød O. Alginate based new materials. International Journal of Biological Macromolecules 1997;21:47-55.
[103] Marra K, DeFail A, Clavijo-Alvarez J. FGF-2 Enhances Vascularization for Adipose Tissue Engineering. Plastic and Reconstructive Surgery 2008;121:1153-64.
[104] Badylak SF, Freytes DO, Gilbert TW. Extracellular matrix as a biological scaffold material: Structure and function. Acta Biomaterialia 2009;5:1-13.
[105] Gilbert TW, Sellaro TL, Badylak SF. Decellularization of tissues and organs. Biomaterials 2006;27:3675-83.

[106] Chen R-N, Ho H-O, Tsai Y-T, Sheu M-T. Process development of an acellular dermal matrix (ADM) for biomedical applications. Biomaterials 2004;25:2679-86.
[107] Altman AM, Chiu ES, Bai X, Yan Y, Song YH, Newsome RE, et al. Human adipose-derived stem cells adhere to acellular dermal matrix. Aesthetic Plastic Surgery 2008;32:698-9.
[108] Spiegel JH, Egan TJ. Porcine small intestine submucosa for soft tissue augmentation. Dermatologic Surgery 2004;30:1486-90.
[109] Le Visage C, Yang S-H, Kadakia L, Sieber AN, Kostuik JP, Leong KW. Small intestinal submucosa as a potential bioscaffold for intervertebral disc regeneration. Spine 2006;31:2423-30.
[110] Merguerian PA, Reddy PP, Barrieras DJ, Wilson GJ, Woodhouse K, Bagli DJ, et al. Acellular bladder matrix allografts in the regeneration of functional bladders: evaluation of large-segment (> 24 cm) substitution in a porcine model. BJU International 2000;85:894-8.
[111] Lin P, Chan WCW, Badylak SF, Bhatia SN. Assessing porcine liver-derived biomatrix for hepatic tissue engineering. Tissue Engineering 2004;10:1046-53.
[112] Mirsadraee S, Wilcox H, Korossis S, Kearney J. Development and Characterization of an Acellular Human Pericardial Matrix for Tissue Engineering. Tissue Engineering 2006;12:763-73.
[113] Schmidt CE, Baier JM. Acellular vascular tissues: natural biomaterials for tissue repair and tissue engineering. Biomaterials 2000;21:2215-31.
[114] Uchimura E, Sawa Y, Taketani S, Yamanaka Y, Hara M, Matsuda H, et al. Novel method of preparing acellular cardiovascular grafts by decellularization with poly(ethylene glycol). Journal of Biomedical Materials Research Part A 2003;67:834-7.
[115] Steinhoff G, Stock U, Karim N, Mertsching H, Timke A, Meliss RR, et al. Tissue engineering of pulmonary heart valves on allogenic acellular matrix conduits: in vivo restoration of valve tissue. Circulation 2000;102:III50-5.
[116] Rieder E, Kasimir M-T, Silberhumer G, Seebacher G, Wolner E, Simon P, et al. Decellularization protocols of porcine heart valves differ importantly in efficiency of cell removal and susceptibility of the matrix to recellularization with human vascular cells. Journal of Thoracic and Cardiovascular Surgery 2004;127:399-405.
[117] Kim B-S, Yoo JJ, Atala A. Peripheral nerve regeneration using acellular nerve grafts. Journal of Biomedical Materials Research Part A 2004;68:201-9.
[118] Borschel GH, Dennis RG, Kuzon WM. Contractile skeletal muscle tissue-engineered on an acellular scaffold. Plastic and Reconstructive Surgery 2004;113:595-602.
[119] Flynn L, Semple J, Woodhouse K. Decellularized placental matrices for adipose tissue engineering. Journal of Biomedical Materials Research Part A 2006;79:359-69.
[120] Fodor WL. Tissue engineering and cell based therapies, from the bench to the clinic: the potential to replace, repair and regenerate. Reproductive Biology and Endocrinology 2003;1:102-8.
[121] Pörtner R, Nagel-Heyer S, Goepfert C, Adamietz P, Meenen NM. Bioreactor design for tissue engineering. Journal of Bioscience and Bioengineering 2005;100:235-45.
[122] Godara P, McFarland CD, Nordon RE. Design of bioreactors for mesenchymal stem cell tissue engineering. Journal of Chemical Technology and Biotechnology 2008;83:408-20.
[123] Kang X, Xie Y, Kniss DA. Adipose tissue model using three-dimensional cultivation of preadipocytes seeded onto fibrous polymer scaffolds. Tissue Engineering 2005;11:458-68.

[124] Kang S-W, Seo S-W, Choi CY, Kim B-S. Porous Poly(Lactic-Co-Glycolic Acid) Microsphere as Cell Culture Substrate and Cell Transplantation Vehicle for Adipose Tissue Engineering. Tissue Engineering Part C: Methods 2008;14:25-34.
[125] Malda J, Frondoza C. Microcarriers in the engineering of cartilage and bone. Trends in Biotechnology 2006;24:299-304.
[126] Nam JH, Ermonval M, Sharfstein ST. Cell attachment to microcarriers affects growth, metabolic activity, and culture productivity in bioreactor culture. Biotechnology Progress 2007;23:652-60.
[127] Tebb TA, Tsai S-W, Glattauer V, White JF, Ramshaw JAM, Werkmeister JA. Development of porous collagen beads for chondrocyte culture. Cytotechnology 2007;52:99-106.
[128] Hernández RM, Orive G, Murua A, Pedraz JL. Microcapsules and microcarriers for in situ cell delivery. Advanced Drug Delivery Reviews 2010;62:711-30.
[129] van Wezel AL. Growth of Cell-strains and Primary Cells on Micro-carriers in Homogenous Culture. Nature 1967;216:64-5.
[130] Justice BA, Badr NA, Felder RA. 3D cell culture opens new dimensions in cell-based assays. Drug Discovery Today 2009;14:102-7.
[131] Burke D, Brown MJ, Jacobson BS. HeLa cell adhesion to microcarriers in high shear conditions: evidence for membrane receptors for collagen but not laminin or fibronectin. Tissue & Cell 1983;15:181-91.
[132] Hong Y, Gao C, Xie Y, Gong Y, Shen J. Collagen-coated polylactide microspheres as chondrocyte microcarriers. Biomaterials 2005;26:6305-13.
[133] Tabata Y, Miyao M, Inamoto T, Ishii T, Hirano Y. De Novo Formation of Adipose Tissue by Controlled Release of Basic Fibroblast Growth Factor. Tissue Engineering 2000;6:279-89.
[134] Kimura Y, Ozeki M, Inamoto T, Tabata Y. Time course of de novo adipogenesis in matrigel by gelatin microspheres incorporating basic fibroblast growth factor. Tissue Engineering 2002;8:603-13.
[135] Malda J, van Blitterswijk CA, Grojec M, Martens DE, Tramper J, Riesle J. Expansion of bovine chondrocytes on microcarriers enhances redifferentiation. Tissue Engineering 2003;9:939-48.
[136] Malda J, van den Brink P, Meeuwse P, Grojec M, Martens DE, Tramper J, et al. Effect of oxygen tension on adult articular chondrocytes in microcarrier bioreactor culture. Tissue Engineering 2004;10:987-94.
[137] Varani J, Fligiel S, Inman D, Beals T, Hillegas W. Modulation of adhesive properties of DEAE-dextran with laminin. Journal of Biomedical Materials Research 1995;29:993-7.
[138] Tao T, Ji G, Hu W. Serial propagation of mammalian cells on gelatin-coated microcarriers. Biotechnology and Bioengineering 1988;32:1037-52.
[139] Frye C, Patrick C. Three-dimensional adipose tissue model using low shear bioreactors. In Vitro Cellular & Developmental Biology - Animal 2006;42:109-14.
[140] Bayram Y, Deveci M, Imirzalioglu N, Soysal Y, Sengezer M. The cell based dressing with living allogenic keratinocytes in the treatment of foot ulcers: a case study. British Journal of Plastic Surgery 2005;58:988-96.
[141] Rubin JP, Bennett JM, Doctor JS, Tebbets BM, Marra KG. Collagenous Microbeads as a Scaffold for Tissue Engineering with Adipose-Derived Stem Cells. Plastic and Reconstructive Surgery 2007;120:414-24.

[142] Curran SJ, Chen R, Curran JM, Hunt JA. Expansion of human chondrocytes in an intermittent stirred flow bioreactor, using modified biodegradable microspheres. Tissue Engineering 2005;11:1312-22.
[143] Chung HJ, Kim IK, Kim TG, Park TG. Highly Open Porous Biodegradable Microcarriers: In Vitro Cultivation of Chondrocytes for Injectable Delivery. Tissue Engineering Part A 2008;14:607-15.
[144] Senuma Y, Franceschin S, Hilborn JG, Tissières P, Bisson I, Frey P. Bioresorbable microspheres by spinning disk atomization as injectable cell carrier: from preparation to in vitro evaluation. Biomaterials 2000;21:1135-44.
[145] Halberstadt C, Austin C, Rowley J, Culberson C, Loebsack A, Wyatt S, et al. A hydrogel material for plastic and reconstructive applications injected into the subcutaneous space of a sheep. Tissue Engineering 2002;8:309-19.
[146] Choi J, Yang H, Kim B, Kim J, Kim J, Yoo B, et al. Human extracellular matrix (ECM) powders for injectable cell delivery and adipose tissue engineering. Journal of Controlled Release 2009;139:2-7.
[147] Lavik E, Langer R. Tissue engineering: current state and perspectives. Applied Microbiology and Biotechnology 2004;65:1-8.
[148] Kimura Y. Adipose tissue engineering based on human preadipocytes combined with gelatin microspheres containing basic fibroblast growth factor. Biomaterials 2003;24:2513-21.
[149] Choi YS, Park S-N, Suh H. The effect of PLGA sphere diameter on rabbit mesenchymal stem cells in adipose tissue engineering. Journal of Materials Science: Materials in Medicine 2008;19:2165-71.
[150] Melero-Martin JM, Dowling M-A, Smith M, Al-Rubeai M. Expansion of chondroprogenitor cells on macroporous microcarriers as an alternative to conventional monolayer systems. Biomaterials 2006;27:2970-9.
[151] Tsai S, Jeng M, Tsay R, Wang Y. Gel beads composed of collagen reconstituted in alginate. Biotechnology Techniques 1998;12:21-3.
[152] Olde Damink L, Dijkstra P, Luyn M, Wachem P, Nieuwenhuis P, Feijen J. Glutaraldehyde as a crosslinking agent for collagen-based biomaterials. Journal of Materials Science: Materials in Medicine 1995;6:460-72.
[153] Mladenovska K, Cruaud O, Richomme P, Belamie E, Raicki RS, Venier-Julienne M-C, et al. 5-ASA loaded chitosan-Ca-alginate microparticles: Preparation and physicochemical characterization. International Journal of Pharmaceutics 2007;345:59-69.
[154] Eisenbarth E. Biomaterials for Tissue Engineering. Advanced Engineering Materials 2007;9:1051-60.
[155] Choi Y, Park S, Suh H. Adipose tissue engineering using mesenchymal stem cells attached to injectable PLGA spheres. Biomaterials 2005;26:5855-63.
[156] Phillips BW, Horne R, Lay TS, Rust WL, Teck TT, Crook JM. Attachment and growth of human embryonic stem cells on microcarriers. Journal of Biotechnology 2008;138:24-32.
[157] Friedl P, Zänker KS, Bröcker EB. Cell migration strategies in 3-D extracellular matrix: differences in morphology, cell matrix interactions, and integrin function. Microscopy Research and Technique 1998;43:369-78.
[158] Hansen R, Bissell M. Tissue architecture and breast cancer: the role of extracellular matrix and steroid hormones. Endocrine-Related Cancer 2000;7:95-113.
[159] Wu C, Pan J, Bao Z, Yu Y. Fabrication and characterization of chitosan microcarrier for hepatocyte culture. Journal of Materials Science: Materials in Medicine 2007;18:2211-4.

[160] Lu G, Zhu L, Kong L, Zhang L, Gong Y, Zhao N, et al. Porous Chitosan Microcarriers for Large Scale Cultivation of Cells for Tissue Engineering: Fabrication and Evaluation. Tsinghua Science & Technology 2006;11:427-32.
[161] Nimni M, Cheung D, Strates B, Kodama M, Sheikh K. Chemically modified collagen: a natural biomaterial for tissue replacement. Journal of Biomedical Materials Research 1987;21:741-71.
[162] Liu JY, Hafner J, Dragieva G, Seifert B, Burg G. Autologous cultured keratinocytes on porcine gelatin microbeads effectively heal chronic venous leg ulcers. Wound Repair and Regeneration 2004;12:148-56.
[163] Kania G, Blyszczuk P, Czyz J, Navarrete-Santos A, Wobus AM. Differentiation of mouse embryonic stem cells into pancreatic and hepatic cells. Methods in Enzymology 2003;365:287-303.
[164] Rowley JA, Madlambayan G, Mooney DJ. Alginate hydrogels as synthetic extracellular matrix materials. Biomaterials 1999;20:45-53.
[165] Newman K, McBurney M. Poly (D, L lactic-co-glycolic acid) microspheres as biodegradable microcarriers for pluripotent stem cells. Biomaterials 2004;25:5763-71.
[166] Mercier NR, Costantino HR, Tracy MA, Bonassar LJ. Poly(lactide-co-glycolide) microspheres as a moldable scaffold for cartilage tissue engineering. Biomaterials 2005;26:1945-52.
[167] Hong L, Peptan IA, Colpan A, Daw JL. Adipose Tissue Engineering by Human Adipose-Derived Stromal Cells. Cells Tissues Organs 2006;183:133-40.
[168] Fischbach C, Seufert J, Staiger H, Hacker M. Three-Dimensional in Vitro Model of Adipogenesis: Comparison of Culture Conditions. Tissue Engineering 2004;10:215-29.
[169] Hemmrich K, von Heimburg D, Cierpka K. Optimization of the differentiation of human preadipocytes in vitro. Differentiation 2005;73:28-35.
[170] Zhang Y, He Y, Bharadwaj S, Hammam N, Carnagey K, Myers R, et al. Tissue-specific extracellular matrix coatings for the promotion of cell proliferation and maintenance of cell phenotype. Biomaterials 2009;30:4021-8.
[171] van Harmelen V, Skurk T, Röhrig K, Lee Y-M, Halbleib M, Aprath-Husmann I, et al. Effect of BMI and age on adipose tissue cellularity and differentiation capacity in women. International Journal of Obesity 2003;27:889-95.
[172] Flynn L, Prestwich G, Semple J, Woodhouse K. Adipose tissue engineering with naturally derived scaffolds and adipose-derived stem cells. Biomaterials 2007;28:3834-42.
[173] Sellaro TL, Ravindra AK, Stolz DB, Badylak SF. Maintenance of hepatic sinusoidal endothelial cell phenotype in vitro using organ-specific extracellular matrix scaffolds. Tissue Engineering 2007;13:2301-10.
[174] Chung HJ, Park TG. Injectable cellular aggregates prepared from biodegradable porous microspheres for adipose tissue engineering. Tissue Engineering Part A 2009;15:1391-400.
[175] Chung H-M, Won C-H, Sung J-H. Responses of adipose-derived stem cells during hypoxia: enhanced skin-regenerative potential. Expert Opinion on Biological Therapy 2009;9:1499-508.

Appendix A: Standard Curves

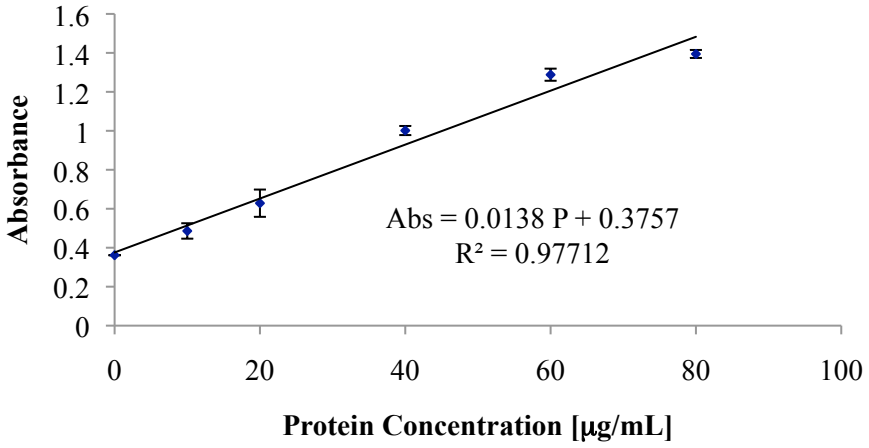

Figure A.1: Bio-Rad protein assay standard curve.
Measuring absorbance of prepared bovine albumin standards with concentrations of 0 µg/mL, 10 µg/mL, 20 µg/mL, 40 µg/mL, 60 µg/mL, and 80 µg/mL, at 595 nm.

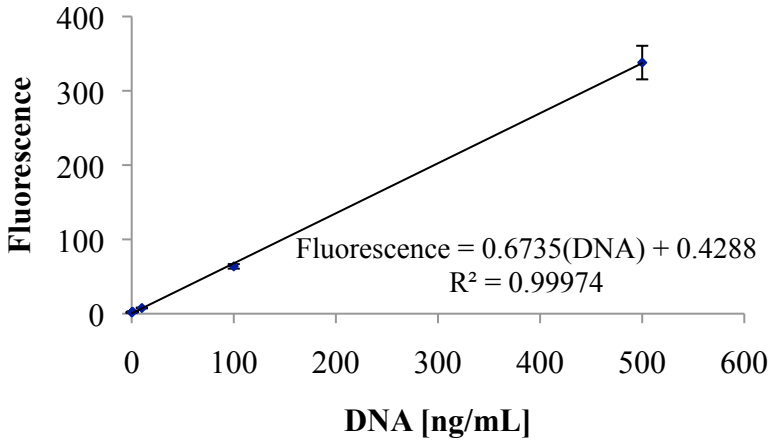

Figure A.2: DNA standard curve.
Generated by measuring the fluorescence (excitation 485 nm, emission 530 nm) of standards prepared by diluting 2 µg/mL Lamda DNA working solution, prepared from the Quant-iT™ PicoGreen® dsDNA kit. Standard concentrations are 0 ng/mL, 1 ng/mL, 10 ng/mL, 100 ng/mL, and 500 ng/mL.

Appendix B: Gelatin-Based Microcarrier Stability Data

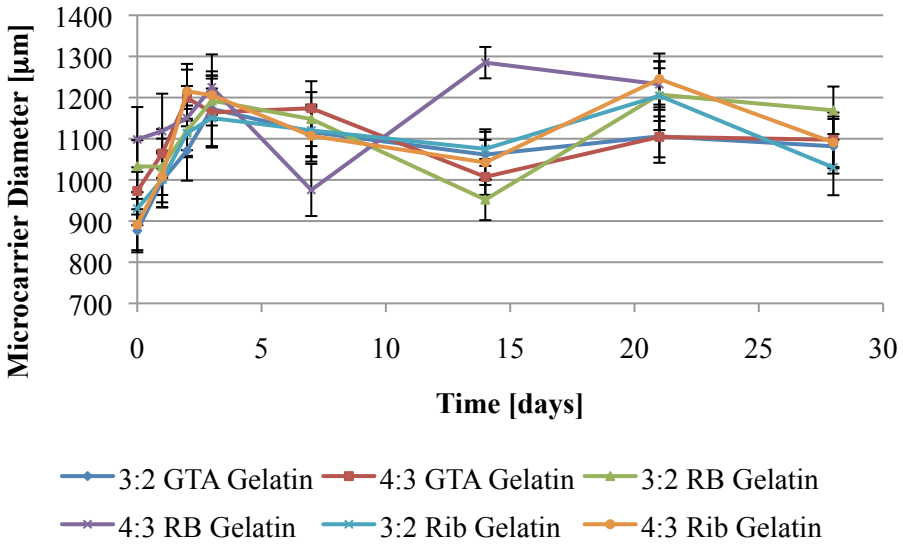

Figure B.1: Gelatin-based microcarrier stability as a function of diameter over 28 days.
Glutaraldehyde, GTA; Rose bengal, RB; Riboflavin, Rib. All data are expressed as the mean ± SD.

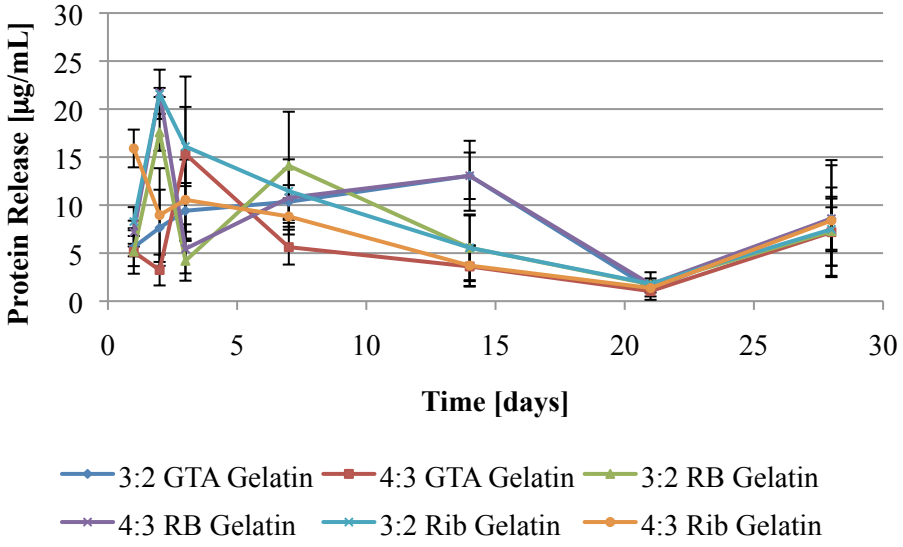

Figure B.2: *In vitro* protein release from gelatin-based microcarriers over 28-days.
Glutaraldehyde, GTA; Rose bengal, RB; Riboflavin, Rib. All data are expressed as the mean ± SD.

Appendix C: Microcarrier Swelling Data

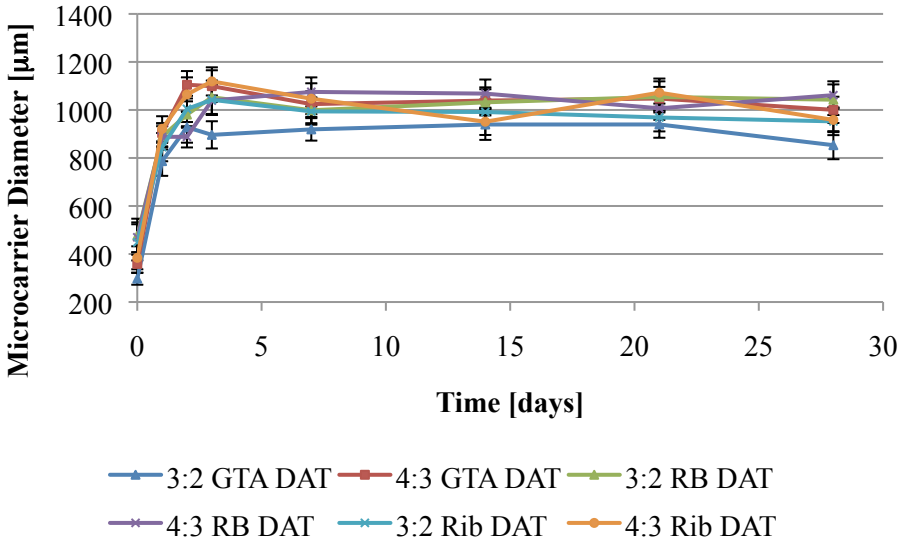

Figure C.1: DAT-based microcarrier swelling as a function of diameter over 28 days.
Glutaraldehyde, GTA; Rose bengal, RB; Riboflavin, Rib. All data are expressed as the mean ± SD.

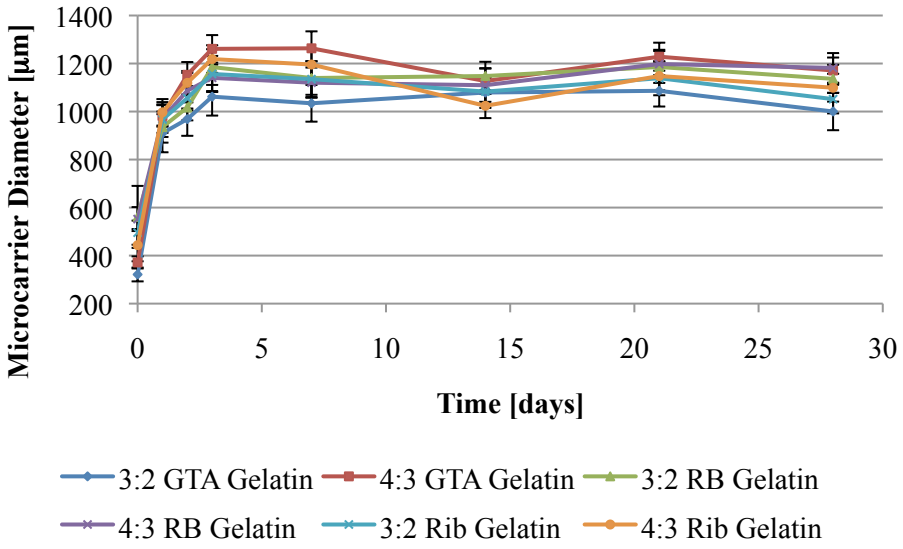

Figure C.2: Gelatin-based microcarrier swelling as a function of diameter over 28 days.
Glutaraldehyde, GTA; Rose bengal, RB; Riboflavin, Rib. All data are expressed as the mean ± SD.

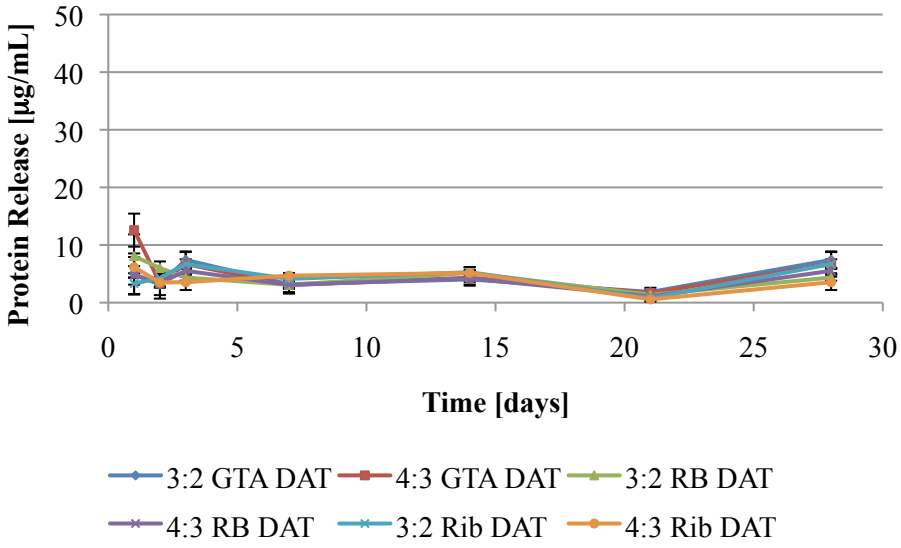

Figure C.3: *In vitro* protein release upon rehydrating DAT-based microcarriers (28 days).
Glutaraldehyde, GTA; Rose bengal, RB; Riboflavin, Rib. All data are expressed as the mean ± SD.

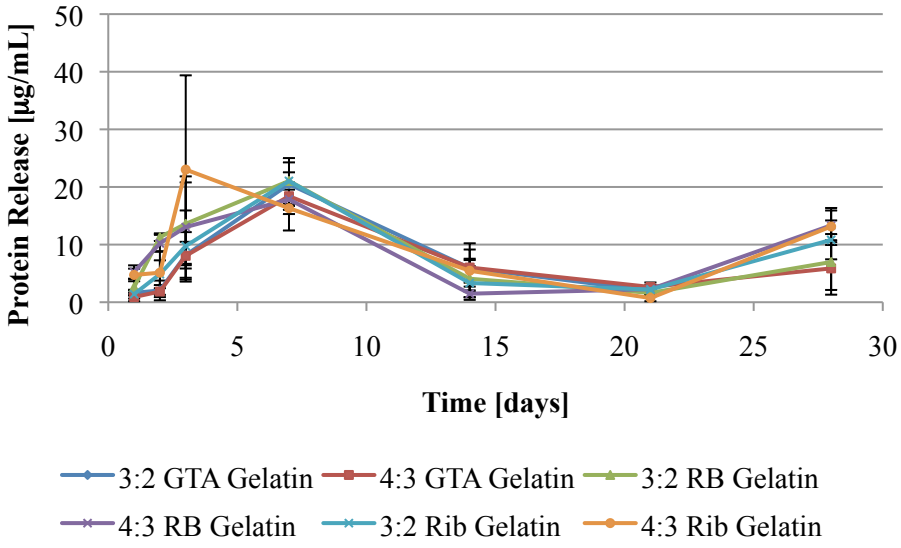

Figure C.4: *In vitro* protein release upon rehydrating gelatin-based microcarriers (28 days).
Glutaraldehyde, GTA; Rose bengal, RB; Riboflavin, Rib. All data are expressed as the mean ± SD.